Science
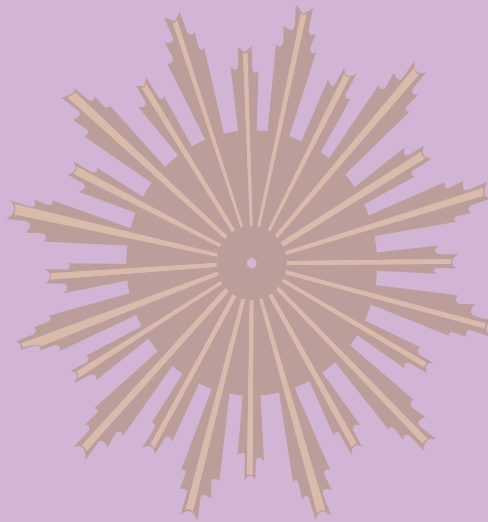
AUREOLE

An Academic Journal

Volume 8 (No. 1)

A Publication on Science 2022

BARASAT GOVERNMENT COLLEGE

AUREOLE – An Academic Journal

ISSN : 0976-9625

EDITORIAL BOARD

AUREOLE

An Academic Journal

Volume 8 (No. 1)

ISSN 0976-9625

A Publication on

Science

2022

BARASAT GOVERNMENT COLLEGE

From the Principal & Chief Editor's Desk

Yours obediently is glad to announce that the peer reviewed esteemed College Academic Journal 'Aureole' since its inception in 2009, is being published this year too, although after a little bit gap due to Covid 19 pandemic and other reasons. The Journal has made an indelible imprint in the field of intellectual and academic discourse.

My heartfelt greetings are conveyed to the authors for their untiring efforts in submitting the scripts. This time this volume is dedicated in the field of Science.

At the same time, yours obediently expresses his regrets for failing to consider some of the writings so sent due to various reasons.

As the number of articles received exceeds our limit a few might have to be put on hold to be published in the next issue and here – the first come first serve principle has been followed in addition to the quality of writings.

Yours obediently deeply expresses his gratitude to all those eminent scholars in their own field, who have reviewed the writings sent to them without any killing of time considering our busy and tight schedule.

I convey my thanks to all the members of Editorial Board for their relentless effort to make it a grand success.

I hope the journal will be a stand out in the field of academia.

I tender my apology for any mistake if there be and welcome suggestions from every corner.

Hoping further whole hearted assistance in future.

Barasat

Dr. Samar Chattopadhyay

Principal& Chief Editor

(West Bengal Senior Education Service)

Review Article

Physiology of Shade Plants: Strategies and Adaptations

Dibyendu Sekhar Mahanty[1*], Poorna Kumari Tiwari[2], Antara Das[3]

[1]Assistant Professor of Botany, [2]MSc in Botany, [3]MSc in Botany, Plant Physiology, Plant Biochemistry and Plant Molecular Biology Laboratory, Post Graduate Department of Botany, Barasat Government College, Kolkata, India
*Corresponding author email: dibyendu.mahanty@gmail.com

Abstract: For performance and sustainability of every ecosystem in every biome availability of light is critical and obligatory. Plants proliferating in full sunlight have different rate of water absorption, transpiration, carbon reduction, respiration, signal transduction, developmental regime and reproduction in comparison to certain plants which normally thrive in diffused light or shade. Shade loving plants thrive under low light condition and under a canopy shade whereas shade avoiding plants develop under optimum light condition which have acclimatized to such condition of low light intensity through morphological, anatomical, and biochemical adaptations. In contrast shade avoiding plants have a high rate of photosynthesis, transpiration, respiration, plants development in the form of elaborate sexual reproduction, seed production, and termination of life cycle through controlled apoptosis of cells as well or whole plant senescence when the growing period is over in case of annuals. Shade plants are mostly herbaceous often are with showy, variegated leaves, thus serve as ornamentals in various indoor areas. These plants are relatively easy to maintain which involves occasional watering, no weeding, limited light exposure and with low amount of nutrients requirements in contrast to the crop plants which grow in full sunlight. In the modern time urban indoor areas these plants offer room for increase in the oxygen and can play a greater role to contain the increase in green house gases (GHG) namely carbon dioxide in the environment through photosynthetic CO_2 reduction.

Key words: Shade plants, crop plants, carbon assimilation, ornamentals, green house gases.

INTRODUCTION

Life on earth depends on the sun. Sun is the sole and ultimate source of energy on earth. Except for some non-photosynthetic chemoautotrophs located in the deep sea, and darkest terrestrial habitat life on earth is fully dependent on the sun and energy transduction through the phenomenon of photosynthesis. For performance and sustainability of every ecosystem in every biome availability of light is critical and obligatory. Energy flow in all ecosystems starts with the sun to the highest trophic level. Plants and cyanobacteria chemically harvest light energy through photosynthesis, a light driven process in which carbon dioxide is reduced to carbohydrate level

utilizing products of the light reactions. In addition to abiotic factors soil composition, temperature, precipitation, composition of gases light has played the most important role in the origin and evolution of autotrophs and supporting other heterotrophs through its energy in the ecosystems. Tropical region of the earth with high insolation is a home to the great diversity of plants and thus taken the name of 'Lungs of the World'. This is because tropical rainforests perform as a giant machine that absorb a large amount of carbon dioxide and liberating oxygen, thus with largest primary product in this natural region [21].

The vegetation in the tropical rainforests is composed of four distinct layers namely, emergent (uppermost) followed by canopy, understory and forest floor. Canopy in the top layer is formed by the crowns of the trees which grow in association which block the sunshine and wind. The bottom layer in the forest floor in the tropical rainforest biomes do not receive adequate light and thus show herbaceous and shrubby plants with broad to moderate sized leaves. Owing very low light availability, primary produce by this section of the plants is considerably low. All physiological processes in plants are driven directly and indirectly by light viz. photosynthetic yield, transpiration, development seed germination, flowering, pollination, seed production and dissemination and propagation of both types [21].

Shade loving plants are those plants that thrive under low light condition and under a canopy shade whereas shade avoiding plants develop under optimum light condition [11]. Due to their propensity for shady environments, shade plants also known as sciophytes or sciophytic plants generally growing under the canopy of huge trees in forest floors where conditions are typically dim, hot, and humid, as in tropical rain forest biomes with high humidity, as a result of protracted periods of low light intensity exposure [4]. Two shade conditions are classified namely partial shade (with light intensity range of 250–350 lux) and complete shade (175–200 lux). Plants in partial shade require 3-6 hours of sunshine per day whereas in full shade it require 2 hours of sunlight or no direct sunlight. There are shade plants which do not require direct sunlight at all and they have acclimatized to such condition of low light intensity by employing morphological, anatomical, and biochemical adaptations in them. In addition to the morpho-anatomical differences leaves, pulvinous, petiole, root systems of plants living under shades, possess distinct physiological characteristics some of which are permanent some are temporary.

In forests a major proportion of light intensity is absorbed by tree vegetation and light reaching to the lower part of the bottom layers reduced by 90-98% of what in the exposed areas.

The sciophytes or the shade plants are of diverse types has stark difference from the crop plants which are selected by human for life and economic purposes. Crop plants are exposed to a high light intensity and engage in high rate of photosynthesis, transpiration, routine flower, fruit and seed development and senescence in many cases. Crop plants have an extensive primary production in contrast to the shade loving plants. Shade loving plants on the other hand are of great significance as they are of high aesthetic value. Shade plants do not have a high rate of photosynthesis, transpiration, and resort to vegetative propagation and thereby do not engage in senescence. Shade plants thus serve as ornamentals in various indoor areas. These plants are very easy maintained viz. occasional watering, no weeding, light exposure is for obvious and with low amount of nutrients requirements in contrast to the crop plants. In the modern time urban indoor areas these plants offer room for increase in the oxygen and can play a greater role to contain the increase in carbon dioxide in the environment.

AIMS AND OBJECTIVES

Aims and objectives of the review work are –

1. Identification of the shade plants around us grown for aesthetic value.
2. Comparison of the morphological, anatomical, physiological and biochemical characteristics of both the groups of plants taken for the study.
3. Screening of such plants.
4. Observation the morphological and anatomical features like leaf morphology, orientation, type of tissue present in the leaves of both categories of plants.
5. Anatomical peculiarities associated with shade plants namely, stomatal apertures, types, stomatal indexes, stomatal frequencies of the shade plant versus crop plants.
6. Internal structures of leaves - arrangement of the photosynthetic cells namely palisade and spongy parenchyma, cuticule, epidermis etc.
7. Pigment system and constitution in these plants taken for the review work and compare viz. chl-a, chl-b, carotenes, xanthophylls etc. among them.

8.   Ascertaining shade plants are plants with low maintenance and recommend for plantation.

LITERATURE REVIEW

Heliophytes are the plants which grow vigorously in the full sunlight in contrast to the sciophytes. Interestingly, no trees are sciophytes meaning trees do a great deal of photosynthesis with high carbohydrate reserves. Though there are heliophytes which grow best in the sun, but can grow fairly well under shade, such plants are facultative sciophytes [21]. Similarly there are facultative heliophytes which grow best in the lower light intensities but can grow well in full sunlight. There are plants which grow in shades but are economically important like *Piper betel, P. nigrum, P. longum* etc. Young leaves in shade plants are normally not masked by carotenoids or anthocyanins as a measure against photo-oxidation [2].

Shade plants may get injured in high light intensities. In addition to the light compensation point, the light saturation irradiance, and the chlorophyll a/b ratio, the light saturation rate of photosynthesis in plants living in the direct sunlight is much higher than in shade leaves [25]. In contrast, shade leaves have a larger chlorophyll content per unit of leaf mass and area, as well as a higher allocation of nitrogen to light-harvesting complexes [25] .

In contrast to shade plants crop plants are some vigorously growing plants where leaf serves as the primary site for photosynthesis. Over the course of evolution, leaves have developed specific structural adaptations that allow them to thrive in various environmental conditions while efficiently carrying out photosynthesis. These adaptations include:

- Large, broad, flat leaf lamina for so as to provide a significant surface area for capturing sunlight.
- Crop plants like rice, wheat, jute, bean require a full day viz. more than 8 to 9 hrs of direct sunlight with light intensity more than 1000 to 1250 lux.
- Presence of protective coating in the abaxial and adaxial surfaces of the leaves: Both surfaces of the leaves are coated with waxy cuticle, this helps in minimising the water loss and protect the leaves from undesirable water loss and protection from environmental stresses.

- **High stomatal density:** Leaves of the crop plants possess comparatively higher number of stomata per unit area (also termed as stomatal frequency). Stomata allow for the exchange of gases, such as carbon dioxide and oxygen, necessary for photosynthesis also water loss for cooling of the leaf surface [4].

- **Detailed and intricate inner surface and air spaces:** Inside the leaf, there is a complex network of internal surfaces and air spaces that facilitate the movement of gases throughout the leaf, ensuring efficient gaseous exchange. It has been observed that the leaves of crops or sun leaves are much thicker than the leaves of the shade plants [24].

- **Abundance of chloroplasts in each cell**: Chloroplasts, the organelles responsible for photosynthesis, are present in large numbers within leaf cells. Abundance of chloroplasts increases the photosynthetic yield in these types of plants. Variegated leaves are purely absent in crop plants.

- **Orientation of leaves**: Orientation of leaves towards incoming light in crop plants is such that it maximizes the absorption of light energy. Limiting crop plants with sunlight hampers the yield drastically [19].

- **Relation between the vascular tissue and photosynthetic cells:** There lie a close association between vascular tissue system and photosynthetic cells (palisade cells and mesophyll cells) in crop plants. The vascular tissues, composed of xylem and phloem, are in close proximity and connection with the photosynthetic cells of the leaf. This connection ensures the efficient exchange and translocation of water, nutrients, and sugars between the leaf and the rest of the plants.

Collectively, these structural features of leaves enable the crop plants them to withstand environmental challenges while efficiently absorbing light and taking up carbon dioxide for photosynthesis. Such adaptations have contributed to the success of leaves as the primary photosynthetic organs in higher plants, including many important crop species [7].

Fluctuations in light conditions can have a negative impact on the carbon gain and productivity of field crops, as their photosynthetic responses are not immediate. This is especially crucial in the case of vegetable crops, where light plays a significant role in their

growth and development [23]. Manipulating the light environment can be a valuable strategy to optimize nutrient absorption capacity and increase the yield and economic value of leafy crops. In melon and fruit vegetables, imbalances in nutrient supply can result in substantial economic losses and impact the flavor and quality of the fruits. Therefore, regulating the light environment presents a viable approach to provide suitable growing conditions for high-yield and high-quality horticultural crops while reducing the dependence on chemical fertilizers. Previous research has demonstrated that nitrate uptake in soybean seedlings reaches its peak during the light period. This increase in nitrate acquisition stimulates photosynthesis and subsequently promotes sucrose transport, ultimately contributing to enhance plant performance under well-illuminated conditions [14].

Following significant parameters are taken while comparing the two groups of plants namely sciophytes and heliophytes:

- Requirement for light or exposure to light and capture of light
- Leaf orientation, chloroplast per unit area of leaf or unit mass of leaf
- Rate of photosynthesis -energy requirement of the plant
- Optimum temperature range for growth and development
- Requirement for water and nutrient
- Mode of reproduction,
- Fruit/seed production in the such plants
- Life cycle patterns.
- Mode of propagation vegetative or reproductive.

Sun leaves also have a significantly higher capacity for Non-Photochemical Quenching (NPQ), a kind of photo-defense that depends on the violaxanthin cycle and the plastidic protein Psb [25]. Sun and shade leaf also differ in terms of chloroplast size, shape, and number For instance, compared to shade leaves, sun leaves have smaller chloroplasts and a lower thylakoid/grana ratio. Leaves in the sun and the shade exhibit different morphological and biochemical traits: Shade leaves have more total chlorophyll per reaction centre, a higher ratio of chlorophyll b to chlorophyll a, and often thinner laminae than sun leaves, which all boost light capture. More rubisco in sun leaves increases CO_2 uptake, while a large concentration of

xanthophyll-cycle components in sun leaves allows them to dissipate extra light energy. When compared to shade leaves, shade avoiding leaves have thicker leaves and larger palisade layers. Because shade plants have very low respiration rates, only a small amount of net photosynthesis is required to bring the net rates of CO_2 exchange to zero, resulting in lower values for shade plants. Low respiration rates appear to be a fundamental adaptation that enables shade plants to thrive in environments that have little light [19]. According to prior research, the morpho-anatomical and physiological adaptations/responses of sun leaves are similar to the foliar characteristics of drought-tolerant plants, but the situation in shade leaves is similar to that of drought-intolerant plants [25].

One of the most important environmental elements for crop biochemistry and physiology is light quantity and quality. Previous comparison research revealed that low light levels resulted in a decrease in the dry matter of the plant's roots, stems, leaves, and entire body as well as in photosynthetic rate, transpiration, stomatal conductance, and stem diameter. Additionally, crop plants grow leaves that are thinner and smaller when exposed to low light levels than they do when exposed to full sunlight. However, the presence of shade environments led to an increase in plant height and lodging, which impedes the movement of water, nutrients, and photosynthetic products and ultimately results in significant losses in agricultural output. When combined, light intensity is the primary factor that regulates the central processes of plants, including germination, leaf growth and development, photosynthesis, the start of buds and flowers, and cell division. In fact, as the amount of light rises to a moderate level, many plant processes become more effective, causing dramatic physiological and developmental changes that result in the rapid expansion of these processes [17]. Plants use phytochromes to perceive the red: far-red ratio (R: FR), which mediates the shade-avoidance syndrome, in the natural light environment. Plant elongates more quickly and blossom more quickly if the ratio is low, as it is in areas covered in dense plant canopies, which helps them generate seeds earlier for survival. In trials with a controlled R:FR ratio under artificial lighting, the shade-avoidance syndrome is plainly visible. However, under low R: FR conditions, flowering and acceleration of elongation do not always happen simultaneously [6]. Leaf morphology and anatomy are determined by shade. The shape of leaves, which are the primary organs for photosynthesis and transpiration in plants, provides insight into how the environment affects plants or how they respond to a changing environment. Palisade tissue lengthens and expands the area of the chloroplast channel via which

CO_2 enters under typical lighting conditions, increasing leaf thickness and enhancing photosynthetic capacity. As more carbon is devoted to the elongation of the stem and petiole at the expense of leaf and root development, plants in shade typically have increased stem height, longer petioles, and smaller stem diameter. Such a design aids plants in their search for light when they are in shadow. But shady conditions lead to weaker, slender stems that have low mechanical strength. By decreasing the activity of enzymes, low light levels or shade circumstances function as a limiting factor in the formation of lignin. The morphological and anatomical structures of the stem are likewise regulated by light quality [22]. Plants absorb red and blue light more readily than green light hence blue or red light has a significant impact on their physiology and development. Low light circumstances cause the majority of plants to reduce their stomatal count, which is clearly seen in both natural and managed environments. Additionally, stomatal conductance decreases at lower irradiances, which results in higher levels of intercellular CO_2 amount. Shade stress may also lessen stomatal opening because guard cells' ABA levels rise in low light conditions, which causes them to bind to a soluble receptor and cause closure of stomatal pores. Chlorophyll (Chl a, Chl b, Chla+b, and Chl a/b), which is an essential pigment involved in absorbance, transmission, and conversion of solar energy into electrochemical energy, changes the photosynthetic pigment composition of plants in low light or shadow. According to several research, lower chlorophyll concentrations under shaded conditions, which is also a common sign of oxidative stress, may be caused by chlorophyll photo-oxidation, a lack of chlorophyll synthesis, or chlorophyll breakdown [12]. Under shade, a plant's growth is directly influenced by the quantity and quality of light (specifically, the red-to-far-red (R/Fr) ratio). Gibberellins (GAs) and auxin [indole-3-acetic acid (IAA)] are key mediators of plants' adaptation to shade [27].

The group of leaf-level features that allow for maximum net carbon fixation in presence of low irradiance are collectively referred to as "shade tolerance" in scientific literature. The set of architectural characteristics that promote to good vertical development in plants growing under low irradiance have been referred to as "shade avoidance" less frequently [10]. It is therefore hypothesized that species adapted to low light levels, or shade-tolerant species, have a wide crown to intercept light across a vast region and a shallow crown to reduce self-shading. Light demanders, or species that have acclimated to high light levels, must monopolize any openings. These plants can maintain rapid growth rates because of the high light conditions in

gaps [18]. Major differences were found between the sun and shade leaves of *Abies alba* in terms of their morphology, anatomy, and physiology. For example, the sun leaves were larger, contained a palisade parenchyma and a hypodermis, and had more stomata [25]. The photosynthetic structures of leaves in shade-tolerant species like *Alocasia* mycorrhiza show modifications to maximize productivity in low light conditions. These include mesophyll tissue with lens-shaped epidermal cells that focus light within thinner leaves with higher chlorophyll concentration. Shade tolerance is defined under the "carbon gain hypothesis" as the maximum amount of light captured and used for photosynthesis along with the least amount of respiration costs for maintenance. The growth and survival trade-off theory, which is an extension of the carbon gain hypothesis, states that growth rates in high light and survivability in low light are inversely associated across species [8].

UNDERSTANDING THE METHOD OF SHADE TOLERANCE

There are numerous physiological and anatomical differences across species with different shade tolerances. Maximization of net carbon gain in low light as well as maximization of resistance to biotic and abiotic stresses in the understory, i.e., the stress tolerance hypothesis, are two partially competing hypotheses on the suites of traits responsible for a species' tolerance to shade [8].

THE CARBON GAIN HYPOTHESIS

According to the carbon gain hypothesis, any trait that improves the use efficiency of light, and therefore improves carbon gain, increases species shade tolerance. These characteristics include a high proportion of biomass invested in organs that contribute to light interception in the understory (i.e., leaves and branches), a low leaf mass per unit area (LMA), and a high quantum yield of photosynthesis (QY) that results in a low photosynthetic light compensation point (LCP) [5]. According to the carbon gain hypothesis, shade-tolerant species have larger leaf chlorophyll levels and more photosynthetic potential in low light than shade-intolerant species do at the level of the individual leaf. According to the carbon gain hypothesis, plants that can tolerate shade have larger leaves than species that cannot. Angiosperms that can tolerate shade typically have larger seeds than non-tolerant species, and this difference in seed size is linked to larger seedlings. Compared to canopy trees of intolerant species, those of shade-tolerant species often collect more leaf area, produce denser crowns, and have poorer light

transmittance. Denser crowns show increased branching density (number of twigs per unit leaf area) and perhaps also greater foliage shade tolerance in shade-tolerant species [5]. In addition to the overall variations in crown leaf area density, there is evidence that shade-tolerant species have a more complex contour of the crown surface with a higher degree of piercing cavities, which enables the plants to support more leaves inside the canopy.

THE STRESS TOLERANCE HYPOTHESIS

Kitajima in1994 proposed that the carbon gain hypothesis should be rejected and that survival in shade is more strongly related to plant resistance to biotic and abiotic stresses (stress tolerance hypothesis) based on the observation that LAR and RGR were higher and MA lower in young seedlings of shade intolerant species in both high and low light [15, 14].These characteristics include a high level of defense metabolites, a high wood density, and LMA [5].

The stress hypothesis is similar to the storage hypothesis for shade tolerance.This theory holds that shade-tolerant species invest more of their output in storage rather than maximizing growth in low light, allowing the plants to withstand periods of low light that are near to or below the whole-plant light compensation point. The concept is supported by several empirical research that show shade-tolerant plants to have larger storage capacity. The stress tolerance and carbon gain ideas, however, are not mutually exclusive [8], but it is conceivable that both aid in elucidating shade tolerance [26]. Our understanding of shade tolerance has been greatly influenced by the carbon gain hypothesis, although this theory is currently being contested. Although most studies found that Shade Tolerant seedlings had lower relative growth rates (RGR) when growing in both high and low light settings, the theory originally predicted that Shade Tolerant species should have greater relative growth rates (RGR) than Shade Intolerant species when growing in the shade. Although some research with tropical trees found the contrary, the carbon gain hypothesis also supports lower LMA for Shade Tolerant species compared with shade intolerant species to maximize light interception [5].

SHADE AVOIDANCE AND SHADE TOLERANT PLANTS

PIGMENT CONTENT AND LEAF STRUCTURE

The leaves of shade plants are commonly thought to be thinner and have larger, more chlorophyll-rich chloroplasts than the leaves of sun plants. Compared to chlorophyll a, shade

plants have a higher percentage of chlorophyll b. These differences can be easily seen in the leaves of numerous species, both those that grow in the sun and those that grow in the shade, as well as when one species is grown under various light intensities [20,3]. The thickening of the palisade tissue, which has been shown to transport light more effectively than spongy mesophyll, is one of the most obvious changes in sun leaves [8]. The morphological characteristics of the *Spinacia oleracea* leaves that grew in high and low light were similar to those of leaves in the sun and the shade. The leaves grown in strong light were 28% thicker compared to those grown in low light. The growth of cells in the palisade and spongy cell layers of sun loving leaves, with the palisade exhibiting the biggest variations, mediated this transition. In contrast to shade leaves, which only had three layers of palisade cells, sun leaves typically had five. In sun loving plants palisade cells were substantially smaller and more compact than their shade counterparts. However, the chlorophyll concentration of shade plants is frequently smaller per unit leaf area. Although several rainforest species, such *C. rubra* and *Lomandra longifolia*, possess thick leaves, a high ratio of dry matter to leaf area, and a much higher chlorophyll content per unit area of leaf, they are not usually associated with shade plants. Shade plants contain lower amounts of soluble protein and significantly lower ratios of soluble protein to chlorophyll than sun species, regardless of how thick the leaves area. Although several rainforest species, such *C rubra* and *Lomandra longifolia*, have thick leaves, a high ratio of dry matter to leaf area, and a high chlorophyll content per unit area of leaf, narrow leaves are not usually a defining feature of shade plants [20]. The carotenoid composition of sun leaves of annual agricultural plants (some with several variants) was compared to shade leaves of many other plant groupings, including sun and shade leaves of six species of perennial shrubs and vines, as well as deep-shadow leaves of seven rainforest species. The components of the xanthophyll cycle violaxanthin, antheraxanthin, and zeaxanthin, as well as beta-carotene, were much higher in sun leaves than in shade leaves. These crop species' sun leaves did not contain a-carotene, which was present in considerable levels in all shade leaves and in lower amounts in three of the four perennial shrubs and vines' sun leaves [1].

STRUCTURE OF CHLOROPLAST

The huge grana stack in shade plant chloroplasts, which can have up to 100 thylakoids per granum, are a noteworthy characteristic. In contrast to sun plant chloroplasts, which have the grana aligned in a single plane, the grana are randomly organized within chloroplasts [20].

Chloroplasts obtained from the leaves of three tropical rainforest plant species, namely *Alocasia macrorrhiza, Cordyline rubra*, and *Lomandra longifolia,* which are known as shade plants, exhibited a significantly higher chlorophyll content compared to chloroplasts from spinach. In fact, the shade plant chloroplasts contained approximately 4-5 times more chlorophyll than the chloroplasts from spinach. Furthermore, the ratio of chlorophyll a to chlorophyll b in the shade plant chloroplasts was measured to be 2.3, whereas it was found to be 2.8 for the chloroplasts from spinach. Leaf sections were examined using electron microscopy, and the results displayed that chloroplast in shade plants possessed remarkably large stacks of grana. A significant difference was observed between *Alocasia* and spinach chloroplasts in terms of the ratio of the total length of partitions to the total length of stroma lamellae, with *Alocasia* exhibiting a notably higher ratio. Additionally, when isolated chloroplasts were subjected to freeze-etching, both the small and large particles commonly observed in spinach chloroplasts were also detected [13].

Recent research conducted on various shade plants has revealed that there is no universal chloroplast structure that applies to all shade plants. Different shade plant species exhibit diverse chloroplast characteristics. For instance, liverworts such as *Neohodgsonia mirabilis* H. Perss and *Marchantia foliacea* Mitt. found in deeply shaded environments possess grana with only 5-10 thylakoids. A *Cyathodium species* collected from Singapore also exhibits a similar range of granal stacking and size, as observed in unpublished observations by C.R. Sheue and V. Sarafis [2].

Similarly, many bryophytes adapted to shady environments lack massive grana and stacking. For example, the shining moss *Schistostega pennata*, which typically inhabits low-light habitats such as rock cracks, caves, and holes, does not possess large grana. Instead, it usually has several large chloroplasts and normal-sized grana in the aerial part of its protonema.

Furthermore, it has been noted that *Trichomanes speciosum* Willd., a plant thriving in deep shade, owes its success to its low metabolic rate. Neither the gametophyte filaments nor the

sporophyte leaves of this species exhibit chloroplasts with extreme forms. In summary, the adaptations and characteristics of shade plant chloroplasts vary among different species, reflecting the diverse strategies employed by plants to thrive in low-light environments [2].

RATE OF RESPIRATION

Leaf respiration plays a crucial role in the overall productivity of plants by influencing various aspects such as daily carbon assimilation, nutrient uptake, and growth. It is widely recognized that leaf respiration exhibits significant variations between periods of darkness and light, not only in terms of its rate but also in terms of the metabolic pathways and biological functions involved [9].

The shade plants, originating from densely shaded environments within California's redwood forests, exhibited lower rates of dark respiration (CO_2 evolved dm^{-2} min^{-1}) and lower compensation points compared to the sun-adapted species found in open sunny habitats. Conversely, the sun species displayed dark respiration rates of CO_2 evolved dm^{-2} min^{-1}. When it came to light-saturated rates of CO_2 uptake, the shade species demonstrated values between 2.1 and 3.1 mg CO_2 dm^{-2} hr^{-1}, while the sun species exhibited rates ranging from 21 to 36 mg CO_2 dm^{-2} hr^{-1}. Notably, the shade species experienced photoinhibition even at relatively low light intensities of 70,000 erg cm^{-2} sec^{-1}[20]. To investigate the contrasting respiratory rates between sun-adapted *Spinacia oleracea* L. (a sun species) and shade-adapted *Alocasia odora* (Lodd.) a shade species, particularly focusing on nocturnal variations, certain respiratory properties of their leaves were examined. Throughout the night, CO_2 efflux and O_2 uptake rates in *S. oleracea* gradually declined, whereas *A. odora* maintained relatively constant rates at lower levels. In *S. oleracea*, the addition of sucrose resulted in increased rates of O_2 uptake, which remained consistent throughout the night. Surprisingly, the addition of an uncoupler (carbonyl cyanide p-(trifluoromethoxy)-phenylhydrazone; FCCP) did not affect the rates. In contrast, *A. odora* exhibited enhanced rates of O_2 uptake when FCCP was added, but sucrose did not have the same effect. Throughout the night, both species experienced a decrease in tissue carbohydrate concentrations, while *A. odora* consistently exhibited a higher ATP/ADP ratio. These findings suggest that the respiratory rate in *S. oleracea* is influenced by the availability of respiratory substrates, whereas the lower respiratory rate in *A. odora* can be attributed to its lower demand for ATP [16]

LIST OF SHADE PLANTS

A list of few plants that are actually shade-loving species:

Abutilon pictum, Acanthus mollis, Aglaonema sp., *Astilbe japonica, Blechnum gibbum, Digitalis purpurea, Asystasia gangetica, Podranea ricasoliana, Fatsia japonica, Alpinia zerumbet, Asparagus sp., Athyrium filix-femina Nephrolepis exaltata, Liriope muscari, Schefflera arboricola, Oxalis triangularis, Oxalis corniculata, Abutilon pictum, Acanthus mollis, Acampe carinata, Acorus gramineus, Aerides maculosa, Aesculus californica, Ajuga sp., Alchemilla mollis, Amorphophallus sp., Anemone japonica, Anthriscus sylvestris, Arum italicum, Asplenium sp., Bergenia ciliata, Bromelia sp., Callicarpa bodinieri, Camellia sp., Campanula garganica, Carpenteria californica, Clerodendrum bungei, Cleodendrum trichotomum, Colocasia esculenta, Cornus kousa, Correa pulchella, Cryptomium sp., Dicentra formosa, Euphorbia hirta, Disksonia sp., Fraxinus latifolia, Hedychium coronarium, Hellelleborus foetidus, Helleborus orientalis, Heuchera micrantha, Hibiscus rosa-sinensis, Houttuynia cordata, Hydrangea macrophylla, Iris douglasiana, Iris ensata, Lamium maculatum, Leptinella sp., Liriope muscari, Lonicera sempervirens, Lonicera cilosa, Lysimachia congestiflora, Melianthus major, Mimulus cardinalis, Nandina domestica, Oxalis deppei, Osmunda claytoniana, Pedicularis densiflora, Pentagramma sp., Phygelius sp., Physocarpus capitatus, Primula polyanthus, Pseudosasa owatarii, Rumex dentatus, Rumex sanguineus, Sasaella masamuneana, Sedum makinoi, Senecio sp., Silene sp. Spirraea douglasii*

Significance of shade plants:

When Henry Austin wrote of 'shadows large and long' in a garden song, he could have been referring to many of our garden spaces. Shade tolerant plants are thus adapted to be efficient energy-users. In simple terms shade tolerant plants grow broader, thinner leaves to catch more sunlight to the cost more sunlight relative to the cost of producing the leaf. Shade plants are mostly ornamental plants. Ornamental plants are grown for decorative purposes in gardens and landscape design projects as house plants, for cut flowers and specimen display. Besides ornamental plants play important role in human health and psychology. It may grow in small homes and create a relaxed and happy ambience. Shade plants are actually indoor plants. Indoor

plants sequester CO_2 and keep Oxygen flowing, they purify the air by removing toxins, help to deter illness. One of the easiest indoor plants to maintain, the Spider Plant (***Chlorophytum*** *sp*.) produces oxygen whilst purifying the air in your home and office by absorbing carbon monoxide, formaldehyde and xylene.

Fig.1. Clockwise from top left (a) *Chlorophytum* sp*., (b) Sansevieria* sp*., (c) Aglaonema* sp*., (d) Spathiphyllum* sp*., (e) Stromanthe sanguinea* and (f) *Calathea zebrina*

The Snake plant (*Sansvieria* sp.), Peace Lily's (*Spathiphyllum* sp.), English Ivy (**Hedera helix**), cleans air better than most other indoor plants as it has the ability to absorb excessive levels of carbon monoxide. They can withstand water stress and has the ability to remain viable in elevated temperature.

As one of the most user-friendly indoor plants, Chinese Evergreen (*Aglaonema* sp.) cleans and purify indoor air, absorbing formaldehyde, carbon monoxide and benzene.

Most of the species of Orchidaceae are shade loving plants. To name a few --

Acanthophippium bicolor, Acampe carinata, Aerides multiflora, Aerides maculosa, Aerides odorata, Agrostophyllum callosum, Bulbophyllum sp., Brachycorythis spelendida, Chiloschista lunifera, Coelogyne sp., Conchidium microchilos,Cryptochilus sanguineus, Cymbidium sp. Dendrobium aqueum, Dendrobium chrysanthum, Dienia ophrydis, Diphylax urceolata, Disperis neligherrensis, Eulophia pulchra, Oberonia verticillata, Otochillus sp., Phalaenopsis amabilis, Smithsonia sp.,Vanda cristata, Vanilla walkeriae,
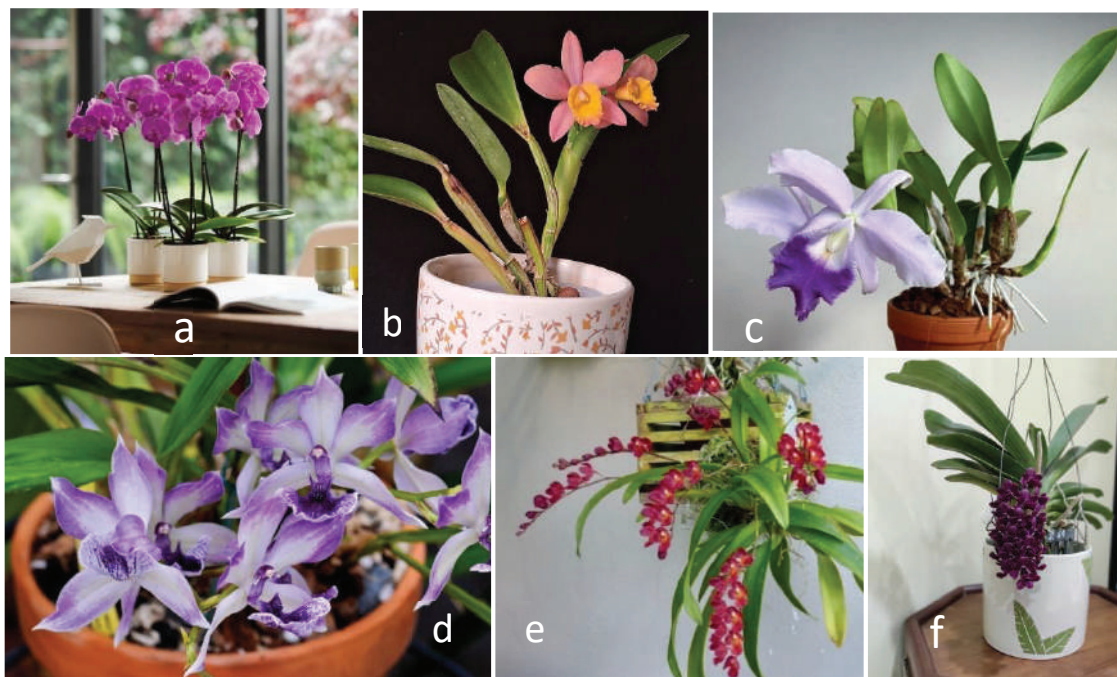
Fig. 2 Clockwise from left (a) *Phalaenopsis* sp., (b) *Sophrocattleya* sp., (c) *Cattleya* sp., (d) *Zygonisia* sp., (e) *Howeara lava* and (f) *Rhynchostylis* sp.,

Most of the shade loving plants are perennial thus whole plant senescence is normally not observed in normal course in these plants [4]. This is may be due to the fact that they do not engage in sexual reproduction and formation of fruit giving signal for senescence. This is not true for orchids as they flower but do not undergo senescence in contrast to other plants. So they live more years than crop plants.

- They have a great aesthetic value and help to make people calmer and happier and reduce workplace negativity.

- Trees, walls, fences, buildings can all interfere with the amount of sunlight received in a given area, particularly on urban properties. Despite the challenges a lack of sunlight may present and shade loving indoor plants can create an attractive, relaxing atmosphere.

- They are also low in cost and require low maintenance than others.

- Orchids are indoor shade loving plants though delicate they do not have high requirement for water. They perform carbon reduction employing Crassulacean Acid Metabolism (CAM) which makes them well equipped to thrive under water stress also [28]. Therefore they can serve as ideal indoor plants in sophisticated milieu.

DISCUSSION

Upon study of stomata from the groups of shade plants and crop plants it was found that general number of stoma per unit area in shade plants are less in number compared to sun loving plants viz. stomatal frequency of sciophytes are considerably lower than the sun loving crop plants or heliophytes. It was observed that most the shade plants do not contain stomata in the upper surface rather only confined to the lower surface of the leaves. This may be attributed to low rate of transpiration in these plants. In sun plants average number stoma per unit area was much higher than the former types of plants. As discussed in the literature review section leaves of the shade plants are not exposed to direct sunlight, this results in the low rate of heating effect occurring on the leaf lamina and low rate of transpiration required to cool the plant body. In most of the sun loving plants stomata are distributed in both the surfaces may be owing to the need for greater cooling effect in these plants.

When potted shade plants watered in the indoor rate of evapo-transpiration in these plants are lower in comparison to the plants growing in the direct sunlight as the soil in such heliophytes dries up faster than the shade plants. Total chlorophyll content and chlorophyll –a content in crop plants were seen to be higher than the shade plants as these plants are more robust with short internodes and greater rate of photosynthate production in the form of fruits, seeds etc. Chl-a form the recation centre of the light harvesting complexes (LHCs) and initiates the light reactions in presence of light. Higher quantity of chl-a confirms higher rate of photosynthesis in crop plants or sun loving plants.. Presence of higher leaf proteins in crop plants

is significantly higher than the shade plants. It was reported that shade plants exhibited lower rates of dark respiration thus low rate of other metabolic works in comparison to the crop plants growing in the direct sunlight.

CONCLUSION

It can be said that shade plants are comparatively less vigorously photosynthesizing plants and remain idle most very often. Crop plants grow faster in comparison to the shade plants. Shade plants are generally with low stomatal frequency and stomatal index it means they lose water in much less quantity may owe their adaptation in the tropical forest floor. As they grow less vigorously, with showy and variegated leaves, low water requirement, low light requirement and comparatively less delicate they are grown as foliar or foliage plants in various facilities like, offices, administrative buildings, stations, indoor areas, banquets, hotels, ships, airports and in urban houses for obvious reasons. The aesthetic sense they add to the environment is excellent. They also act as air purifiers as they perform photosynthesis in the indoor areas. This plants thus has the potential to reduce the carbon dioxide content if grown collectively can result in a cumulative effect on carbon dioxide (green house gases) sequestration.

Conflict of interests

The authors declare that they have no known competing financial interests or personal relationships that could have appeared to influence the work reported in this paper.

References:

[1] B. Demmig-Adams and W. W. Adams III: Carotenoid composition in sun and shade leaves of plants with different life forms. *Plant, Cell & Environment*, **15(4)**, 411-419 (1992).

[2] C. R. Sheue, V. Sarafis, R. Kiew, H.Y. Liu, A. Salino, L. L., Kuo-Huang and M.S. Ku: Bizonoplast, a unique chloroplast in the epidermal cells of microphylls in the shade plant *Selaginella erythropus* (Selaginellaceae). *American Journal of Botany*, **94(12)**,1922-1929. (2007).

[3] C. S. Cooper and M. Qualls: Morphology and Chlorophyll Content of Shade and Sun Leaves of Two Legumes 1. *Crop Science*, **7(6)**, 672-673. (1967).

[4] D. S. Mahanty: Physiology of shade loving plants: A comparative analysis with shade avoiding plants. *Indian J. Applied & Pure Bio.* **38(2)**, 536-546 (2023).

[5] E. B. Ntawuhiganayo, F. K. Uwizeye, E. Zibera, M. E. Dusenge, C. Ziegler, B. Ntirugulirwa and J. Uddling: Traits controlling shade tolerance in tropical montane trees. *Tree Physiology*, *40* **(2)**, 183-197 (2020).

[6]E. Goto: Effects of light quality on growth of crop plants under artificial lighting. *Environment Control in Biology*, *41***(2)**, 121-132 (2003).

[7] F.P. Gardner, R.B. Pearce and R. L. Mitchell: *Physiology of crop plants*. Scientific publishers (2017).

[8] F. Valladares and Ü. Niinemets, Shade tolerance, a key plant feature of complex nature and consequences. *Annual Review of Ecology, Evolution, and Systematics*, *39*, 237-257. (2008).

[9] G. Tcherkez and O.K. Atkin: Unravelling mechanisms and impacts of day respiration in plant leaves: an introduction to a Virtual Issue. *New Phytologist*, *230***(1)**, 5-10. (2021).

[10] H. A. Henry and H. A. Aarssen: On the relationship between shade tolerance and shade avoidance strategies in woodland plants. *Oikos*, 575-582 (1997).

[11] I. Ruberti, G. Sessa, A. Ciolfi, M. Possenti, M. Carabelli and G. J. B. A. Morelli: Plant adaptation to dynamically changing environment: the shade avoidance response. *Biotechnology advances*, *30***(5)**, 1047-1058 (2012).

[12] I. Shafiq, S. Hussain, M.A. Raza, N. Iqbal, M. A. Asghar Ali and Y. A. N. G. Feng: Crop photosynthetic response to light quality and light intensity. *Journal of Integrative Agriculture*, *20***(1)**, 4-23 (2021).

[13] J.M. Anderson, D. J. Goodchild and N.K. Boardman: Composition of the photosystems and chloroplast structure in extreme shade plants. *Biochimica et Biophysica Acta (BBA)- Bioenergetics*, *325***(3)**, 573-585 (1973).

[14] J. Xu, Z. Guo, X. Jiang, G. J. Ahammed and Y. Zhou: Light regulation of horticultural crop nutrient uptake and utilization. Horticultural Plant Journal, **7(5)**, 367-379 (2021).

[15] K. Kitajima: Relative importance of photosynthetic traits and allocation patterns as correlates of seedling shade tolerance of 13 tropical trees. *Oecologia* **98**, 419–428 (1994).

[16] K. Noguchi and I. Terashima: Different regulation of leaf respiration between *Spinacia oleracea*, a sun species, and *Alocasia odora*, a shade species. *Physiologia Plantarum*, *101***(1)**, 1-7 (1997).

[17] L. Feng, M.A. Raza, Z. Li, Y. Chen, M. H. B. Khalid and F. Yang: The influence of light intensity and leaf movement on photosynthesis characteristics and carbon balance of soybean. *Frontiers in plant science*, *9*, (2019).

[18] L. Poorter, F. Bongers, F.J. Sterck and H. Wöll: Architecture of 53 rain forest tree species differing in adult stature and shade tolerance. *Ecology*, *84***(3)**, 602-608 (2003).

[19] L. Taiz, E. Zeiger, I.M. Møller, & A. Murphy: *Plant physiology and development* (No. Ed. 6). Sinauer Associates Incorporated (2015).

[20] N.T. Boardman: Comparative photosynthesis of sun and shade plants. *Annual review of plant physiology*, *28***(1)**, 355-377 (1977).

[21] P.D. Sharma: Ecology and Environment, 13th Edition (2018) Rastogi Publications (2018).

[22] P.R. Burkholder: The Rôle of Light in the Life of Plants. I. Light and Physiological Processes. *Botanical Review*, *2***(1)**, 1–52. http://www.jstor.org/stable/4353120 (1936).

[23] R.H. Bohning and C.A. Burnside: The effect of light intensity on rate of apparent photosynthesis in leaves of sun and shade plants. *American Journal of Botany*, 557-561 (1956).

[24] T.C. Vogelmann: Plant Tissue Optics. *Annu. Rev. Plant Physiol. Plant Mol.Bio.* **44**, 231-251 (1993).

[25] V. M. Dörken and B. Lepetit: Morpho-anatomical and physiological differences between sun and shade leaves in *Abies alba* Mill. (Pinaceae, Coniferales): a combined approach. *Plant, cell & environment*, *41***(7)**, 1683-1697 (2018).

[26] V. Paul, L. Sharma, R. Pandey and R.C. Meena: Measurements of stomatal density and stomatal index on leaf/plant surfaces. *Manual of ICAR Sponsored Training Programme for Technical Staff of ICAR Institutes on―Physiological Techniques to Analyze the Impact of Climate Change on Crop Plants*, *27* (2017).

[27] F. Yang, Y. Fan, X. Wu, Y. Cheng, Q. Liu, L. Feng and W. Yang: Auxin-to-gibberellin ratio as a signal for light intensity and quality in regulating soybean growth and matter partitioning. *Frontiers in plant science*, *9*, 56 (2018).

[28] L. Zhang, F. Chen, G. Q. Zhang, Y.Q. Zhang, S. Niu, J. S. Xiong, Z. Lin, Z.M. Cheng and Z. J. Liu:Origin and mechanism of crassulacean acid metabolism in orchids as implied by comparative transcriptomics and genomics of the carbon fixation pathway. The Plant Journal https://doi.org/10.1111/tpj.13159 (2016).

Research Article

Studies on Genetic Diversities in *Allium cepa* L. Based on Cytomorphological and Biochemical Parameters

Shreya Das[1], Sonali Dey (Sengupta)[2]* and Gargi Sengupta[3]

[1]M.Sc. in Botany, [2,3] Associate Professor, PG Department of Botany, Barasat Govt. College, Barasat, WestBengal, India
*Corresponding author email: sonalidey71@gmail.com

Abstract: Three onion (*Allium cepa* L.;Family: Alliaceae) cultivars namely red single bulb, red multi bulb and white single bulb were characterized with an objective to study intraspecific genetic diversity for further exploration of the species to produce superior plant types. Present investigation revealed that three onion cultivars varied among themselves regarding morphological (bulb characters - length, weight and equatorial diameter), cytological (cell length, cell breadth, mitotic index, nucleolar frequency and karyotype analysis) and biochemical (total protein content) parameters. Further genetic analysis has been suggested in onion including cluster analysis to study genetic interrelationship and evolutionary pattern among the cultivars.

Key Words: *Allium cepa* L., genetic diversity, selection criteria, characterization.

INTRODUCTION

Onion (*Allium cepa* L., Family: Alliaceae, 2n =16) is by far most important bulb crop throughout the world. Onion bulb is rich in carbohydrate and minerals like phosphorus, potassium and calcium [1] and is largely used in domestic as well as in pharmaceutical purposes [2, 3]. However, exploitation of onion genotypes in plant improvement program through induced mutation, polyploidy, hybridization etc. to produce superior plant types is rather meagre. Moreover, studies on onion genetics based on association of yield with yield contributing characters, character association patterns, heritability, genetic advance, genotype–environment interaction etc. is also limited. Improvement of any species depends on genetic diversity present within it. Further, genetic diversity serves as a way for a population to adapt to changing environment thereby helping the population to have a greater chance of surviving and flourishing. Genetic diversity can be evidenced from morphological, anatomical, cytological, biochemical and molecular analysis of the genotypes within a population. With a view it, present investigation has been undertaken to characterize three onion cultivars namely red single bulb, red multi bulb and white single bulb on the basis of cytomorphological and biochemical parameters aiming to further exploration of the species.

Materials and Methods

Three cultivars of *Allium cepa* L. namely red single bulb (RSB), red multi bulb (RMB)and white single bulb (WSB) were used as germ plasm sources. Mean value for each morphological parameter were determined from fifteen bulbs of each plant types. Mitotic

studies were made from root tips. Excised root tips were pretreated in saturated PDB solution for three hours at 16°C temperature. Pretreated root tips were then fixed in 1:3 acetic alcohol for overnight. The fixed root tips stained and hydrolysed in 2% aceto orcein- 1(N) HCl (9:1) solution and squashed in 45% acetic acid. Nucleolar frequency was estimated from root tip cells of the cultivars.

For karyotype analysis, photomicrographs were taken (x100) from well spread metaphase plate. Karyotype was described by Levan et al. [4]. Disparity index (DI) and total form percent(TF%) were determined as per Mohanty et al. [5] and Huziwara [6] respectively. Cell length and cell breadth were measured from peeled onion scale (x100) with the help of ocular and stage micrometer. Total protein content was estimated using the method described by Lowry et al. [7].

ANOVA was performed to know the significant variations among the cultivars. The p values less than 0.05 were considered as significant.

Result and Discussion

Present investigation showed a great variation among the cultivars regarding morphological characters (Table 1, Fig.1). Morphological studies revealed that the white bulb cultivar had a maximum bulb weight (range: 39.5gm -63.6 gm, mean 48.62 gm ± 4.43, CV- 20.42%) followed by the red single bulb (range: 22.12 gm-57.22gm, Mean 39.84 gm±5.96,CV-33.30%) and red multi bulbs (range:1.696gm-3.55gm, Mean2.52 gm±0.305,CV-27.14%). Similarly, bulb length (highest in RSB:4.76 cm± 4.74; lowest in RMB: 2.8cm±2.42) and equatorial diameter of the bulb (maximum in WSB: 5012cm±0.178; minimum in RMB: 1.22cm ±0.058) vary considerably among the cultivars.. Morphological variations may indicate that genome diversity is present among the cultivars.

Figure1. Figure showing three onion cultivars.

Epidermal cell length (highest in WSB: 192.5 μ ±5.31; lowest in RMB: 95.0 μ ±2.89) and cell breadth (maximum in RSB: 70.0 μ ±5.04; minimum in RMB: 46.9 μ ±2.61) were found to differ greatly among the cultivars (Table1). The shape of the epidermal cells (Fig.2) of these three cultivars of onion also showed a distinct variation among themselves.

RSB   RMB   WSB
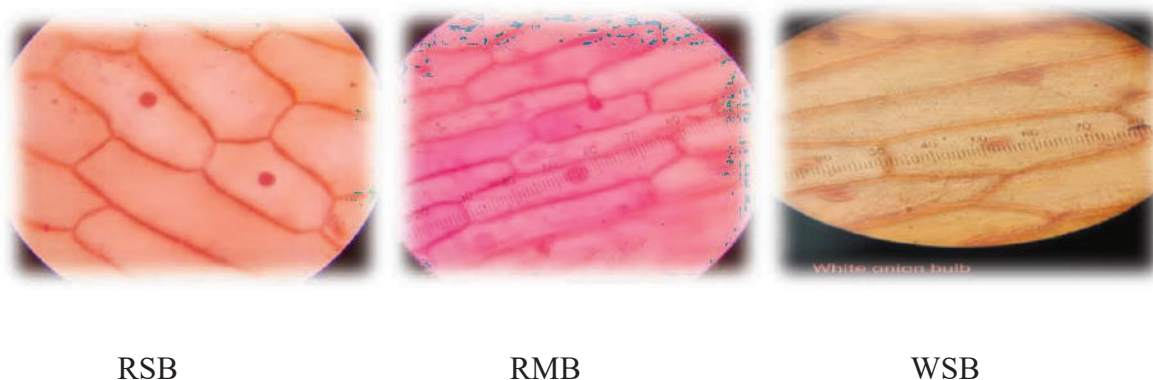
Figure2. Epidermal cell types in three onion cultivars.

Mitotic index (Table 1) did not differ significantly between red single-bulb and red multi-bulb cultivars (RSB -21.68%, RMB-21.82%) whereas the white bulb showed significantly lower mitotic index (18.64%) than the other two. The mitotic index can be considered as a biomarker of cell proliferation [8]. The increase and decrease of the mitotic index indicate cellular growth and death respectively [9]. Therefore, red bulb cultivars exhibited a higher rate of cell division. Multiple bulb formation on a single plant may be due to the higher mitotic index.

Nucleolar frequency (Table 2, fig 3) showed significant variations among the cultivars (RSB -1.71/cell, RMB -1.0/cells, WSB-1.67/cells). Red multiple bulb showed only mononucleolate cells, while red single bulb cultivar had more binucleolate cells than mononucleolate ones. On the other hand, the white bulb cultivar showed more or less equal frequencies of mononucleolate (43.76%) and binucleolate cells (46.15%). It also contains a significant amount of trinucleolate cells (10.61%). Tetra nucleate cells were noted to be present in very low frequency (0.001%) in only red single bulb cultivar (Fig.5)**.** The nucleolar analysis clearly exhibited genomic diversity among the cultivars. Nucleolar frequency is directly related to different metabolic processes like synthesis of ribosomes and proteins, storage of rRNA, regulation cell cycle, responses to stress, and growth and proliferation of cell cells.

RSB   **RMB**   **WSB**

Figure3. Root tip cells showing nucleolus in three onion cultivars.

In the present investigation, karyotype analysis showed that chromosome number was same (2n= 16) in all three cultivars, but chromosome morphology and chromosome types differed am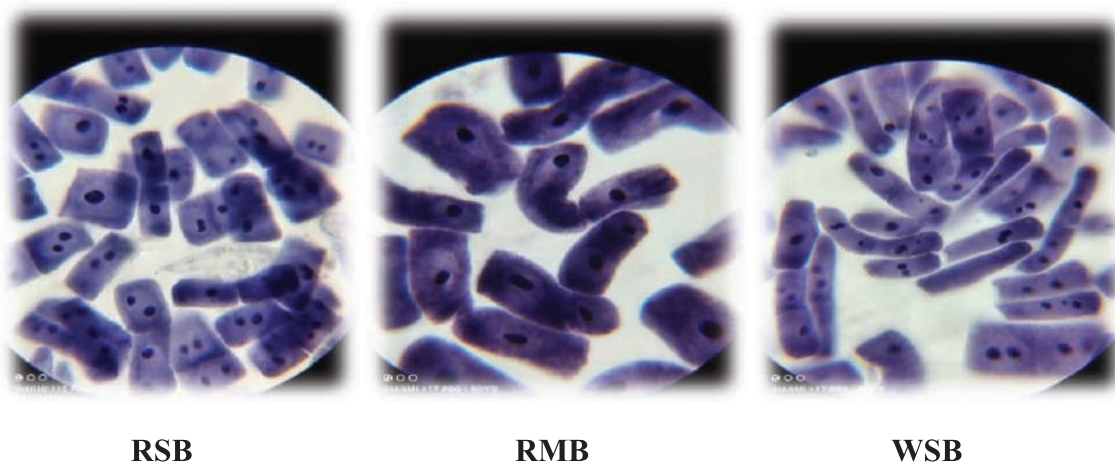ong genotypes (Table2, Fig.4). Red multi bulb had symmetrical (TF%- 41.75%) karyotype (karyotype formula: 2Lm+2L^{sc}m+6Mm+2Msm+2Sm+2Ssm) with lowest disparity index (25.01%) indicating its primitiveness. On the other hand, white bulb cultivar manifested nearly symmetrical (TF%- 38.92%) karyotype (karyotype formula: 6Lm+2L^{sc}sm+4Mm+2Mst+2Sm) with highest disparity index (36.84%) showing that white bulb is advanced among three genotypes and probably be evolved through recombination or through other plant breeding techniques. Karyotype formula of red single bulb is 2Lm+6Mm+2M^{sc}m+2Msm+2Mst+2Sm. Total and average chromosome length also varied considerably among genotypes. No chromosomal marker has been found in this investigation.

Karyotype analysis has been extensively carried out in plant phylogenetics and diversity studies for more than hundred years. The informations like chromosome number, size and morphology are considerd as valuable tools in understanding interrelationship and delimitation of taxa [10]. Comparative karyotype analysis of related species has been used to describe patterns and directions of chromosomal evolution within a group [11-16]. In onion, several karyomorphological works [17- 19] contributing to the understanding of the *Allium* biodiversity have been made.

Total protein content (Table1) also showed significant variations (RSB-10.50%, RMB- 25.88% and WSB- 7.53%) among the cultivars indicating clear genome diversity within the species.

Present study manifested intraspecific genetic diversity (among three cultivars namely red single bulb, red multi bulb and white single bulb) in *Allium cepa* L. For improvement of a genotype, studies on association of yield and yield contributing characters are necessary [20]. Thus, it is of utmost importance to ascertain selection criteria for exploration of the genotypes

to produce superior plant types and also to analyse genetic interrelationship and evolutionary pattern among the cultivars of *Allium cepa* L..

RSB   RMB   WSB
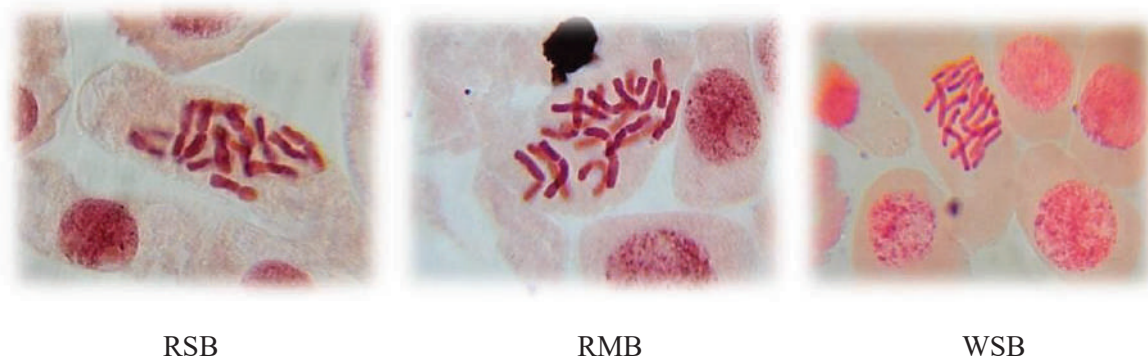
Figure4: Chromosomes of three onion cultivars

Table1. Quantitative characters in three onion cultivar

Cultivar	Morphological Parameters											Total protein content(%)
	Bulb Weight(gm)		Bulb Length(gm)		Equatorial Diameterof Bulb(cm)		Celll Length(μ)		Celll Breadth(μ)			
	$\overline{x} \pm SE$	CV(%)	$\overline{x} \pm SE$	CV (%)	$\overline{x} \pm SE$	CV (%)	$\overline{x} \pm SE$.	CV(%)	$\overline{x} \pm SE$	CV (%)		
RSB	39.84± 5.96	33.3	4.76± 0.474	22.27	3.98± 0.275	15.45	101±5.94	13.4	70±5.04	16.13		10.50
RMB	2.52± 0.305	27.14	2.8± 0.242	19.29	1.22±0.058	10.68	95±2.89	10.47	46.9±2.61	12.45		25.88
WSB	48.62± 4.43	20.42	4.1± 0.151	8.27	5.12± 0.178	7.81	192.5±5.31	6.14	63±3.84	13.62		7.53

P<0.05 for all the parameters in ANOVA test.
RSB- Red single bulb, RMB- - Red multi bulb, WSB- White bulb

Table2. Chromosomal characters in three onion cultivars

Cultivars	Total no. of cells observed	Mitotic Index(%)	Total no. of cells observed	Nucleolar frequency/cell	Chromosomal Indices			
					TCL	ACL	TF(%)	DI(%)
RSB	2697	21.68	359	1.71	19	1.188	37.89	16.67
RMB	2842	21.82	549	1.00	29.4	1.838	38.09	36.84
WSB	3195	18.64	377	1.67	24.8	1.5	38.70	26.66

RSB- Red single bulb, RMB- - Red multi bulb, WSB- White bulb TCL – Total chromosome length, ACL- Average chromosome lengthTF-Total Form Percent, DI- Disparity Index
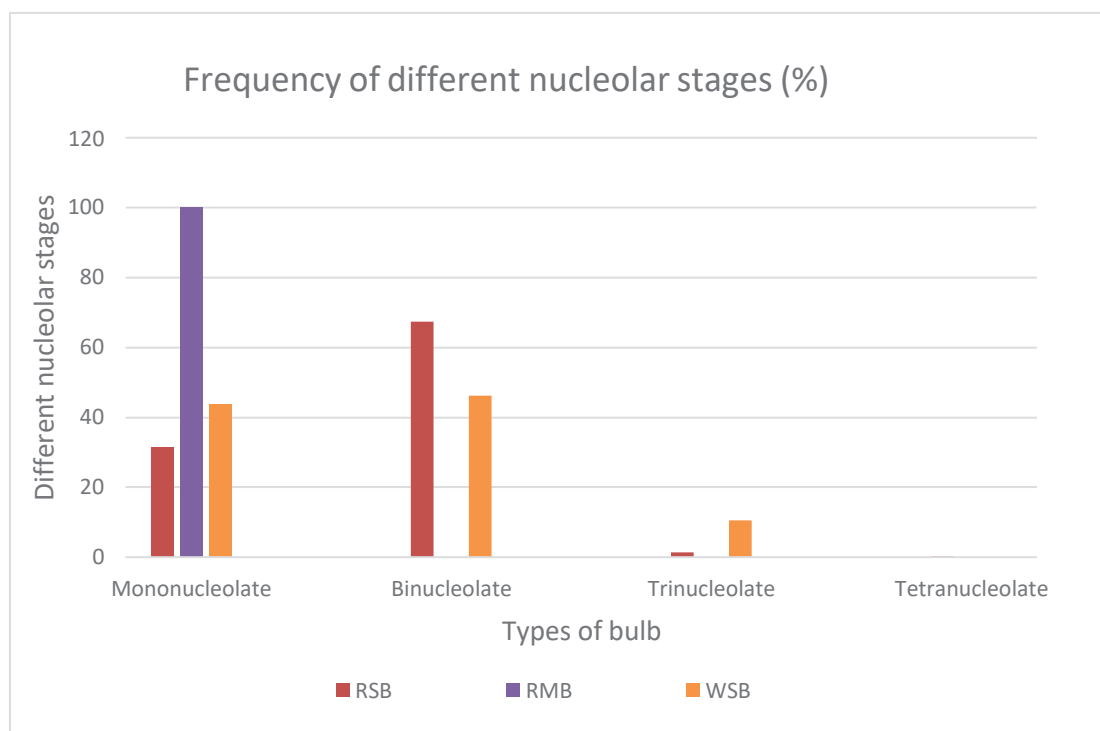
Figure5. Frequency of different nucleolar stages in the root tip cells of three onion cultivars.

References

[1] M.H. Ullah, S.M.I. HuQ, D.U. Alam and M.A. Rahman: Effects of nitrogen, phosohorus and potassium on nutrient content in onion. *Bangladesh J. of Agric. Res.*, **30(1),** 41-48.

[2] S. L. Kochhar: Economic Botany in the Tropics, published by Macmillan India Ltd., Madras, pp 233-234(1992).

[3] J. F. Dastur : Medicinal plants of India and Pakistan, published by DBT araporevala Sons & Co. Pvt. Ltd., pp14. (1977).

[4] A. Levan, K. Fredga and A. A. Sandberg: 'Nomenclature of centromeric position on Chromosomes', *Hereditus*, **52**, 201-220 (1964).

[5] B. D. Mohanty, P.D. Ghosh and S. Maity: 'Chromosomal analysis in cultured cells of Barley (*Hordeum vulgare* L.), Structural alteration in chromosomes', *Cytologia,* **56,** 191-196(1991).

[6] Y. Huziwara: 'Karyotype analysis in some genera of Compositae viii. Further studies in chromosome of Aster', *American J. of Bot.*, **49**, 116-119 (1962).

[7] O. H. Lowry, N.J. Rosebrough, A.L. Farr and R.J. Randal: 'Protein measurement with Folin phenol reagent', *J. of Biol. Chem.*, **193**, 265-275 (1957).

[8] A. Paul, A. Roy and N. Banerjee: 'Phylogenetic relationship of some species of allium l. On the basis of morphological, biochemical and cytological study'. *International Journal of Recent Scientific Research,* **10(8B)**, 34098-34103(2019).

[9] M. R. Rojas, R. L. Gilbertson, D. R. Russell and D. P. Maxwell: Use of degenerateprimers in the polymerase chain reaction to detect whitefly transmitted Gemini viruses, *Plant Disease,* **77**, 340-347(1993).

[10] N. Naruhashi and Y. Iwatsubo: Cytotaxonomic study on two putative hybrids in the genus Duchesnea (Rosaceae), *The Botanical Magazine*, Tokyo,104,137-143(1991).

[11] A. K. Sharma and A. Sharma: Recent advances in the study of chromosomal alterations with to speciation, *Bot. Rev.*, **25**, 514-544(1959).

[12] B. L. Stebbins: Chromosomal evolution in higher plants, Edward Arnold Ltd., London (1971).

[13] K. Watenabe, R.M. King, T. Yahara, M. Ito, J. Yokoyama, T. Suzuki and D. J. Crawford: '*Chromosomal cytology and evolution in Eupatorieae (Asteraceae), Annals of Mussorie Botanical Gardens',* **82**, 581-592 (1995).

[14] A. B. Das, S. Mohanty, R .H. Marrs and P. Das: '*Somatic chromosome number and karyotype diversity in fifteen species of Mammilaria of the family Cactaceae.Cytobios',* **97**, 141-151(1999).

[15] A. L .L. Vanzela, M. Luceno and M. Guerra: '*Karyotype evolution and cytotaxonomyin Brazilian species of Rhynchospora Vahl. (Cyperaceae), Botanical J. of the Linnean relation Society'*, **134**, 557-566 (2000).

[16] F. Shan, G. Yan and J.A. Plummmer: ' *Karyotype evolution in the genus Boronia (Rutaceae),' Botanical J. of the Linnean Society'*, **142,309-320 (2003).**

[17] S.Saensouk and P. Saensouk:'*Karyotype analysis of three species of Allium (Amaryllidaceae) from Thailand. Biodiversitas',* **22**, 3458-3466 (2021).

[18] R. Paknia, G. Karimzadeh and M. Khodadadi: Studies of morphological variations and path analysis in some Iranian native onion (*Allium cepa*L.) populations.Iranian J. of Agric. Sciences, **38-1(1),** 131-140 (2007).

[19] R. Paknia and G. Karimzadeh: Karyotypic study and chromosome evolution in some Iranian local onion populations. '*Journal of Plant Physiology and Breeding'*, **1(1)**, 49-62(2011).

[20] A. Hayder, N. Sharkar, B.Ahmed, M.M. Hannan, M.A. Razvy, M. Hossain, A. Hoque and R.Kamir: '*Genetic variability and interrelationship in onion(Allium cepa L.)' Middle East J. of Sci. Res.*, **2,** 132-134 (2007).

Review Article

Magnetic Interactions in azido and thiocyanato bridged Manganese complexes

Soma Nath (Deoghoria)

Assistant Professor, Department of Chemistry, Barasat Govt. College, Barasat, Kolkata-700124
Email : somadeoghoria@gmail.com

Abstract: This review describes the recent amalgamation of two long-established areas, manganese cluster chemistry and transition-metal azide (N_3^-) / thiocyanate (NCS⁻) chemistry. The combination of azide and thiocyanate in Mn chemistry has led to a variety of new polynuclear clusters, high-spin molecules. The azide and thiocyanate ligands have ability to transmit moderate or strong magnetic interactions and easily generate polynuclear system. Complexation process can be affected by ligand, molar ratio, donor strength of the ligand and type of solvent used for crystallization.

Keywords: *Manganese, ferromagnetic, antiferromagnetic, pseudohalide-bridged*

Introduction:

The combination of the organic and inorganic components allows obtaining new materials with promising applications in magnetism, molecular adsorption, luminescence and catalysis [1, 2]. The complexation process can be affected by counter anions, coexisting neutral ligands, temperature, pH, and solvents used for crystallization. In some cases, two or more complexes of different composition were obtained by manipulating the solvent, ligand–metal molar ratio. The main aim of the current review is to study magnetic interactions in complexes formed between Mn(II) ions, pseudohalide (N_3^-/ NCS⁻) and a ligand. The speciality of Mn(II) ions in the synthesis of coordination compounds results from the highest possible number of unpaired electrons for 3d metal (with spin of S = 5/2), which leads to interesting superexchange magnetic interactions [3]. On the other hand, pseudohalide ions have been proven to be versatile ligands that can bind transition metal ions in a wide variety of ways [4, 5] . They can act as monodentate ligands and as bridging ligands leading to the formation of mononuclear and polynuclear species with different dimensionality and nuclearity.

The strategy is to use potential bridging ligands, such as azide or thiocyanate having versatile binding modes and conformational flexibility in the synthesis of new Mn(II) complexes. It is well-known that the azide anion is an efficient and versatile mediator for magnetic coupling, and pseudo halide-bridging ligands were more commonly employed in

the design of poly nuclear transition-metal complexes with remarkable diversity in structure and magnetism. Magnetic coupling mediated through an pseudohalide bridge is normally ferromagnetic [6-8] for the end-on mode (μ-1,1 or EO) and antiferromagnetic for the end-to-end mode (μ-1,3 or EE) [9] . On the other hand, the appropriate choice of metal ions along with the bridging ligands is also an important factor for such works. Among the first-row transition metal ions, high-spin Mn(II) centers are quite desirable because they contain the highest possible number of unpaired electrons [10].

Coordination modes of azide (N_3^-):

In coordination complexes the azide ion has different kinds of binding modes like N-bonded terminal, *μ*-(1,3), *μ*-(1,3/1,1), *μ*-(1,1), *μ*-(1,1,1), *μ*-(1,1,3) as shown in Scheme1. Depending upon the coordination mode of the azide ion, the IR spectra of the compounds are different.

Terminal

(2020-2040 cm^{-1})

μ-(1,3)

(2030-2050 cm^{-1})

μ-(1,3/1,1)

(2040-2060 cm^{-1})

μ-(1,1)

(2045-2075 cm^{-1})
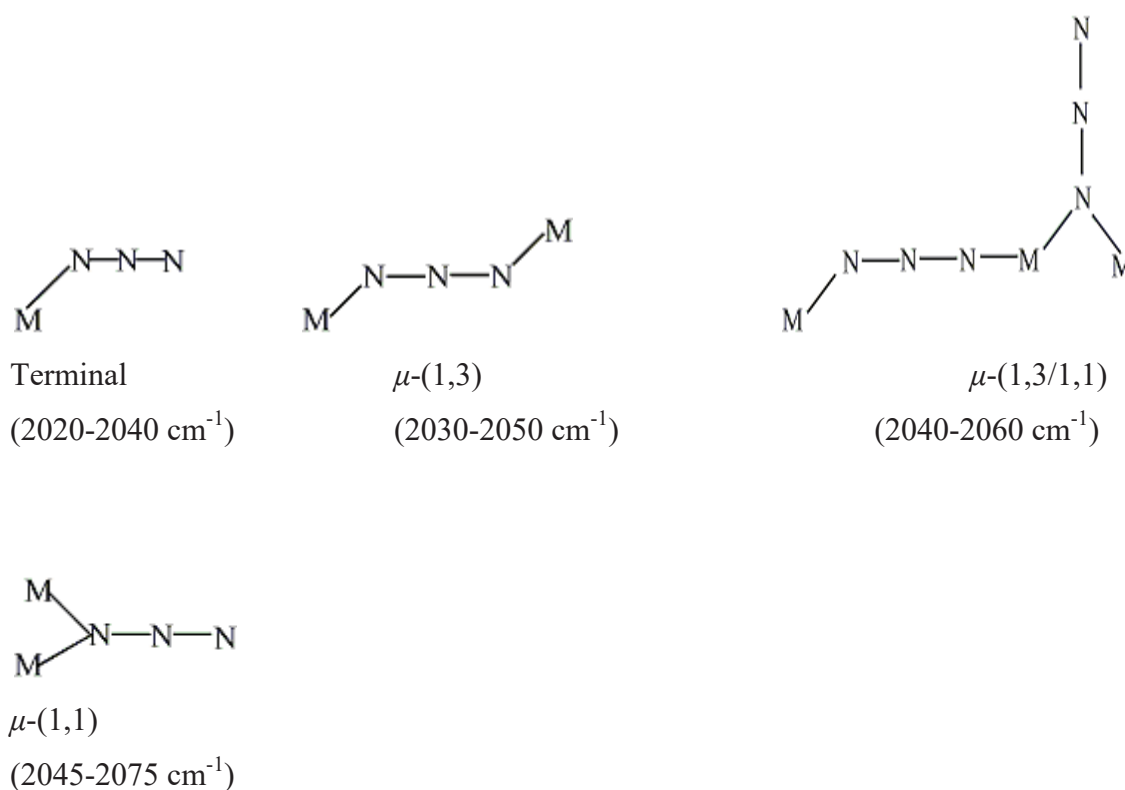
Scheme - 1

Coordination modes of thiocyanate (NCS^-): Being an ambidentate ligand thiocyanate may coordinate the metal center through the nitrogen (M-NCS) or thesulfur (M-SCN) or both (M-NCS-M). The CN stretching frequency of the N-bonded compound is nearly 2050 cm^{-1}, lower than that of S-bonded complex (nearly 2100 cm^{-1}).

N—C—S

M

N-bonded terminal

N—C—S (with M above S)

M

μ-(1,3)

S—C—N (with M below S)

M

S-bonded terminal

M (two M above N) N—C—S

M

μ-(1,1)-N bonded

M (two M above S) S—C—N

M

μ-(1,1)-S bonded
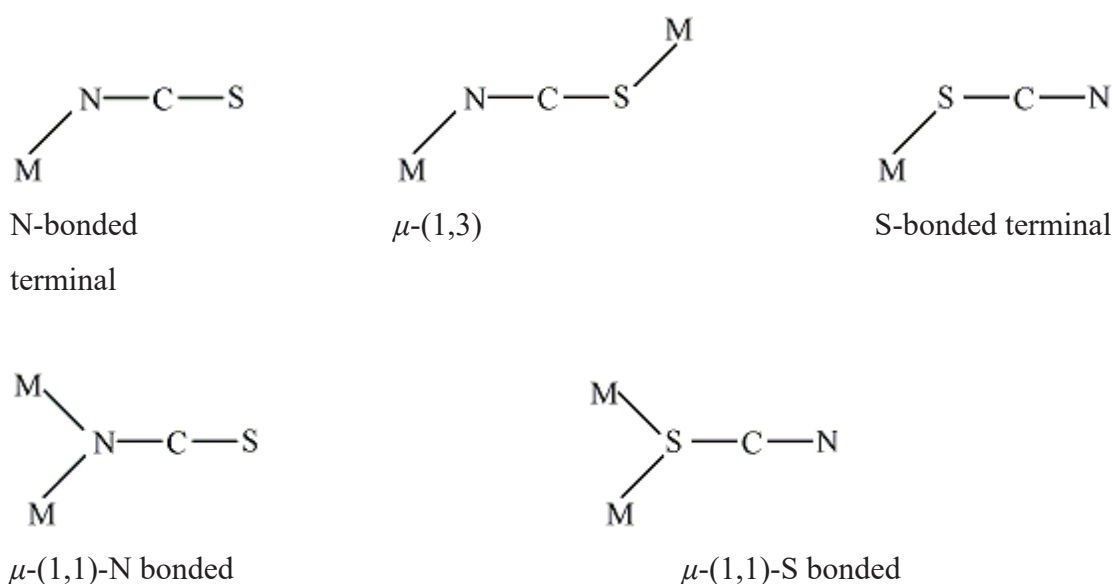
<u>**Scheme – 2**</u>

Complexes with terminal azide and μ1,3 -thiocyanato bridge

In this review, the first two complexes of azide/ thiocyanate (reported by Deoghoria et al.) and a flexible hexadentate ligand (L2) with Mn-ion [11] were described. The hexadentate ligand resulting from the bis-condensation reaction of 2-benzoylpyridine and triethylenetetramine. While $[Mn^{II}L2](ClO_4)_2$ (**1**) resulted from the reaction of L2 with manganese(II) perchlorate, the dinuclear complex $[Mn^{III}_2(L3)(N_3)_6]$ (**2**) and the 1D polymer $[Mn^{II}_2(L3)_2(NCS)_4]_n$ (**3**) resulted from the reaction of L2 and manganese(II) salts, in the presence of sodium azide for **2** or ammonium thiocyanate for **3**, respectively.

$Mn^{II}(ClO_4)_2.6H_2O \ + \ L2 \ (1:1) \ \longrightarrow \ [Mn^{II}L2](ClO_4)_2 \ (1)$

$Mn^{II}(ClO_4)_2.6H_2O \ + \ L2 \ + \ NaN_3 \ (2:1:4 \ or \ 2:1:6)$

$\downarrow$ *Aq. MeOH / Air* $\downarrow$ *Aq. CH₃CN / Air*

$[Mn^{III}_2(L3)(N_3)_6]$ (2) $[Mn^{II}L2](ClO_4)_2$ (1)
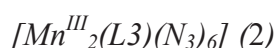
*Oxidation state of the Mn in the complex is +3 whereas in starting material it is Mn^{+2}, so oxidation occur through complexation.

$Mn^{II}(ClO_4)_2.6H_2O$ +   L2   + NH_4SCN (2 : 1 : 4 or 2 : 1 : 6)

$\downarrow$ *Aq. MeOH / Air* $\downarrow$ *Aq. CH₃CN / Air*

$[Mn^{II}L2](ClO_4)_2$ (1) $[Mn^{II}_2(L3)(NCS)_4]_n$ (3)
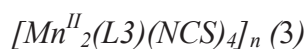
*Required solvent for complexation is methanol for complex 2 whereas acetonitrile for complex 3.

The rearrangement from L2 to L3, consisting in an alkylating cyclization centred on the two secondary amine functions of L2, occurred exclusively along the course of complexation [12].

L2

L3
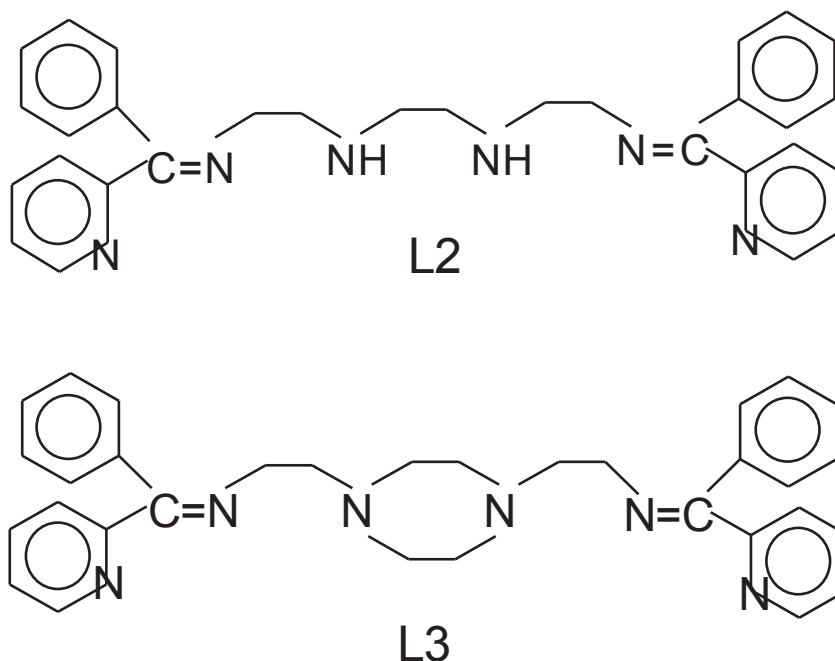
The role of the solvent with regard to the formation of compounds **2** or **3** is remarkable here. While formation of **3** only requires the L2 to L3 rearrangement, formation of **2** requires manganese **oxidation from the + 2 to the + 3 state**, in addition to the L2 to L3 rearrangement. A possible explanation is that the stronger σ donor ability of the azido anion favours oxidation of the manganese centres in the presence of methanol, allowing formation of the $[Mn^{III}_2(L3)(N_3)_6]$ (**2**) species. This oxidation may be further assisted by coordination of two extra azido ligands per dinuclear unit, yielding the neutral hexacoordinated complex **2**. On the other hand, while the weaker σ donor ability of NCS does not favour oxidation of manganese centres, the presence of the very weakly coordinating acetonitrile solvent allows bridging of manganese(II) dinuclear units into the 1D chain of **3** through $\mu_{1,3}$-NCS anions.

The IR spectrum of **2** exhibits a very strong absorption at 2040 cm^{-1} corresponding to the azido asymmetric stretching vibrations. The IR spectrum of **3** exhibits strong absorptions at 2098 and 2053 cm^{-1} corresponding to the N,S-bonded thiocyanate ions.

The molecular structure of **2** consists of isolated dinuclear units. Each manganese atom is located in a distorted octahedral (MnN$_6$) coordination environment, with three nitrogen atoms from L3 and three nitrogen donors from terminal azido groups. It is worth noting that none of the azido anions behaves as a bridging ligand.

The structure of **3** consists of [Mn$^{II}_2$(L3)(NCS)$_4$] dinuclear repeat units doubly μ1,3-NCS bridged into 1D chains. The octahedral coordination sphere around each manganese (II) consists of three nitrogen donors from L3 two nitrogen donors from thiocyanate anions from an end-to-end NCS bridge and other from a terminal NCS), and one sulfur donor from another end-to-end NCS. The MnN$_5$S coordination sphere is severely distorted from octahedral symmetry, with quite large deviations from the regular cis and trans angles.

As expected **2** has a paramagnetic behaviour. Its χ$_M$T product of 5.97 cm^{3}Kmol^{-1}, close to the spin-only value for two non-interacting S = 2 ions, is constant over the whole 300-25 K temperature range and decreases from 5.78 (25 K) to 2.44 cm^{3}Kmol^{-1} (1.95 K) due to single-ion zero field splitting (ZFS) of high-spin Mn^{III}.

The experimental χ$_M$T product of **3** smoothly decreases from 8.48 cm^{3}Kmol^{-1} at 300 K (slightly below the spin-only value for two non-interacting S = 5/2 ions) to 7.61 cm^{3}Kmol^{-1} at 80 K, and then sharply, down to 0.67 cm^{3}Kmol^{-1} at 1.96 K, clearly indicating operation of antiferromagnetic interactions in **3** mediated by the double end-to-end thiocyanate bridges between dinuclear [Mn$^{II}_2$(L3)(NCS)$_4$] repeat units along the 1D chains.

<u>Complexes with alternating Manganese azido chain</u>

Similar type of azido complex was reported [13] by Morsy et al, where both type of bridging azides (EO and EE) were present. The ligands 3-ethyl-4-methylpyridine (3-Et,4-Mepy) and azide coordinate to Mn(II) forming an alternating chain with the formula [Mn(3-Et,4-Mepy)$_2$(μ-N$_3$)$_2$]$_n$.

The IR spectrum of the complex shows a very intense split band in the region 2000-2100 cm-1, that can be assigned to the asymmetric stretching vibrations of the azide group, centered at 2056 and 2080 cm^{-1} which indicate the presence of two different symmetric and asymmetric azido groups. This was tentatively rationalized in terms of the coexistence of both EO and EE bridging azido groups, which was supported by the X-ray structural data.

The compound consists of chains of octahedrally coordinated manganese atoms alternately bridged by double end-to-end (μ-1,3) and double end-on (μ-1,1) azido bridges, which results in a structurally and magnetically alternating chain. The 3-ethyl-4-methylpyridine ligands are arranged *trans*, completing the six-fold coordination spheres of the manganese atoms.

The magnetic properties of the compound, as studied in the temperature range 300–4 K, show bulk antiferromagnetic interaction. Fitting the magnetic data for alternate Ferro (EO) and Antiferro (EE) magnetic systm for S=5/2 gives the parameters JAF = –13.7(1) cm–1, JF = 2.4(1) cm–1, This is the first case with a trans arrangement of alternate end-on and end-to-end azido bridges.

Complexes with end to end (EE) azido linkages

Another complex of this type is reported by Mohamed et al. [14] where azido linkages are all end-to-end type. Reaction of sodium azide with manganese (II) and diethylnicotinamide (DENA) leads to the two-dimensional system *trans*-[Mn(DENA)$_2$(N$_3$)$_2$]$_n$.

Structural determination shows layers of manganese atoms bridged by means of single μ-1,3- azido bridges. The polymeric structure is achieved by means of two different μ-1,3-azide bridges, one of them with Mn–N–N azido bridge has the unusual feature of quasi-linear coordination with Mn–N–N bond angles of 171.7(2)°. Manganese atoms are placed in a centrosymmetric octahedral environment. The coordination polyhedrons formed by two DENA and four azido ligands coordinated in a trans arrangement. Each azido ligand acts as a bridge to the next manganese atom in the end-to-end coordination mode, allowing a two-dimensional polymer.

Structural data proposed two different superexchange pathways one through the azido bridge, with Mn–N–N bond angles of 148.4° (J1), and a second through the azido bridge, with Mn–N–N bond angles of 171.7° (J2). Structural data suggest that two J superexchange coupling constants are required to fit the susceptibility data. Molecular orbital calculations and susceptibility data show antiferromagnetic interaction.

Complexes with end on (EO) azido linkages

Three new azide bridged dinuclear Mn(II) complexes were derived by Ray et al [10] of the type [Mn(L$_1$)(μ1,1-N$_3$)(N$_3$)]$_2$, [Mn(L$_2$)(μ1,1-N$_3$)(N$_3$)]$_2$, and [Mn(L$_3$)(μ1,1-N$_3$)(N$_3$)]$_2$ where L= pyrimidine derived primary Schiff base ligands Ln (n = 1–4), with azide as bridging ligands.

All the complexes contain Mn(II)-azido links in which the Mn(II) centres are bridged by a di-μ1,1-azido (double EO) group. The double EO bridging fragments in the complexes are similar with bridging angles (Mn–N–Mn) ranging from 102.59° to 104.81°. Magnetic property studies reveal that intramolecular ferromagnetic interactions are mediated in all the complexes through the EO azido bridges with J parameters in the range 4.3–5.12 cm^{-1}.

Complexes with μ1,3 –thiocyanato bridged polymer

Similar type of thiocyanato complexes also reported by Sailaja et al. [15] where Dimeric [Mn(salpn)NCS]$_2$ which is a ligand bridged dimer and polymeric [Mn(salpn)NCS]$_n$ are formed by the reaction of Mn(CH$_3$CO$_2$)$_2$·4H$_2$O, the schiff base (salpnH$_2$ = N,N‘-Bis(salicylidene)-1,3-diaminopropane), and thiocyanate. Each monomeric unit of the polymer is related to its adjacent ones by a 2-fold screw axis leading to a helix. From the magnetic susceptibility of the helical chain, $J = -3.2$ cm^{-1} and shows a weak ferromagnetic ordering below 7 K due to spin canting effects.

Other reported μ1,3 –azido bridged complexes with Mn(III)/Mn(II)

One dimensional chain compounds of the type [Mn(L)N$_3$] were prepared [16] where Mn exists in its +3 oxidation state, L is a Schiff base ligand and bridging of azide is μ 1,3- type. Each Mn(III) ion exhibits a characteristic Jahn-Teller elongation along the chain direction and shows antiferromagnetic interactions between Mn(III) spins within a chain are transmitted through the end to end azide ligands.

Same type of work had been done [17] where three different one dimensional polymers were prepared from different tetradentate Schiff bases and azide bridge. Here also Mn exists in +3 oxidation state and the bridging mode of azido is μ 1,3- type. Each Mn atom adopts a typical Jahn–Teller distortion. Magnetic measurements show the presence of apparent spin canting. Complexes exhibit an antiferromagnetic interaction.

A group of scientists also prepared [18] this type of interesting molecular magnets from complexation of Mn(II), EO azido bridge and simple non Schiff base ligand where bidentate doubly azido-bridged Mn(II) complexes produced, show ferromagnetic coupling.

Another Interesting recent work [19] where antiferromagnetic coupling was observed in Mn(II) complex prepared through EO cyanato bridging. This type of unusual magnetic behavior is due to big counter anion inducement and small Mn-N-Mn angle. Recently derived similar type metal complexes with anti-cancer and antimicrobial activities were also examined by a group of scientist .

Concluding remarks:

Transition metal complexes containing Schiff bases are stable and have wide applications as model compounds for the investigations of the role of polymetallic active sites in biological systems. Schiff base complexes have been reported in literature also possessing analytical, industrial, clinical, biochemical, antimicrobial, anticancer, antibacterial, antifungal and antitumor activities. Incorporation of bridging ligands to this type of Schiff base complexes have been of much interest over the last years as they have potential applications in designing new magnetic molecular materials due to different types of bridging mode and super exchange pathways.

References:

[1] O. Kahn: Molecular Magnetism, VCH, New York, **(**1993**)**.

[2] V. L. Pecoraro: Manganese Redox Enzymes, VCH, New York, (1992**)**.

[3] C. Theocharis, Stamatatos and G. Christou: Azide Groups in Higher Oxidation State Manganese Cluster Chemistry: From Structural Aesthetics to Single-Molecule Magnets *Inorg. Chem.*, *48 (8)*, 3308–3322, (2009)

[4] K. Vrieze ; G. Van Koten; : Comprehensive Coordination Chemistry, G. Wilkinson, R. D. Gillard and J. A. Mcleverty", Eds., *Pergamon Press, Oxford, England,* **2**, 225, (1987**)**.

[5] J. Ribas ; A. Escuer ; M. Monfort ; R. Vicente ; R. Cortes ; L. Lezama ; T. Rojo: Polynuclear Ni^{II} and Mn^{II} azido bridging complexes. Structural trends and magnetic behavior *Coord. Chem. Rev.*, **193-195**, 1027-1068, **(**1999**)**.

[6] E. Ruiz ; J. Cano, S. Alvarej ; P.Alemany: Magnetic coupling in end-on azido bridged transition metal complexes:A density functional study *J. Am. Chem. Soc.*, **120**, 11122-11129, (1998).

[7] M. F. Charlot ; O. Kahn ; M. Chaillet ; C. Larrieu: Interaction between copper(II) ions through the azido bridge: concept of spin polarization and ab initio calculations on model systems *J. Am. Chem. Soc.*, *108*, 2574-2581, **(**1986**)**.

[8] J. M. Clemente-Juan ; C. Mackiewicz ; M. Verelst ; A. Bousseksou ; F. Dahan ; J. –P. Tuchagues: Synthesis, Structure, and Magnetic Properties of Tetranuclear Cubane-like and Chain-like Iron(II) Complexes Based on the N_4O Pentadentate Dinucleating Ligand 1,5-Bis[(2-pyridylmethyl)amino]pentan-3-ol *Inorg. Chem.,* **41**, 1478-1491, (2002**)**.

[9] F. F. de Biani ; E. Ruiz ; J. Cano ; J. J. Novoa ; S. Alvarej: Magnetic Coupling in End-to-End Azido-Bridged Copper and Nickel Binuclear Complexes: A Theoretical Study *Inorg. Chem.*, **39**, 3221-3229, **(2000).**

[10] S. Ray, S. Konar, A. Jana, A. Dhara, K. Das, S. Chatterjee, M. S. El Fallah, J. Ribas, S. K. Kar: Five new pseudohalide bridged Mn(II) complexes of pyrimidine derived Schiff base ligands: Synthesis, crystal structures and magnetic properties *Polyhedron*, **68** , 212–221, **(2014).**

[11] S. Deoghoria, S. K. Bera, B. Moulton, M. J. Zaworotko, J. –P. Tuchagues, G. Mostafa, T. -H Lu, S. K. Chandra: Synthesis, crystal structure, and magnetic properties of binuclear Mn^{III}-azido and 1D polymeric Mn^{II}-$\mu_{1,3}$-thiocyanato novel species based on a neutral hexadentate Schiff base *Polyhedron*, **24**, 343-350, **(2005).**

[12] S. Deoghoria, S. Sain, M. Soler, W.T Wong, G. Christou, S. K. Bera, S. K. Chandra: Synthesis, crystal structure and magnetic properties of a new ferromagnetic nickel(II) dimer derived from a hexadentate Schiff base ligand *Polyhedron*, **22**, 257-262, **(2003).**

[13] A. M. Morsy, A. Youssef, A. Escuer, A. Mohamed, S. Goher, F. A. Mautner, R. Vicente : Structural Characterization and Magnetic Behaviour of the Ferro-Antiferromagnetic Alternating Manganese–Azido Chain [Mn(3-Et,4-Mepy)2(ì-N3)2]*n* (3-Et,4-Mepy 5 3-Ethyl-4-methylpyridine) *Eur. J. Inorg. Chem.*, 687-691,(1999**).**

[14] A. Mohamed, S. Goher, A. M. Morsy, A. Youssef, A. Franz, Mautner, R. Vicente , A. Escuer: Superexchange Interactions through Quasi-Linear End-to-End Azido Bridges:Structural and Magnetic Characterisation of a New Two-Dimensional Manganese–Azido System [Mn(DENA)$_2$(N$_3$)$_2$]*n* (DENA= 5- diethylnicotinamide) *Eur. J. Inorg. Chem.,* 1819-1823,**(2000).**

[15] S. Sailaja , K. Rajender Reddy , M. V. Rajasekharan , C. Hureau , E. Rivière , J. Cano , and J.-J. Girerd :Synthesis, Structure, and Magnetic Properties of [Mn^{III}(salpn)NCS]*n*, a Helical Polymer, and the Dimer [Mn^{III}(salpn)NCS]$_2$. Weak Ferromagnetism in Mn^{III}(salpn)NCS]*n* to the Strong Magnetic Anisotropy in Jahn−Teller Mn(III) (salpnH$_2$ = *N,N*'-Bis(salicylidene)-1,3-diaminopropane) *Inorg. Chem.*, **42 (1***)*, 180–186, **(2003).**

[16] J.H. Song; K.S.Lim; D.W. Ryu; S.W.Yoon; B.J. Suh; C.S.Hong: Synthesis, structures, and magnetic properties of end-to-end azide-bridged manganese(III) chains: Elucidation of direct magnetostructural correlation, *Inorganic Chemistry,***53**, 7936-7940 (2014).

[17] J.H. Yoon; W.R. Lee; D.W. Ryu; J. W. Lee; S. W. Yoon; B. J. Suh; H. C. Kim; C. S. Hong: End-to-End Azide-Bridged Manganese(III) Chain Compounds: Field-Induced Magnetic Phase Transitions and Variation of T_C to 38 K Depending on the Side Groups of the Schiff Bases, *Inorg. Chem*, **50(21),** 10777-10785 (2011).

[18] Z. Zhang, L. Zhang, Z. Ni,: Synthesis, crystal structures, and magnetic properties of a series of double end-on-azido-bridged dinuclear manganese(II) complexes, *Trans. Met. Chem,* **39(5),** 527-534, (2014).

[19] D. Yang, Z. Zhang, L. Zhang: Two double end-on cyanato-bridged dinuclear manganese (II) complexes exhibiting abnormal magnetic coupling for the Mn(II)-N-Mn(II) linkage, *Trans. Met. Chem.*, **40 (7),** 749-754, (2015).

Agricultural Wages and Crop Prices in India: A Cointegrated Relationship

Rajnarayan Gupta

Associate Professor, Department of Economics, Barasat Government College, Barasat, North 24 Pgs, West Bengal, 713124, Email: rajngupta75@yahoo.co.in

Abstract: Labour is an important input in agriculture and for that matter wage bill is a major constituent of cost of production in the agricultural sector. The increased wage rate may be a reason for the upward movement in the prices of agricultural crops. The causality goes the other way round. The hike in the prices of crops also causes wage escalation. The present study examines this relationship. The standard time series techniques, e.g., ADF test and cointegration have been used for that purpose. The study period ranges from July, 1999 to June,2013.The study finds a cointegrated relationship between wages and prices in the agricultural sector.

Keywords : Agricultural wages, Crop prices, ADF, Cointegration.

Introduction

The movement in the level of prices is always a sensitive issue in an economy. Inflation adversely affects the living condition of the people in general and poor in particular. The prices of consumer goods are more important in this context, most of which are agricultural products. Thus price fluctuations of agricultural crops–mainly upward movements, intervene with the living standard of the people. The movements of agricultural prices are, therefore, a cause for concern. The present study addresses this issue and tries to identify the underlying factors.

The price rise in agricultural commodities is due to a combination of two types of factors viz.,cost-push and demand-pull. Cost-push factors include cost of labour,cost of fertiliser, cost of irrigation etc. Increasing diversion of food consumption from human being to animal and poultry use or, in other words, for non-food use, changes in consumption pattern, population growth and most important, the increase in the level of wages are some of the significant demand-pull factors. The present study concentrates on the wage level and examines its capacity to influence the prices of agricultural goods.

Wage level affect price level in two ways, both as a supply side factor and as a demand side factor. On the supply side, it is an important determinant of cost of production. But, at the same time, it also determines demand. Any hike in the level of wages increases the purchasing power of the people and thus has obvious effect on the level of demand in the economy.

While wages affect prices, prices also affect wages. Thus, the causality goes the other way round. Workers always need protection against inflation. Thus, whenever there is price escalation in the economy, wages are also likely to increase, although it depends to a great extent on the strength of workers' union. The causality from prices to wages is more applicable to agricultural goods which constitute what are called wage goods.

On the basis of the above theoretical underpinning which suggests two-way causality between agricultural prices and wages, the present study attempts to measure the degree of association between them. The study contains six sections. Second section reviews the existing literatures on the relationship between agricultural wage rate and agricultural prices in India. Third describes the trend of agricultural wage rate and agricultural prices in India. In the agricultural sector, wage bill seems to be a commendable part of crop prices. For that reason, the relationship between wage rate and agricultural prices has been considered in the study. The methodology and data sources are explained in next section. Fifth Section presents and analyses the empirical findings and finally the study is concluded inprecise way at the end.

Review of the Literature

The relationship between agricultural wages and prices has been investigated by various studies. A Narayanmoorthy (2007) [1] mentioned that the cost of cultivation of crops has been increasing over the years because of increase in the wage rate, input prices and othermanagerial costs. In this regard,the author finds that it is wage cost that determines the cost of agricultural production. For that reason, movements in agricultural wage rate should mostly cause fluctuation in agricultural prices.

M Raghavan (2008) [2] discusses the wage of machine labour and identified somereasons behind the upward trend of wage rate.He mentions that wage of machine labour reaches above 23 per cent of the operational cost in 2004-05 in India. The widespread mechanization of almost all farming operations (like ploughing, irrigating, weeding, harvesting and threshing), according to the author, significantly affects agricultural production cost, and consequently, crop prices.

Atulan Guha, Ashutosh Kr Tripathi (2014) [3] explores the link between food price inflation and rising rural real wages. They mention that the bargaining power of workers increased due to public works programmes and this induced them to bargain for more wages because of food priceinflation. The increase in agricultural wages has been pushing up food prices primarily through raising the cost of production. According to the authors the increase in the rural real wage has adverse effect on rising food inflation, influences the living standard of rural unskilled and agricultural workers who constitute a large majorityof the population.

Ashima Goyal and Akash Kumar Baikar (2014) [4] investigate the causes of wage fluctuation for rural unskilled male labourers in India, and examine their impact on inflation. They point out that the impact of wages on rural food prices is not so large, since some supply shocks impacted food prices, and special circumstances drove the unusual rise in real wages and large nominal wage growth may not persist if food inflation and the fiscal deficit moderate.

Yash P. Mehra (1993) [5] investigates relationship between movements in labor costs and price level in the short run. The author concludes that consumer prices and unit labor costs are Granger-causal in both directions and it is also consistentwith the presence of Granger-causality running one way from consumer pricesto wages.

Kenneth M. Emery and Chih-Ping Chang (1996) **[6]** examine the impact of labour costs on consumer prices and also investigate whether the relationship is stable over time during the post-1980 period in the United States. Both consumer prices for all items (CPI)

and consumer prices excluding food and energy (CPIC) and unit labour costs for the non-farm business sectorare considered in the article. They concluded that the causal effect of wage growth on inflation depends on the choice of the price series. For CPIC, wage growth is significant at the 1-percent level, implying causality.However, for CPI, wage growth is not significant, implying no causality. The results also show that inflation always Granger-causeswage growth, regardless of the choice of the price series.

Wage Level and Agricultural Prices in India

In India, there is no uniform and proper wage policy for all sectors. In the economy, a mechanism has been practiced for wage determination in the Organized and Unorganized sectors. Wages in the organized sectors are determined through negotiations and settlements between the employer and employees. But in the unorganized sector the negotiation is not made properly. Due to illiteracy and lack of effective bargaining power, labourers have been exploited in this sector. The government intervention improves wage rate in the unorganized sector. As a result, increasing trend of wage may affect the agricultural price movement significantly.

There are three types of labour –men, women and children. Among these, male workers are largely associated with the agricultural work. In many states women and children come to this field as part time workers in India. Naturally, female workers would not be a bigger part in respect of overall rural labour. And it is seen that women and children are considered as casual section of labour and they enjoy comparatively much low wage. For that reason the present study mainly concentrates on the male wage and examines the relation between male wage and agricultural prices.

The upward trend in the male wage raises a question whether it is the reason behind the increase in the prices of agricultural goods over time. The conjecture appears sensible with the fact that male wage is a necessary and important input in the farm sector. Male wage is a significant cost component in agriculture.

For crops like maize, bajra or jowar, agricultural wage constitutes more than 50% of the total cost of production. Figure 1 depicts the trend of male wage and agricultural prices for the period from July'99 to June'09.
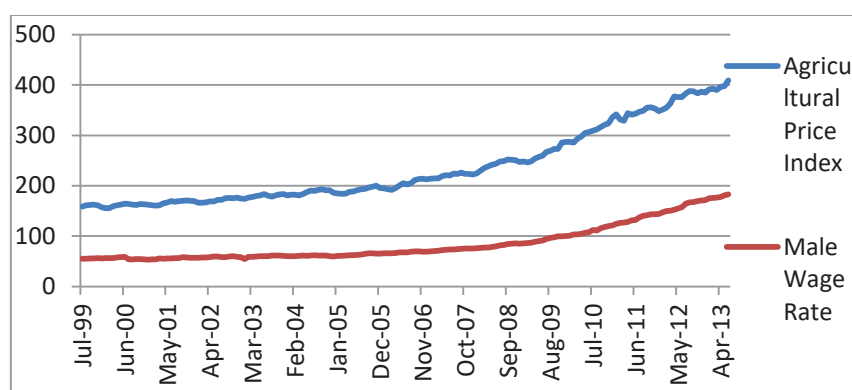
Source: (1) Office of the Economic Adviser, Ministry of Commerce and Industry, Government of India,New Delhi (2) Wage Rates in Rural India, Government of India, Ministry of Labour& Employment, Labour Bureau, Shimla /Chandigarh

Figure 1: Male Wage Rate and Agricultural Price Index in India
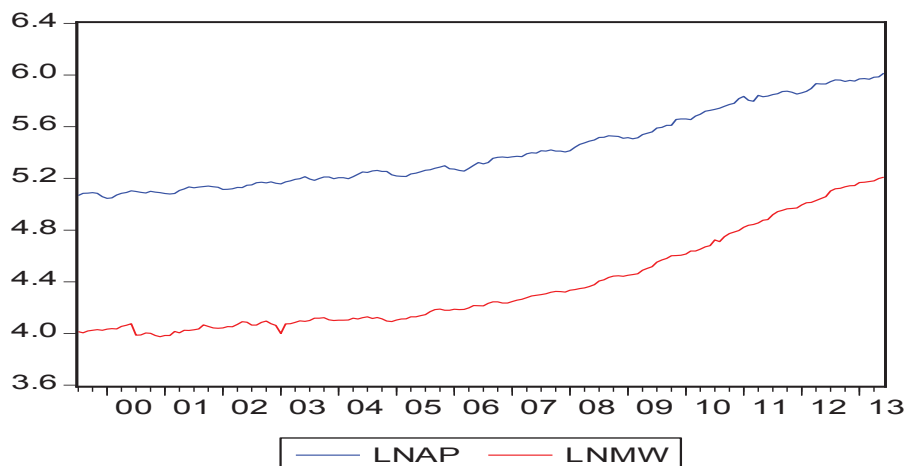
Figure 2: Agricultural Prices (AP) and Agricultural wage for Men (MW)

Table 1: Percentage of wage cost to total production cost for major crops in India

Year	Rice	Maize	Bajra	Jowar	Cotton	Rapeseed	Groundnut	Wheat	Pulses	Sugarcane
1997-98	44.7	54.9	54.6	53.7	40.3	40.2	40.9	34.5	33.5	37.4
1998-99	45.5	52.1	55.4	52.5	45.0	40.5	41.3	33.6	36.3	36.8
1999-00	44.7	46.5	54.3	52.1	41.9	34.1	43.3	32.1	35.0	35.1
2000-01	46.2	47.5	55.9	52.0	41.0	41.0	44.1	33.7	34.3	45.3
2001-02	44.8	52.4	59.7	55.0	45.3	41.1	46.7	36.1	35.0	37.1
2002-03	46.2	50.1	55.7	53.0	41.6	41.0	43.3	35.0	35.6	37.4
2003-04	46.4	56.0	57.8	50.9	38.9	43.3	40.3	35.6	35.2	37.3
2004-05	46.0	54.1	56.2	54.0	40.4	53.1	42.6	55.9	34.6	32.9
2005-06	46.2	47.3	52.8	55.3	46.2	40.4	43.1	38.5	34.5	34.7
2006-07	47.1	47.2	52.6	54.7	40.8	41.1	42.3	34.0	31.4	38.8
Average	45.8	50.8	55.5	53.3	41.9	41.6	42.8	36.9	34.5	37.3

Source: Computed from Reports of the Commission for Agricultural Cost and Price, Department of Agriculture and Cooperation, Ministry of Agriculture, Government of India, New Delhi

Methodology and Data Sources

The present study makes an alternative investigation into the relationship between agricultural prices and wages for the Indian economy. For empirical study, male wage rate has been taken to be the representative wage rate for the agricultural sector. The study starts with checking the 'trend' and 'seasonality' of the series of 'Agricultural price Index (AP)' and 'Rural Male Wage (MW)'. ADF (Augmented Dickey Fuller) test is used for testing stationarity of both the series. The long run relationship between AP and MW has been investigated with cointegration test. The work has been carried out with monthly data on both the variables.

Data on male wage have been collected from 'Wage Rates in Rural India' published by NSSO and Labour Bureau. However, NSSO does not provide data on male wage on monthly basis. For that reason the data on male wage (MW) for eleven agricultural occupations have been collected and the average male wage (Ploughing, Sowing, Weeding, Transplanting, Harvesting, Winnowing, Threshing, Picking, Herdsman, Well Digging, Cane Crushing) has been computed from that. Similarly, monthly data on agricultural price index are also not available. Therefore, for the empirical investigation, the present study has considered data on wholesale price index of primary articles from the various publications of OEA (Office of the Economic Adviser), Ministry of Commerce and Industry, Government of India. The range of study period is from July 1999 to June 2013.

Empirical Findings

For investigating into the causal relationship between AP and MW, the series AP and MW have been transformed into logarithm of AP and MW i.e. lnAP and lnMW respectively. The graphs of lnAP and lnMW (Figure 2) seem to be "trending" upward, albeit with fluctuations. The empirical results also show that the time series of lnAP and lnMW have trend. Then the detrending procedure has been used for separating the trend from the series and taking the residual values for lnAP and lnMW as dlnAP and dlnMW respectively. The results of seasonality test for AP and MW (Table 3 and Table 4 respectively) show that there is no seasonality in the series of dlnAP and dlnMW, since all the values of probability are insignificant.

For examining stationarity of dlnAP and dlnMW, ADF test has been used. The results of the tests (Table 5) confirm that both series are non-stationary. However, both series appear stationary at first difference. Then cointegration test has been carried out for examining long run relationship between dlnAP and dlnMW and the results of the test are presented in Table 6. Results suggest that we should reject the null hypothesis of no cointegration at 5% level of significance since the corresponding p-value is 0.0011. Therefore, we conclude that there exists a strong causal relationship between dlnAP and dlnMW.

Table 2: Test for trend in the series lnAP and lnMW

Dependent Variable	Coefficient of the Trend Variable	R²	t-statistics	Probability
lnAP @trend	0.0450	-70.7558	25.1750	0.0000
lnMW @trend	0.0409	-25.9224	26.8065	0.0000

Table 3: Test for seasonality indlnAP

Variable	Coefficient	Standard Error	t-Statistic	Probability
C	-0.0068	0.0207	-0.3307	0.7413
@SEAS(1)	-0.0046	0.0293	-0.1583	0.8744
@SEAS(2)	-0.0099	0.0293	-0.3387	0.7353
@SEAS(3)	-0.0094	0.0293	-0.3219	0.7479
@SEAS(4)	0.0049	0.0293	0.1683	0.8665
@SEAS(5)	0.0074	0.0293	0.2541	0.7997
@SEAS(6)	0.0138	0.0293	0.4709	0.6383
@SEAS(7)	0.0156	0.0293	0.5336	0.5943
@SEAS(8)	0.0156	0.0293	0.5324	0.5952
@SEAS(9)	0.0193	0.0293	0.6582	0.5114
@SEAS(10)	0.0156	0.0293	0.5345	0.5938
@SEAS(11)	0.0140	0.0293	0.4775	0.6337

Table 4: Test for seasonality indlnMW

Variable	Coefficient	Standard Error	t-Statistic	Probability
C	0.5630	0.0989	5.6913	5.6913
@SEAS(1)	0.0064	0.1399	0.0455	0.0455
@SEAS(2)	0.0185	0.1399	0.1322	0.1322
@SEAS(3)	0.0233	0.1399	0.1666	0.1666
@SEAS(4)	0.0353	0.1399	0.2522	0.2522
@SEAS(5)	0.0480	0.1399	0.3434	0.3434
@SEAS(6)	0.0546	0.1399	0.3903	0.3903
@SEAS(7)	-0.0207	0.1399	-0.1477	-0.1477
@SEAS(8)	-0.0132	0.1399	-0.0946	-0.0946
@SEAS(9)	0.0016	0.1399	0.0113	0.0113
@SEAS(10)	0.0075	0.1399	0.0533	0.0533
@SEAS(11)	0.0021	0.1399	0.0153	0.0153

Table 5: ADF Test Results

Dependent Variable	Constant	Coefficient of the Trend Variable	Coefficient of the Lagged Term	Number of Lagged Difference Terms	R^2	ADF
dlnAP	-	-	-0.0214 (-1.6237)	1	0.0370	-1.6237
ΔdlnAP	-	-	0.8513 (-10.9781)	1	0.4221	-10.978*
dlnMW	-	-	0.0123 (7.5789)	1	0.0802	7.5789
ΔdlnMW	-	-	-0.6773 (-6.7875)	1	0.4409	-6.7875*

Note: The values in parentheses show the respective t-values
Δ – First difference
* Significant at 1% level

Table 6: Test for Cointegration

Hypothesized No. of CE(s)	Eigenvalue	Trace Statistic	0.05 Critical Value	Prob.**
None*	0.2176	44.7594	13.3109	0.0011
At most 1	0.0134	1.7102	5.1289	0.1121

Trace test indicates 1 cointegratingeqn(s) at the 0.05 level
 * denotes rejection of the hypothesis at the 0.05 level

Max-eigenvalue test indicates 1 cointegrating eqn(s) at the 0.05 level
* denotes rejection of the hypothesis at the 0.05 level
**MacKinnon-Haug-Michelis (1999) p-values
Note: Lags interval (in first differences): 1 to 2

Conclusion:

Wages and prices are highly interrelated in the agricultural sector. In India, wage rate, and particularly, the male wage in the agricultural sector, exhibits a sharp upward trend and so also the prices of agricultural crops. The present study investigates into the relationship between these two variables and finds a permanent and strong association between them. However, the two-way relationship between agricultural wages and prices has serious implications for the economy. Any factor that raises wages stimulates prices as well and the vice versa. And once the wage-price spiral sets in it continues till exogenous forces dampen either of the two variables.

References:

[1] A. Narayanamoorthy: 'Deceleration in Agricultural Growth: Technology Fatigue or Policy Fatigue?', *Economic & Political Weekly*, June 23, pp 2375-79(2007).

[2] M. Raghavan: 'Changing Pattern of Input Use and Cost of Cultivation', *Economic and Political Weekly*, June 28, 2008, pp.123-129(2008).

[3] A. Guha, and A. K. Tripathi: 'Link between Food Price Inflation and Rural Wage Dynamics', *Economic and Political Weekly*, VOL XLIX, Number 26 & 27, pp-66-73(2014).

[4] A. Goyal, and A. K. Baikar: 'Psychology, cyclicality or social programs: Rural wage and inflation dynamics in India', *Indira Gandhi Institute of Development Research*, Mumbai April 2014,WP-2014-014, Available at http://www.igidr.ac.in/pdf/publication/WP-2014-014.pdf (2014).

[5] Y. P. Mehra: 'Unit Labor Costs and the Price Level', *Federal Reserve Bank of Richmond Economic Quarterly Volume 79/4*(1993).

Assessing Sediment Textural Analysis and Basic Nutrients in the Indian Sundarban: Insights from Field Investigations

Arpan Roy Chowdhury[1] Swapan Paul[2] Chandan Surabhi Das[3]

[1]PG student, Department of Geography, West Bengal State University, West Bengal, India, arpan23rc@gmail.com
[2]Research Scholar, Department of Geography, West Bengal State University, West Bengal, India, spaul5481@gmail.com.
[3]Associate Professor in Geography, Barasat Government College, West Bengal, India. yenisi2002@gmail.com

Abstract: The Indian Sundarban, a vital ecological hotspot, faces increasing anthropogenic pressures, warranting comprehensive assessments of sediment properties and nutrient dynamics. This study presents findings from field investigations aimed at interpreting sediment textural analysis and basic nutrient distribution across a selected transect of Sundarban region. Utilizing surface samples, textural analyses revealed a predominance of fine-grained sediments, indicative of depositional environments influenced by tidal dynamics. Result reveals that potassium exhibits the highest concentration among the measured nutrients, ranging from 80 to 160 kg/ha. Phosphorus follows with a concentration ranging between 18 and 32 kg/ha, and nitrogen with 8 to 20 kg/ha. The organic carbon content varies from 0.2% at the riverfront to approximately 0.80% in the intermediate zone of the mudflats. The spatial distribution of each nutrient reveals higher concentrations in the intermediate zone of the forest floor compared to both the riverfront and the interior areas. This phenomenon can be attributed to the higher litter production and the protective nature of this zone, leading to enhanced trapping of nutrients. Such findings underscore the intricate interplay between ecological processes and sediment nutrient dynamics within the Sundarban ecosystem.

Keywords: Nutrient dynamics; Sediment texture; Mangrove, Mudflat, Sundarban

Introduction

The Sundarban, a UNESCO World Heritage Site, is the largest tidal halophytic mangrove forest in the world, spreading across the delta of the Ganges, Brahmaputra, and Meghna rivers in the Bay of Bengal [1-2]. It is renowned for its unique biodiversity and ecological significance, serving as a crucial habitat for numerous species, including the iconic Royal Bengal Tiger (Panthera tigris tigris) [3]. However, this fragile ecosystem faces numerous threats, including climate change, habitat degradation, and anthropogenic activities. One critical aspect of the Sundarban's ecosystem health is the sediment composition and nutrient dynamics within its waterways [4-6]. Sediment texture, defined by the distribution of particle sizes, plays a fundamental role in shaping the physical and

chemical characteristics of aquatic environments. Moreover, nutrient availability in sediments is a key factor influencing primary productivity and supporting the diverse array of flora and fauna that inhabit the region [7-11].

Understanding sediment textural analysis involves determining the size distribution of sediment particles, including sand, silt, and clay fractions [12]. The composition and distribution of these particles influence sediment stability, erosion susceptibility, and habitat suitability for benthic organisms. Additionally, sediment texture affects nutrient retention and release, with finer particles typically exhibiting higher nutrient retention capacities due to their larger surface area. In tandem with sediment textural analysis, assessing basic nutrient concentrations in sediments is essential for understanding nutrient cycling and ecosystem productivity in the Sundarban [13]. Nutrients such as nitrogen (N), phosphorus (P), and potassium (K) play pivotal roles in regulating primary production and supporting the growth of mangrove vegetation, phytoplankton, and benthic organisms. Furthermore, excessive nutrient inputs can lead to eutrophication, altering ecosystem dynamics and threatening biodiversity [14-15].

Previous research on the Sundarban has predominantly focused on biodiversity assessments, conservation strategies, and the impacts of climate change on this unique ecosystem [19-24]. While these studies have shed light on various facets of the Sundarban's ecology, there remains a conspicuous gap in our understanding of sediment textural analysis and nutrient distributions within its waterways. Few studies have delved into the intricacies of sediment composition and nutrient dynamics, leaving a significant knowledge deficit regarding these critical aspects of the Sundarban's functioning.

Against this backdrop, the primary objective of this study is to conduct comprehensive field investigations aimed at assessing sediment textural analysis and basic nutrient concentrations in a selected stretch of Indian Sundarban.

Material and methods

1. Study area

The active deltaic portion of Indian Sundarban (4260 km^2) is located between Hugli River in the west, Hariabhanga river in the east, Bay of Bengal in the south, and the Dampier-Hodges line in the north, extending from 21°33′51″N and 88°10′13″ E to 22°9′23″N and 89°5′56″ E. The Indian Sundarban is divided into three parts based on restrictions to enter the forest: namely core, buffer, and transition zone. These comprise nineteen

community development blocks under the jurisdiction of North 24 Parganas (6 blocks) and South 24 Parganas district (13 blocks) from its northern to southern end. This biosphere is a meso-tidal (tidal range of 2–4 m), a low-lying coastal region where the maximum elevation is less than 5 m above the mean sea level (amsl) (Payo et al. 2016) with about 70% of the area is under 1 m amsl.

Within this entire setup, A single transect was chosen within the expanse of a mangrove-dominated mudflat zone, situated along the midsection of the Thakuran River, to facilitate various sampling endeavours (Fig. 1).
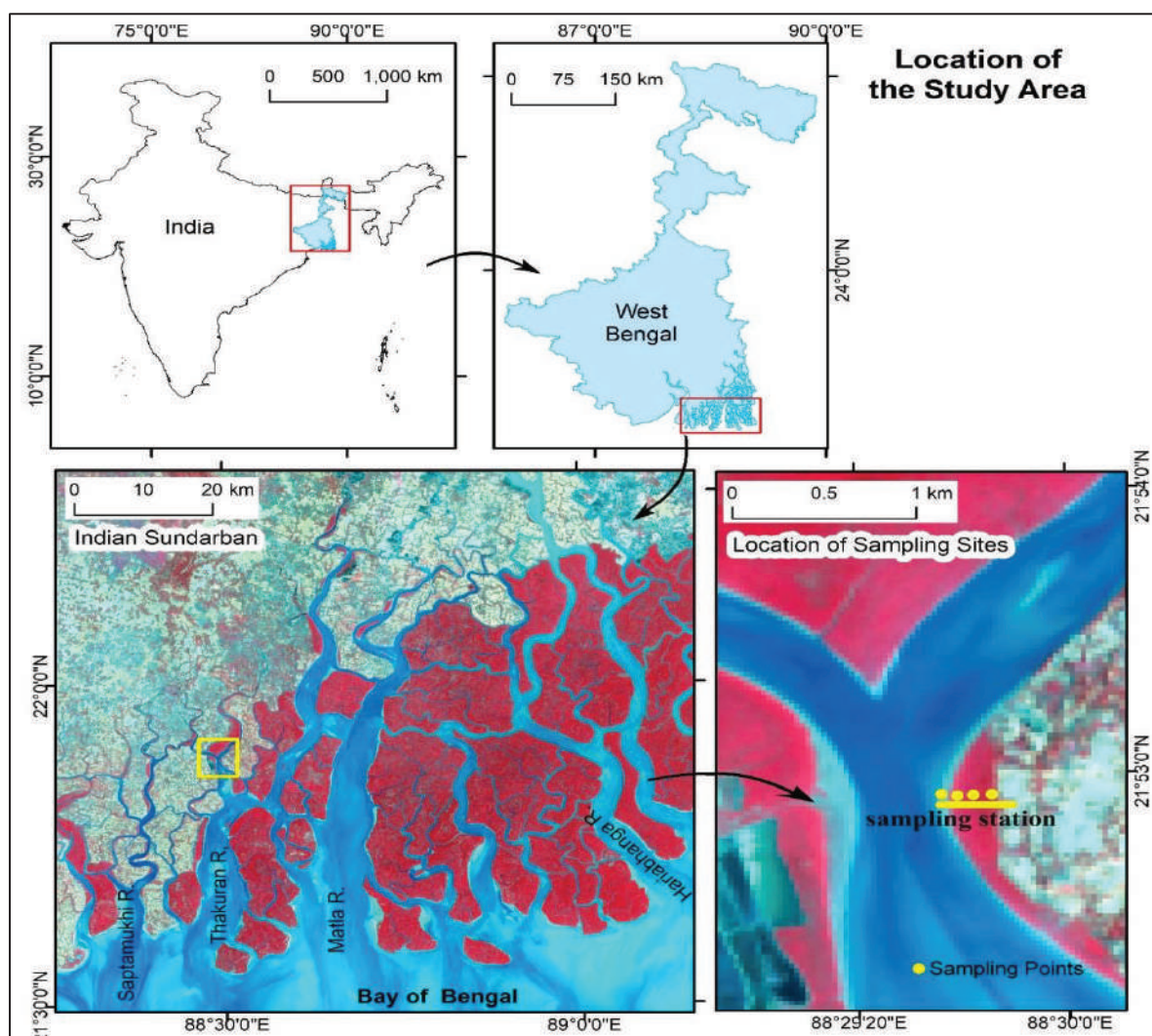

Fig. 1. Location of the study area.

2. Sediment sample collection

Four sites were chosen at intervals of at least 50 meters, extending from the riverbank into the heart of the forest, for the collection of soil samples. Sediment samples were subsequently gathered from these designated locations, meticulously excluding the initial litter zone, and adhering rigorously to established protocols. Following collection, all samples were stored in plastic airtight pouches in preparation for laboratory analysis.

3. Sediment analysis

3.1 Textural analysis

To analyse the textural composition of the sediments, a meticulous process was followed. Initially, the sediments underwent a drying phase in an oven set at 90 degrees Celsius for approximately 72 hours. Subsequently, the dried sediment was subjected to crushing procedures at least three times to ensure uniformity. The sediment then underwent sieving using containers with mesh sizes corresponding to 0.5 phi intervals: 120, 170, 230, and 270. The last container served as a pan to collect sediment unable to pass through the sieves. However, the sediment collected in the pan presented a challenge as traditional sieving methods were no longer applicable. To delve deeper into the textural analysis of these sediments, a pipette analysis was performed using the sediments collected in the pan, following the Folk and Ward method.

3.2 Nutrient measurements

The collected sediment samples were oven-dried at 60°C until constant weight of the samples was obtained. Following the removal of all the exterior components, such as tree roots, gravel, barnacles, Telescopium, etc., all of the dried samples were successively crushed and sieved at Φ3 before being analysed. Total Nitrogen (TN) was analysed using Kjeldahl method after [25]. For determining Total Phosphorus (TP) in sediments, Olsen's method was used for mangrove-dominated alkaline soils [26]. The organic carbon (OC) of sediments was estimated by the wet oxidation method. Salinity was also measured using a digital salinity meter.

4. Mangrove zonation

The mangrove zonation analysis along the selected transect in the Indian Sundarban relied on local expertise and a Mangrove Identification Manual [27]. By utilizing

these resources, the variability of nutrients across mangrove zones was examined. This involved assessing nutrient levels within each zone to understand the ecological implications of nutrient distribution patterns within the Sundarban mangrove ecosystem.

Result and discussion

1. Textural character of surface sediments

The results reveal a distinct pattern in sediment texture along the mangrove-dominated mudflat gradient. Moving from the low tide line towards the high tide line, there is a noticeable shift from very coarse silt to very fine sand. Sediment analysis indicates that riverfront sediment exhibits characteristics of very coarse silt, with mean grain sizes ranging from φ 4.433 to φ 4.715. In contrast, sediment from intermediate zones transitions to very fine sand, with a mean size of φ 3.932 observed in the interior sediments. This variation in sediment texture can be attributed to hydrodynamic processes along the study area. The rapid rising tide velocities facilitate the landward transport of coarser sediment, while the reduced velocity during the receding tide, influenced by tidal asymmetry and the presence of mangrove roots, contributes to the accumulation of finer sediment nearer to the riverbank. Analysis of grain size distribution reveals a bimodal pattern, with a subdued peak observed around 4.5 φ as one moves towards lower zones. This suggests a complex interplay of sediment transport processes influenced by tidal dynamics and local geomorphology. Sediment sorting across all samples appears poor, indicative of the muddy nature of the coast and the fast-rising tide velocity coupled with minimal wave return periods. Samples from the riverfront and intermediate zones exhibit poor sorting, while those from the interior zone display very poor sorting, reflecting distinct patterns of fine silt and clay accumulation within the mangrove zone. Skewness analysis shows a transition from symmetrical characteristics in riverfront sediment to fine asymmetry inland. Riverfront sediment tends to exhibit symmetrical characteristics due to consistent water flow, while the interior of mudflats experiences varying hydrodynamic conditions, leading to the accumulation of finer particles on one side, thus introducing asymmetry. Regarding kurtosis, the leptokurtic tendency (1.169) observed in riverfront sediment suggests a higher proportion of coarse particles, resulting in a more peaked distribution. Sediment from intermediate zones displays mesokurtic characteristics (0.953 and 0.941), indicating a more balanced distribution of particle sizes. In contrast, sediment from the interior zone exhibits platykurtic traits,

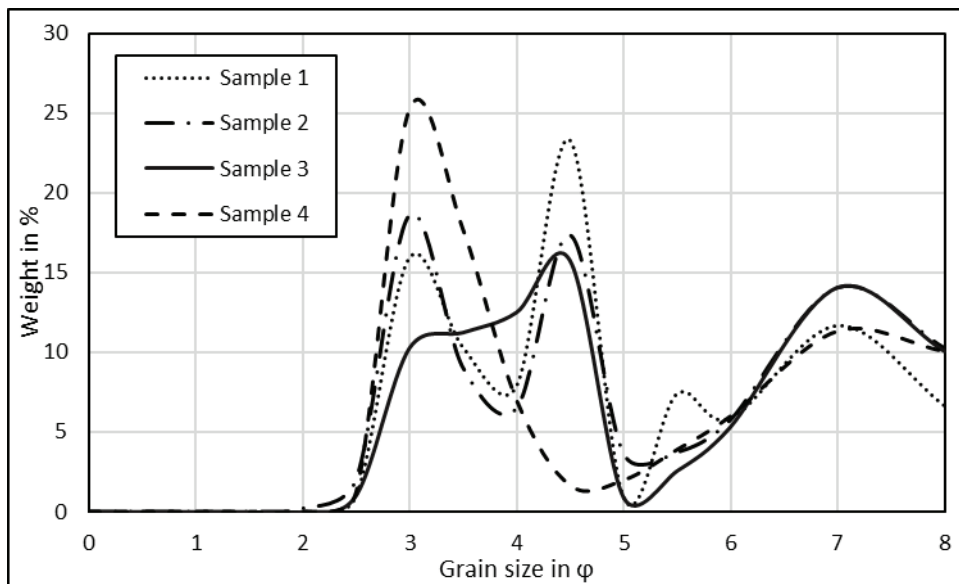suggesting a dominance of fine particles and resulting in a broader and flatter distribution (Fig. 2).

Fig. 2. Sediment texture characteristics of the studied site. Sample 1 is from riverfront zone, Sample 2 and 3 are from the intermediate zone, and Sample 4 is from the interior zone of the mangrove-dominated intertidal mudflat.

2. Amount of nutrients

In the case of salinity, the variability along the transect reveals higher levels near the riverfront zone, with concentrations measuring 14 ‰ (ppt). This elevation in salinity is indicative of prolonged exposure to saline waters due to inundation during both neap and spring high tides. As one moves away from the river, the salinity gradually diminishes, reaching levels between 8-10 ‰. This pattern suggests a complex interaction between tidal dynamics and freshwater input, with the influence of marine waters waning with distance from the river. Regarding the variability of nitrogen, concentrations exhibit a distinct spatial gradient. Near the spring high tide line, nitrogen levels are notably elevated, measuring 20 kg/ha. This observation suggests potential inputs from marine sources or biological processes associated with tidal flushing in this region. However, as one moves further from the river, nitrogen concentrations decline, stabilizing between 12-14 kg/ha. This decline likely reflects a decrease in marine influence and an increase in terrestrial input, highlighting the dynamic interplay between marine and terrestrial nutrient sources along the transect.
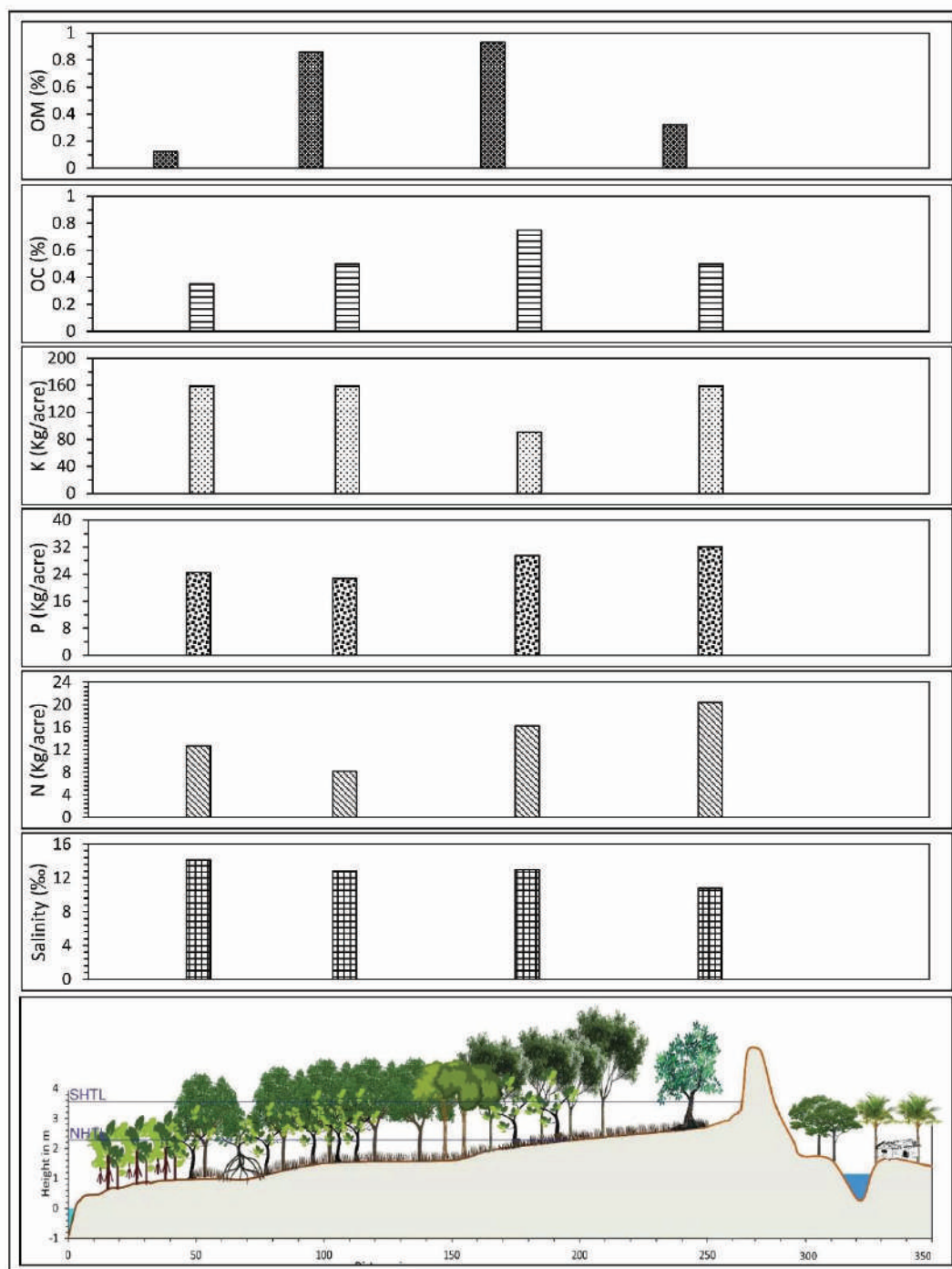
Fig. 3. Variation of major nutrient parameters along the studied transect of the Sundarban.

Similarly, phosphorus demonstrates a spatial pattern mirroring that of nitrogen. Higher concentrations are observed near the spring high tide line, with levels reaching 20 kg/ha. As distance from the river increases, phosphorus concentrations gradually diminish, stabilizing between 12-14 kg/ha. This trend underscores the complex nutrient dynamics within the Sundarban, with inputs from sediment runoff and organic matter decomposition contributing to higher concentrations near the coast. In contrast to salinity, nitrogen, and

phosphorus, potassium exhibits minimal variability along the transect. Concentrations remain relatively uniform throughout the sampled area, suggesting a consistent supply of this nutrient across different zones of the ecosystem. This stability in potassium levels indicates its role as a conservative nutrient within the Sundarban, with limited influence from tidal dynamics or terrestrial inputs. The spatial distribution of organic carbon and organic matter reflects the influence of vegetation patterns, tidal dynamics, and human activities within the Sundarban. Higher concentrations are observed further inland, exceeding 0.6%, indicating areas with dense vegetation cover and reduced exposure to tidal inundation. Conversely, near the spring high tide line, concentrations are lower, falling below 0.4%. This reduction is attributed to sparse vegetation cover and anthropogenic activities such as deforestation and fuelwood collection.

Conclusion

In conclusion, the study elucidates the intricate dynamics governing sediment texture and nutrient distribution along the mangrove-dominated coastal gradient of the Sundarban ecosystem. Hydrodynamic processes, tidal dynamics, and freshwater input significantly influence sediment transport patterns, shaping the observed variation from coarse silt to fine sand across the coastal gradient. The spatial variability in nutrient concentrations reflects the complex interplay between marine and terrestrial sources, with implications for ecosystem health and resilience. Understanding these dynamics is essential for effective management and conservation strategies, particularly in the face of ongoing environmental changes and human activities. Further research is warranted to assess the long-term implications of these dynamics on the stability and sustainability of the Sundarban mangrove ecosystem.

Acknowledgments

References

[1] S. Das, N. Dasgupta and A. Hazra: "Halophytes: A Glimpse of Indian Sundarbans–A World Heritage Site, Its Existing Status, and Sustainability." Handbook of Halophytes: From Molecules to Ecosystems Towards Biosaline Agriculture. 163-197(2021).

[2] S. K. Sarkar, M. K. Ahmed and K. K. Satpathy: "The Sundarban Delta Complex." World Seas: an Environmental Evaluation. Academic Press, 145-168 (2019).

[3] A. Hassan and A. Sharma: "Wildlife Tourism for Visitors' Learning Experiences: Some Evidence on the Royal Bengal Tiger in Bangladesh and India." *Wildlife Tourism, Environmental Learning and Ethical Encounters: Ecological and Conservation Aspects*. 155-168 (2017).

[4] S. N. Islam: "Sundarbans a dynamic ecosystem: an overview of opportunities, threats and tasks." *The Sundarbans: A Disaster-Prone Eco-Region: Increasing Livelihood Security*. 29-58 (2019).

[5] A.C.G. Henderson et al: "The Indian Sundarbans: biogeochemical dynamics and anthropogenic impacts." *Estuarine Biogeochemical Dynamics of the East Coast of India.* 239-260 (2021).

[6] U. K. Mandal et al: "Global climate change and human interferences as risk factors, and their impacts on geomorphological features as well as on farming practices in Sundarbans eco-region*." The Sundarbans: A Disaster-Prone Eco-Region: Increasing Livelihood Security*.405-437 (2019).

[7] R. Chowdhury et al: "Effects of nutrient limitation, salinity increase, and associated stressors on mangrove forest cover, structure, and zonation across Indian Sundarbans." *Hydrobiologia* **842**, 191-217(2019).

[8] M. B. K. Prasad et al: "Sources and dynamics of sedimentary organic matter in Sundarban mangrove estuary from Indo-Gangetic delta." *Ecological processes*. **6**, 1-15(2017).

[9] S. Manna et al.: "Interplay of physical, chemical and biological components in estuarine ecosystem with special reference to Sundarbans, India." *Ecological Water Quality—Water Treatment and Reuse.* 206-238(2012).

[10] M. Bakshi et al. "Sediment quality, elemental bioaccumulation and antimicrobial properties of mangroves of Indian Sundarban." *Environmental geochemistry and health.* **41,** 275-296(2019).

[11] P. Gogoi et al. "Environmental factors driving phytoplankton assemblage pattern and diversity: insights from Sundarban eco-region, India." Ecohydrology & Hydrobiology 21.2 (2021): 354-367.

[12] S. J. Blott and P. Kenneth: "Particle size scales and classification of sediment types based on particle size distributions: Review and recommended procedures." *Sedimentology.* **59.7**, 2071-2096(2012).

[13] M. B. K. Prasad et al: "Sources and dynamics of sedimentary organic matter in Sundarban mangrove estuary from Indo-Gangetic delta." *Ecological processes*. **6**, 1-15(2017).

[14] K. Palit et al: "Microbial diversity and ecological interactions of microorganisms in the mangrove ecosystem: Threats, vulnerability, and adaptations." *Environmental Science and Pollution Research.* **29.22,** 32467-32512(2022).

[15] I. F.-Hanum et al:"Development of a comprehensive mangrove quality index (MQI) in Matang Mangrove: Assessing mangrove ecosystem health." *Ecological Indicators*. **102**, 103-117(2019).

[16] B. Gopal and Malavika Chauhan. "Biodiversity and its conservation in the Sundarban mangrove ecosystem." *Aquatic sciences* **68,** 338-354(2006).

[17] K. Hassan et al: "Climate change and world heritage: a cross-border analysis of the Sundarbans (Bangladesh–India)." *Journal of Policy Research in Tourism, Leisure and Events* **11.2,** 196-219 (2019).

[18] M. Sievers et al: "Indian Sundarbans mangrove forest considered endangered under Red List of Ecosystems, but there is cause for optimism." *Biological conservation.* **251**, 108751(2020).

[19] M. M. A.-A.-Mamun, et al: "Ecosystem services assessment using a valuation framework for the Bangladesh Sundarbans: livelihood contribution and degradation analysis." *Journal of forestry research.* **28**, 1-13 (2017).

[20] S. Samanta et al: "Assessment and attribution of mangrove Forest changes in the Indian Sundarbans from 2000 to 2020." *Remote Sensing.* **13.24**, 4957(2021).

[21] S. N. Islam, S. Reinstädtler and A. Gnauck: "Invasive species in the Sundarbans coastal zone (Bangladesh) in times of climate change: chances and threats." *Impacts of Invasive Species on Coastal Environments: Coasts in Crisis.* 63-85 (2019).

[22] A. Chowdhury, S. K. Maiti and S. Bhattacharyya: "How to communicate climate change 'impact and solutions' to vulnerable population of Indian Sundarbans? From theory to practice." *SpringerPlus.* **5**, 1-17 (2016).

[23] N. Ainun and J. K. Chowdhur:. "Influence of climate change on biodiversity and ecosystems in the Bangladesh Sundarbans." *The Sundarbans: A Disaster-Prone Eco-Region: Increasing Livelihood Security*.439-468 (2019).

[24] A. Raha et al: "Climate change impacts on Indian Sunderbans: a time series analysis (1924–2008)." *Biodiversity and Conservation*. **21,** 1289-1307 (2012).

[25] G. W. Burton and J. E. Jackson: "Effect of Rate and Frequency of Applying Six Nitrogen Sources on Coastal Bermudagrass 1." *Agronomy Journal* **54.1,** 40-43 (1962).

[26] S. R. Olsen: Estimation of available phosphorus in soils by extraction with sodium bicarbonate. No. 939. US Department of Agriculture, (1954).

[27] M. Sitnik: "Mangrove Ecology Workshop Manual." A Field Manual Focused on the (2002).

Research Article

Assessing the Water Quality of Chamta Channel in Darjeeling Himalayan Foothills Region

Gargi Sarkar[1], Chandan Surabhi Das[2], and Subhadip Gupta[3]

[1]Department of Geography, Sree Chaitanya College, Habra, West Bengal
[3]Department of Geography, Barasat Government College, West Bengal
[2]Department of Geography, Asutosh College, Kolkata, West Bengal
[1]e-mail: gsg.presidency@gmail.com

Abstract: The assessment of river health relies on studying water quality, which indicates the overall health of the river habitat. This paper focuses on evaluating the water quality of an ungauged stream in the Darjeeling Himalayan foothills. The task is challenging due to the need for primary data collected through field surveys. Three field visits were conducted in 2022 during different hydrological regimes. The water quality index method, following ICMR guidelines, was used for assessment. The study shows variations in water quality of the Chamta channel, with significant deterioration during the pre-monsoon months. Downstream, the water quality worsens after passing through certain areas near the Chamta-Panchanoi confluence. Water quality of the Chamta channel becomes worst in the lean months of pre-monsoon season. Water quality gradually deteriorates as the channel approaches downstream through the Gaurcharan, Matigarahat, and finally Tomba areas (near Chamta-Panchanoi confluence) following the crossing of the Hawa Singh river bridge.

Keywords: Foothills stream, water quality index, electric conductivity, total dissolved solid, dissolved oxygen,

Introduction

Since the turn of the twenty-first century, river and lake degradation has intensified due to the rapidly growing population and modernization of society. In addition to internal and exterior physical, chemical, and biological forces, various anthropogenic stresses such as habitat degradation, species introductions, pollution, and fishing pressures occur simultaneously [11]. The physicochemical properties and other features of water are altered by the introduction of different types of contaminants and nutrients into water bodies through industrial effluents, sewage, agricultural runoff [1]. Since rivers have characteristics that are both social and natural. Because ecosystem health is shaped by the interplay of river biota and their hydro-geochemical environment, it is a crucial component of river health [6-7, 9-10]. The present paper is dealing

with the issue of river water quality of an ungauged river called the Chamta where the water quality is compromised by the illegal intervention of the local anthropocentric activities. The Chamta is an 8.3 km long, non-perennial foothill stream, located in the Darjeeling district. It is a right bank tributary of the Panchanoi. It originates from the Kurseong hills (26048'50'' N, 88019'44'' E), flows down from the NW to SE through the Sukna forest and finally discharges into the Panchanoi near Sishudangi (26043'05'' N, 88022'05'' E). The Chamta falls under Kurseong and Matigara administrative blocks under Darjeeling district. The Mahananda Wild Life Sanctuary (MWLS) occurs over the first 5 km stretch of the Chamta from its source (out of bounds of the public). The Chamta has two right bank and three left bank tributaries. Its basin has an area of 24 sq. km. Twenty-nine (29) census villages fall under the Chamta basin. The fourteen (14) Chamta-bound villages have a total of 29444 persons in 2011 compared to 17877 persons in 2001. Hence there has been an increase of total 11567 persons (Population Growth Rate [PGR] 64.7%) over a period of 10 years between 2001 and 2011 which is quite similar trend (61.5% PGR) has also been followed by the entire 29 villages under the Chamta basin. The Chamta channel passes through the greater Siliguri area after crossing Gaurcharan in its downstream stretch. Both the banks of the Chamta channel are intensively occupied by displaced and economically poor slum dwellers of the Siliguri township area. They illegally occupy portions of river bed and river bank for their livelihood.

Mondal et. al. (2021) selected fourteen indicators for the measurement of water quality of the Karala River in Jalpaiguri. They observed that river restoration through Nature Based Solution (NBS) is necessary particularly in its downstream reaches, where density of settlement is high [7]. Bigham (2016) considered sediment as the non-point source pollutant in riverine environment [6]. Singh et.al. (2015) found that the presence of different pollutants nearby Domohoni along Teesta due to the unrestricted discharge of tea garden effluents carrying pesticide residues into the river water. The residue of Chlorpyriphos, Dicofol Ethion effected the riverine ecosystem as well as fish community [9]. Gorde and Jadav (2013) found that the quality of natural waterbody is deteriorating day by day due to rapid growth of urbanization, industrialization, released chemical fertilizer and pesticides from the agricultural field. So before use this water, it is very obvious to check the quality of water otherwise people may be affected by different water-borne diseases [8]. Rasid and Romshoo (2013) noted that water quality in the Lidder River in the Kashmir valley was gradually decreasing due to multipurpose use of river water, such as wash out of fertilizers and pesticides and seasonal

tourism which was why river water quality deteriorated mostly between June and August coinciding with the peak season of tourists [5]. Markowitz and Newton (2011) noted that increased suspended sediment supply affected the surface water quality of stream. He observed that the surface water quality was a control of bank induced suspended sediment in Birch creek watershed, New York, USA [4]. Maheshwari et.al. (2011) noted that the surface water quality of Yamuna River is highly polluted due to the discharge of untreated west water directly to the channel. To analyses the quality of water, water samples are being collected during Summer and Winter season from some specific sites of Kailash temple to Taj Mahal area because of the presence of so many chemical fertilizers, iron, leather and other industries. Here various physical as well as chemical properties of surface water are being analyze to compare with the standard limits which is recommended by WHO. Quality of water during winter was found more suitable for domestic uses [1]. The methodology has also been followed in present research for the understanding of the variation of water quality of the Chamta river in pre-monsoon, monsoon and post-monsoon season. Dutta and Misra (2010) found the concentration of heavy metals like Mg, Fe, Ca. Zn in river water and partially contaminated ground water at nearby places, which made a serious in issue in health of local inhabitants of small tea gardens of Sonitpur district of Assam in India [2]. Zhang et.al. (2009) commented that the water quality is the indicator of the river health, which indicate intervened by the due to the anthropogenic effect. To measure the water health, they adopted the entropy method and calculate the weight of index [11]. Similarly, the magnitude of the measured parameters of water of the Chamta channel reflects the health of the river. Brown (2009) highlighted the issues of bank instability and spatial differentiation of surface water quality in Clayburn watershed in Canada [3]. Daniel et al. (1982) stated that river water quality is mostly affected by pollutants from non-point sources [10].

Methodology

The present research paper deals with the spatial (from upstream to downstream direction along the Chamta channel) as well as temporal (pre-monsoon, monsoon and post-monsoon regime) variation of water quality along the Chamta channel. The primary water quality data has been collected from field by using the Aquasol field-kit in the year of 2022 along the Chamta channel. Seven (07) representative monitoring stations are set along the Chamta channel which are Kanyan (at upstream direction, just outside the Mahananda Wild Life Sanctuary), Kamalabarir Chaat, Patharghata (Nichitpur), Gaurcharan, Matigara NH31C

(Matigarahat), Chandmoni, Tomba (at Chamta-Panchanoi confluence). Three (03) field-visits have been conducted in the year of 2022 with an interval of four (04) months to collect the water samples from the Chamta channel. The first visit was executed in the middle-month of April which represents the water quality of the Chamta channel in the lean pre-monsoon months, the second visit was taken place in the middle-month of July (represents the water quality of Monsoon months) and October (represents the water quality of late-monsoon or Post-Monsoon months). Reading of surface water pH (digital meter), electric conductivity (EC through digital meter), total dissolved solid (TDS through digital meter), dissolved oxygen (DO), calcium. magnesium, total hardness, total alkalinity has been recorded standing at the representative monitoring stations along the Chamta channel. Water quality index (WQI) model has been introduced, which is dimensionless number indicates the nature of water. The magnitude of WQI is found higher for the less polluted water, whereas it reduces with the increase of level of water pollution. Water samples are taken into lab to observe the presence or absence of Coliform bacteria in Chamta water samples by using the Bactaslide field kit.

The Chamta channel has neither been measured by the West Bengal Irrigation Department nor monitored by the West Bengal Pollution Control Board (WBPCB). In order to record the variation in magnitude of parameters related to surface water quality of the river, such research relies heavily on primary data that can only be collected by field visits to representative stations along the channel studied in a certain period of time.

Result and Discussion

Magnitude of parameters of water quality has been detected of the Chamta river in pre-monsoon (Fig. 1-8), monsoon (Fig. 9-16) and post-monsoon (Fig. 17-24) months. The measured magnitude of the surface water quality of the Chamta river indicates that the best quality of water flows through the Chamta channel in the post-monsoon months (Fig. 25). The quality of water of Chamta river becomes poorer in the dry months of the year (Fig. 1-8). It improves gradually from June and the trend is continued up to December (Fig. 9-24). Even the quality of the Chamta river is found better in the late monsoon or post-monsoon months than the high discharge monsoon months (Fig. 25). But the presence of coliform bacteria is recorded through the entire studied path of the Chamta channel. The changing correlations among the water quality parameters have been observed in each three hydrological regimes of Chamta channel. It proves the interaction between the dependant and independent variables vary with the

change of hydrological regime along with the combined impact of changing hydro-geomorphological condition and human interference.

There are about nine-seven (97) open drain-outlets are recorded by field surveys which are carrying domestic wastes and sewage (adds more nitrogen and phosphorus in the Chamta channel) onto the Chamta channel that have been marked along the reaches of the Chamta to identify their spatial distribution. These outlets act as point-sources of pollution in river water. Water quality deteriorates at the said sewage disposal points as identified from the study of water quality. Spacing between the drain-outlets and the number of drain outfalls increase gradually from upstream to downstream of the Chamta as the number and size of settlement increase downstream. These negative scenario of water quality and stream water pollution increase rapidly downwards from Gaurcharan. The untreated pesticide residue rich effluent water from the Chamta river-side tea-gardens and agricultural fields can be considered as non-point sources of river water pollution. N-P-K 0-0-60 has been used as fertilizer in the New Chumta, and Chamta tea gardens. It enhances the growth of the tea production as well as the growth of Algae in Chamta channel. It enhances the BOD while reduces the DO level. Residue of used chemical pesticides (Endosulfan) in those TG are harmful for the native fishes of Chamta. The pesticides generally used in TGs in the month of February to April (sowing season) and the toxic residues comes in Chamta river by the irrigational discharges. That is why the water quality of the Chamta channel becomes most polluted in these lean months in presence of load of more pollutants in channel, while flashing by channel discharge is not possible. Effluent of bio-medical wastes from hospitals and nursing homes, located on the left bank of Chamta namely, Dr. Chang's Super-speciality, Neotia Getwell Multi-Speciality Hospital, Avalon Hospital at Gaurcharan add to the pollution level in the Chamta channel. Biomedical waste is potentially infectious and is generated during healthcare procedures involving biological materials. It changes the physical, chemical and biological properties of Chamta river water and modifies natural aquatic ecosystem. The illegal bank-line settlers are actively or passively responsible for the declining stream water quality. The released domestic waste water, solid waste, untreated residue of human and animal's excreta directly make the water quality of Chamta poor. This toxic water has been found to increase incidence of skin diseases among the local people. This is further to mention that the domestic septic tanks are open to the channel of the Chamta. As a result, the river water is neither used as drinking water nor for washing, bathing and cleaning linens.

Fig. 1: Distribution of DO at representative buffer villages along Chamta channel in April 2022

Fig. 2: Distribution of pH at representative buffer villages along Chamta channel in April 2022

Fig. 3: Distribution of EC at representative buffer villages along Chamta channel in April 2022

Fig. 4: Distribution of total alkalinity at representative buffer villages along Chamta channel in April 2022

Fig. 5: Distribution of total hardness at representative buffer villages along Chamta channel in April 2022

Fig. 6: Distribution of magnesium at representative buffer villages along Chamta channel in April 2022
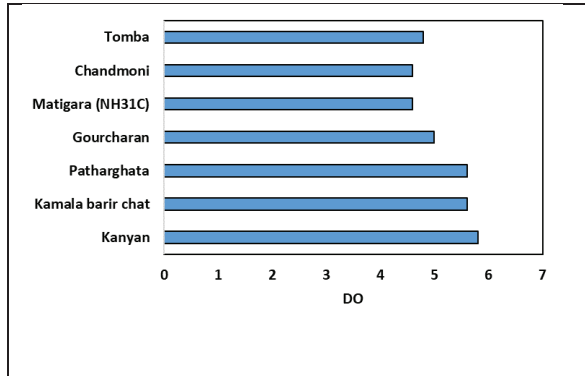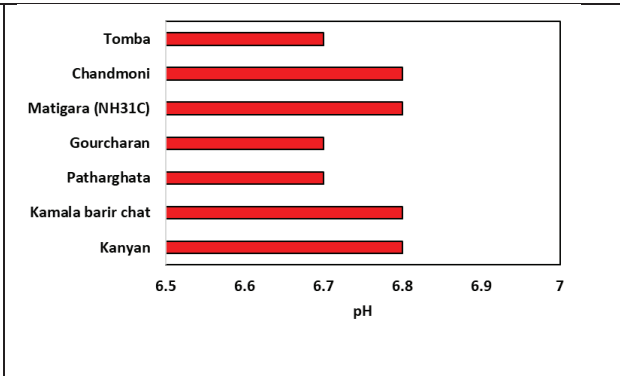
Fig. 7: Distribution of calcium at representative buffer villages along Chamta channel in April 2022	Fig. 8: Distribution of TDS at representative buffer villages along Chamta channel in April 2022
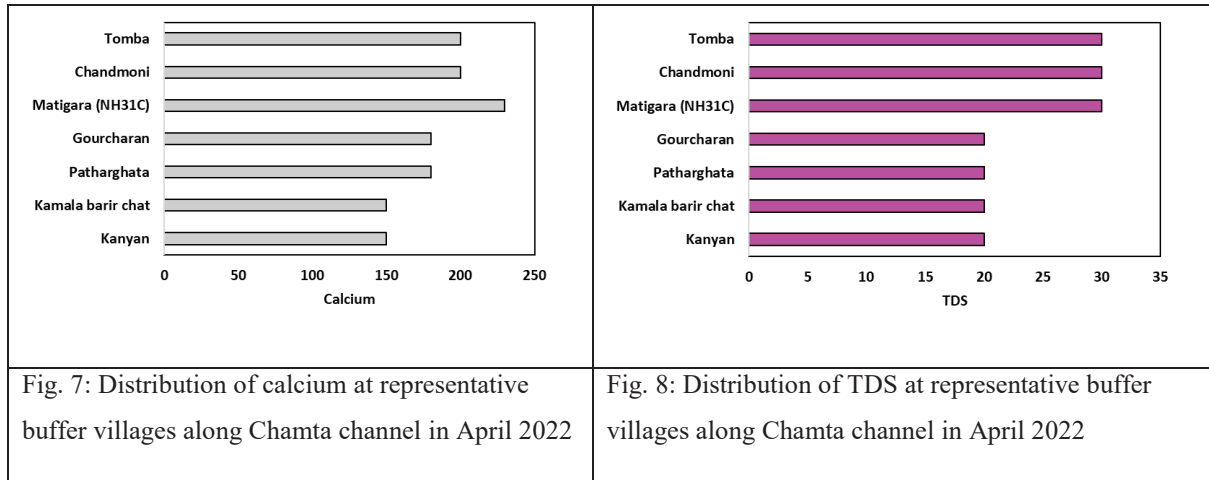
Not only the human beings but also the bio-diversity of Chamta channel gradually declining in recent years. Fish can be considered as one of the proxy indicators of changing habitat. Fish has become rare now-a-days in the Chamta channel. After crossing the Gaurcharan area along Chamta channel, even near the Chamta-Panchanoi confluence near the Chandmoni TG, the reach has become devoid of fish such as Boroli, Sol, Magur, Bami, Kuchia, Gittu, Koi etc. Falling water quality of the Chamta, as per the views of the local people, has a telling effect on the size of the available fish. Large size fishes are available more in the better quality upstream water while in the downstream direction the size of Nodiali fishes gradually decreases. Release of surplus chemical

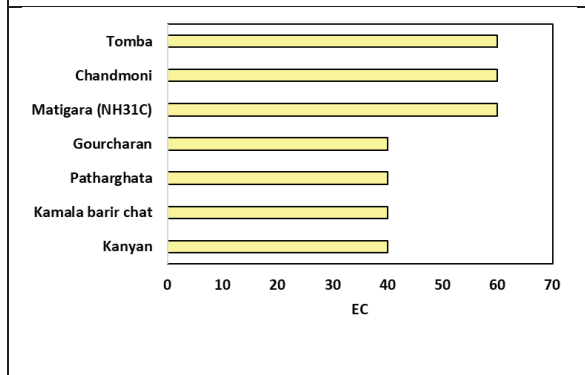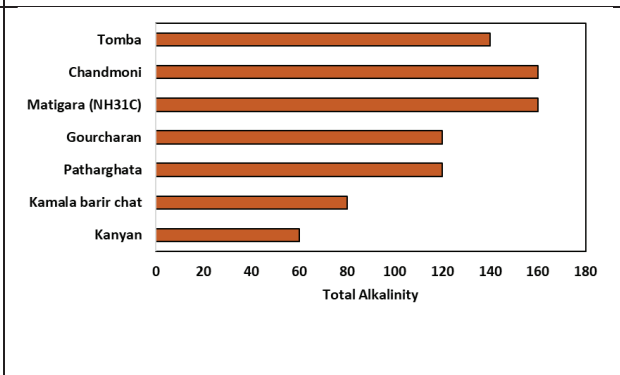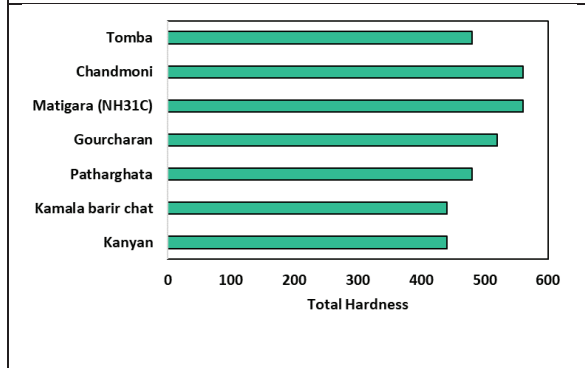| Fig. 9: Distribution of DO at representative buffer villages along Chamta channel in July 2022	Fig. 10: Distribution of pH at representative buffer villages along Chamta channel in July 2022
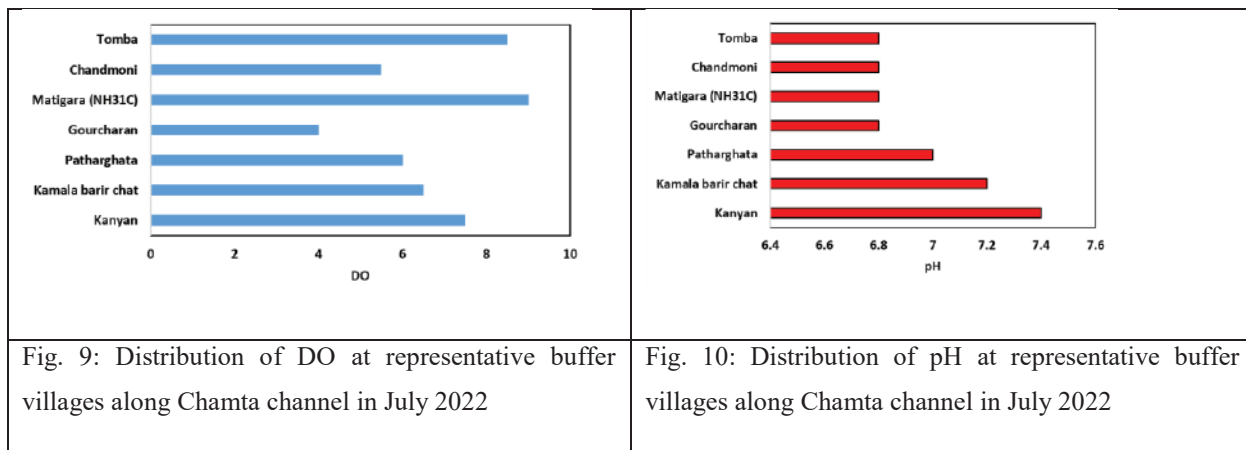
Fig. 11: Distribution of EC at representative buffer villages along Chamta channel in July 2022

Fig. 12: Distribution of total alkalinity at representative buffer villages along Chamta channel in July 2022

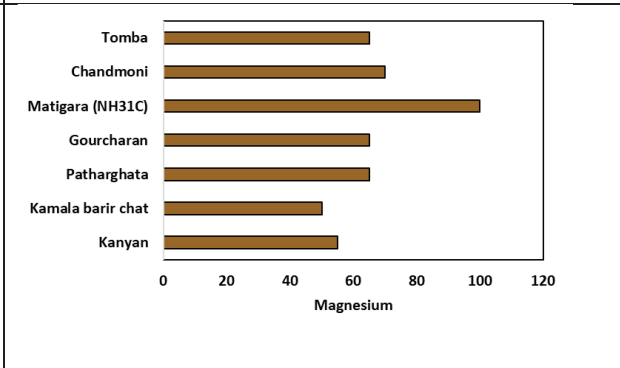Fig. 13: Distribution of total hardness at representative buffer villages along Chamta channel in July 2022

Fig. 14: Distribution of magnesium at representative buffer villages along Chamta channel in July 2022

Fig. 15: Distribution of calcium at representative buffer villages along Chamta channel in July 2022
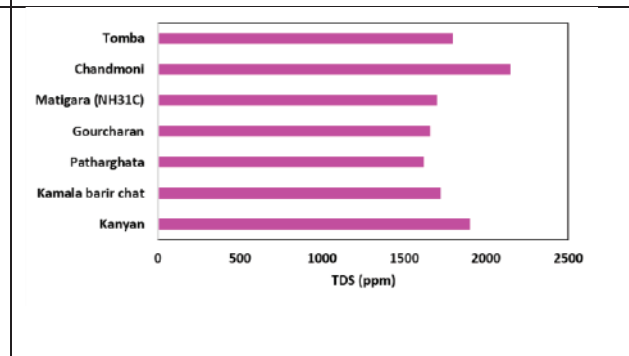
Fig. 16: Distribution of TDS at representative buffer villages along Chamta channel in July 2022

fertilizers from tea-gardens in the upstream areas increases the problem of toxicity which is responsible again for diminishing supply of fishes. As such the reach between Gaurcharan and Chamta confluence has almost become fish-less though it was rich in fishes even a decade ago.
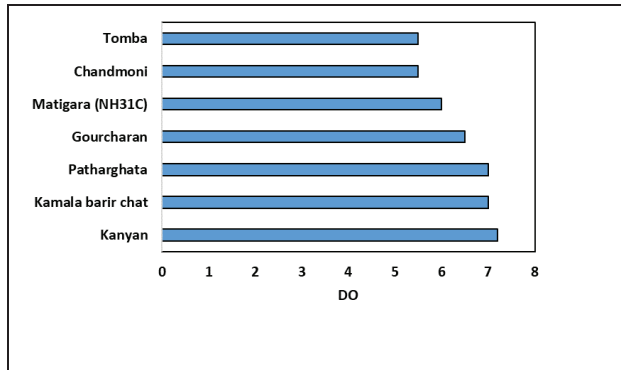
Fig. 17: Distribution of DO at representative buffer villages along Chamta channel in October 2022
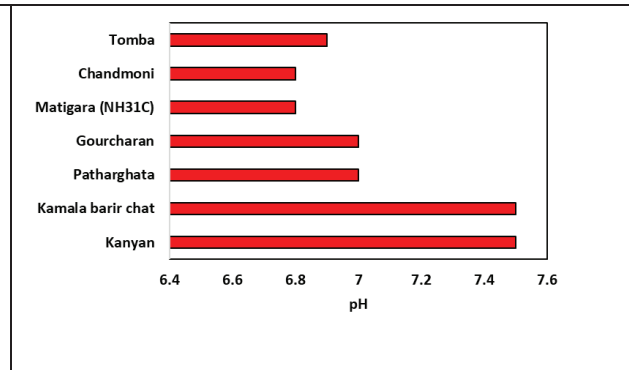
Fig. 18: Distribution of pH at representative buffer villages along Chamta channel in October 2022
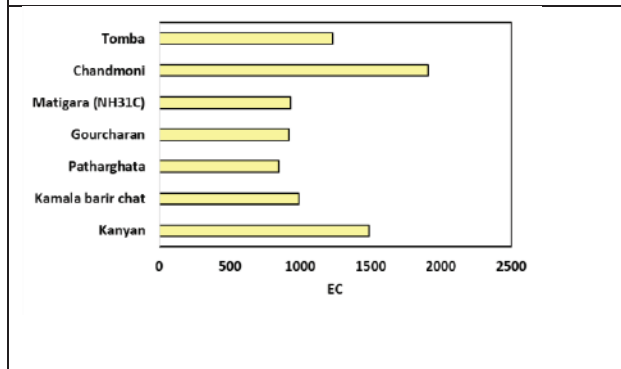
Fig. 19: Distribution of EC at representative buffer villages along Chamta channel in October 2022
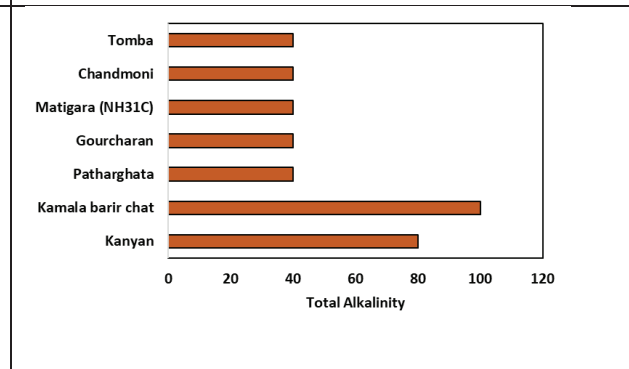
Fig. 20: Distribution of total alkalinity at representative buffer villages along Chamta channel in October 2022
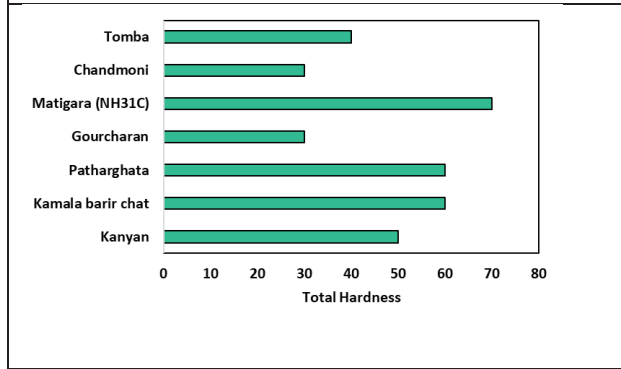
Fig. 21: Distribution of total hardness at representative buffer villages along Chamta channel in October 2022
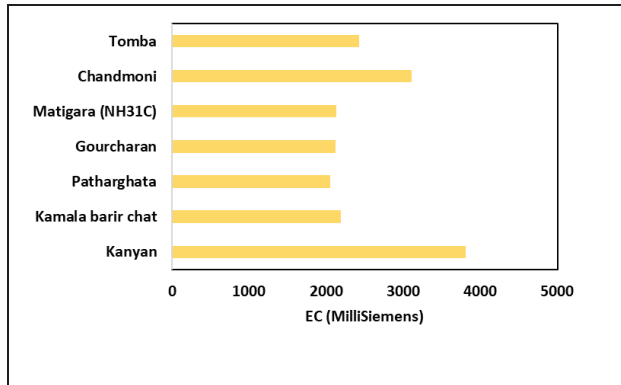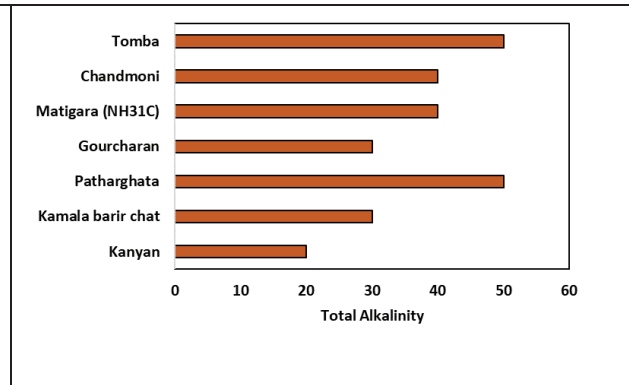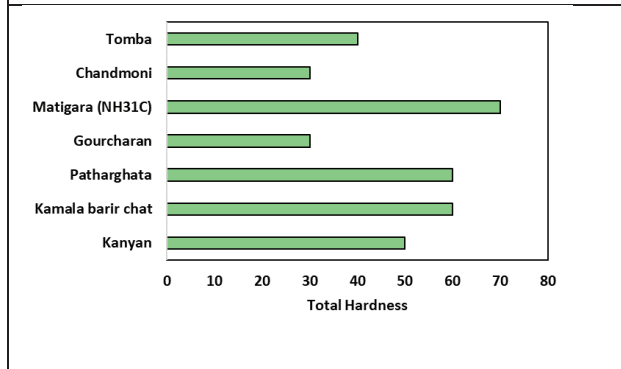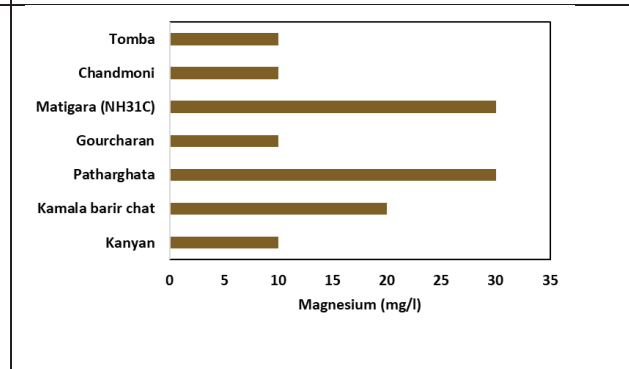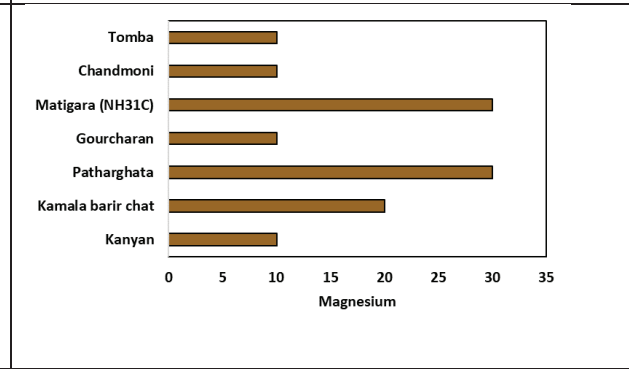

Fig. 22: Distribution of magnesium at representative buffer villages along Chamta channel in October 2022
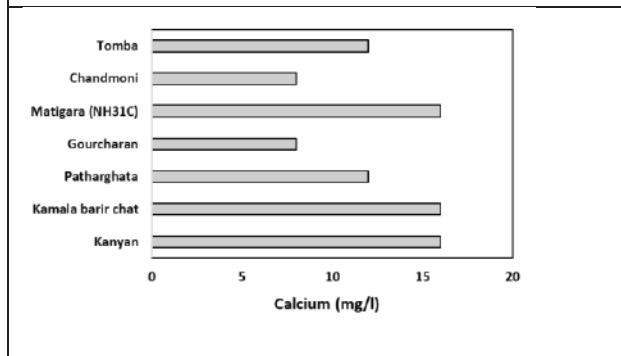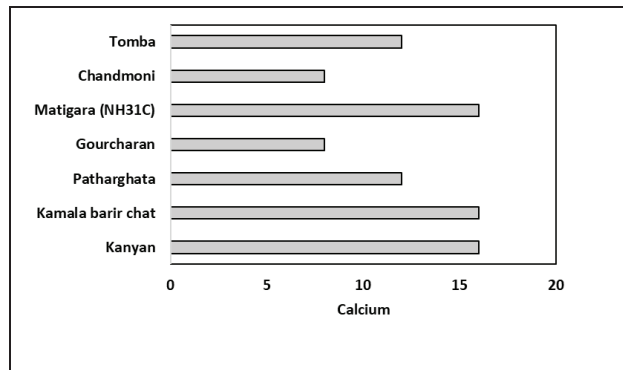
Fig. 23: Distribution of calcium at representative buffer villages along Chamta channel in October 2022
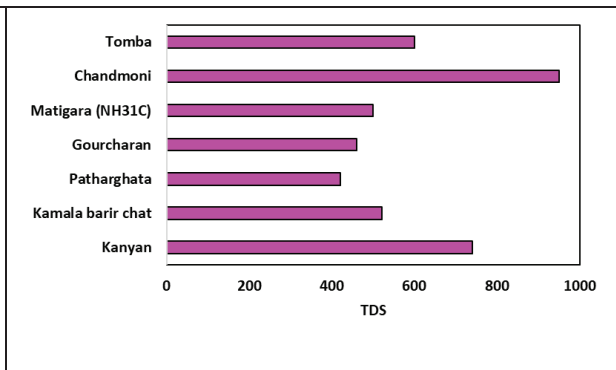
Fig. 24: Distribution of TDS at representative buffer villages along Chamta channel in October 2022

Correlation among the water quality parameters changes with season in the survey year of 2022 in case of the Chamta channel (Table 1-3). It reflects the role of discharge in the channel which regulates all the dependent factors of water quality. Significant association has been observed between pH and DO in the monsoon (Table 2) and post-monsoon months (Table 3), while no association is detected in lean months of pre-monsoon (Table 1) between these two variables. Significant association with Calcium is found with the total alkalinity, TDS, EC, total hardness in the pre-monsoon months which disappears with the increase of discharge in the Chamta channel (Table 2-3). TDS is well associated with pH, total alkalinity and total hardness in the span of monsoon regime (Table 2), which has not found in pre-moon (Table 1) even in post-monsoon season (Table 3).
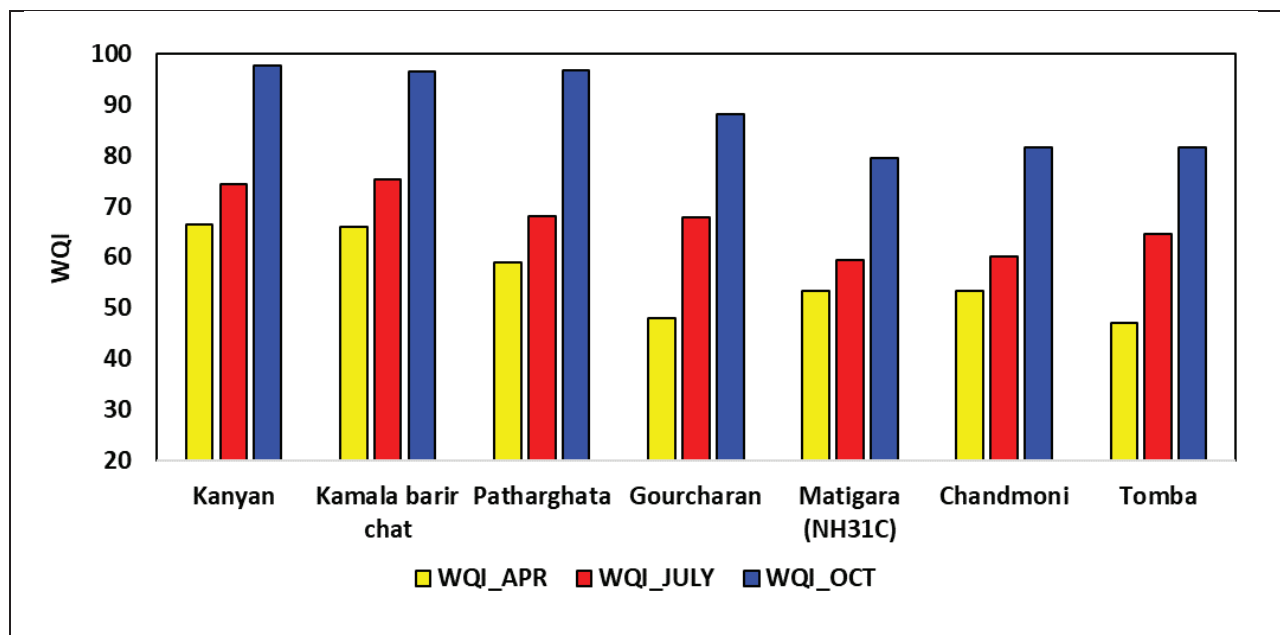
Fig. 25: Spatial variation of water quality index (WQI) at representative buffer villages along Chamta channel in 2022

Table 1: Correlation among the water quality parameters in April 2022 at selected stations along the Chamta river

APR	DO	pH	Total Alkalinity	TDS	EC	Total Hardness	Calcium	Magnesium
DO	1.00							
pH	0.02	1.00						
Total Alkalinity	**-0.92**	-0.16	1.00					
TDS	-0.87	0.17	0.81	1.00				
EC	-0.87	0.17	0.81	1.00	1.00			
Total Hardness	-0.88	0.07	0.89	0.67	0.67	1.00		
Calcium	-0.88	-0.08	**0.94**	**0.84**	**0.84**	**0.85**	1.00	
Magnesium	-0.71	0.13	0.76	0.65	0.65	0.81	**0.92**	1.00

Table 2: Correlation among the water quality parameters in July 2022 at selected stations along the Chamta river

JULY	DO	pH	Total Alkalinity	TDS	EC	Total Hardness	Calcium	Magnesium
DO	1.00							
pH	**0.94**	1.00						
Total Alkalinity	-0.50	-0.32	1.00					
TDS	-0.84	**-0.75**	**0.50**	1.00				
EC	-0.52	-0.47	0.19	0.03	1.00			
Total Hardness	0.64	0.66	0.29	**-0.50**	-0.35	1.00		
Calcium	-0.61	-0.55	-0.11	0.44	0.30	**-0.90**	1.00	
Magnesium	-0.09	0.16	0.34	0.28	-0.31	-0.09	0.42	1.00

Significant correlation has also been observed between the calcium and total hardness in the monsoonal days (Table 2). pH and calcium show significant association with total alkalinity with in post-monsoon season (Table 3) which has not observed in rest of the year in case of the Chamta channel.

Table 3: Correlation among the water quality parameters in October 2022 at selected stations along the Chamta river

OCT	DO	pH	Total Alkalinity	TDS	EC	Total Hardness	Calcium	Magnesium
DO	1.00							
pH	**0.80**	1.00						
Total Alkalinity	0.64	**0.94**	1.00					
TDS	-0.41	-0.06	0.03	1.00				
EC	-0.41	-0.06	0.00	1.00	1.00			
Total Hardness	0.42	0.23	0.31	-0.50	-0.55	1.00		
Calcium	0.46	0.57	**0.63**	-0.25	-0.29	0.84	1.00	
Magnesium	0.26	-0.15	-0.08	-0.59	**-0.63**	**0.86**	0.45	1.00

Conclusion

The current study indicates that the water quality of the Chamta channel is significantly influenced by the volume of water supplied to the channel. Pollution levels tend to rise during the pre-monsoon months as the water supply in the Chamta river decreases. Conversely, pollution levels decrease at monitoring stations along the Chamta channel during the monsoon season, when there is an abundant supply of water that helps flush out pollutants downstream. The local depression-induced shorter but more intense rainfall results in increased water supply to the channel, further reducing the concentration of pollutants in the post-monsoon months. The water quality shows the most improvement during the winter period following the monsoon season. The correlation between water quality parameters varies with changes in the hydrological regime.

References:

[1] A. Maheshwari, M. Sharma and D. Sharma: Hydro chemical analysis of surface and ground water quality of Yamuna River at Agra, India. *J. Mater. Environ. Sci, Vol. **2(4),*** 373-378 (2011).

[2] D. Joydev and A.K. Misra: Analysis of heavy metals in ground water of small tea gardens of Sonitpur District, Assam, India. *International Journal of Chemical Sciences, Vol.8(1),* 397-404 (2010).

[3] D.J. Brown: The effects of non-point source pollution on surface water quality, Clayburn Watershed, Abbotsford, British Columbia, Canada (2009).

[4] G. Markowitz and S. Newton: Project Report: Using Bank Assessment for Non-Point Source Consequences of Sediment (BANCS) Model to Prioritize Potential Stream Bank Erosion on Birch Creek, Shandaken, New York (2011).

[5] I. Rashid & S.A. Romshoo: Impact of anthropogenic activities on water quality of Lidder River in Kashmir Himalayas. Environmental monitoring and assessment, *Vol. 185*, 4705-4719 (2013).

[6] K.A. Bigham: Evaluation and application of stream bank assessment for non-point source consequences of sediment (BANCS) model developed to predict annual stream bank erosion rate, Thesis (Kansas State University) (2016).

[7] S. Mondal, S. Mitra, J. Dey and L. Tamang: Assessment of the anthropogenic interventions and related responses of Karala River, Jalpaiguri, India: a multiple indicator-based analysis. Environmental Monitoring and Assessment, *Vol.193(10),* 667 (2021).

[8] S. P. Gorde and M. V. Jadhav: Assessment of water quality parameters: a review. *J Eng Res Appl,* Vol. *3(6),* 2029-2035 (2013).

[9] S. Singh, D. Bhutia, S. Sarkar, B.K. Rai, J. Pal, S. Bhattacharjee and M. Bahadur: Analyses of pesticide residues in water, sediment and fish tissue from river Deomoni flowing through the tea gardens of Terai Region of West Bengal, India. *International journal of fisheries and aquatic studies, Vol*. *3(2),* 17-23 (2015).

[10]   T.C. Daniel, R.C. Wendt, P.E. McGuire and D. Stoffel: Nonpoint Source Loading Rates from Selected Land Uses, *JAWRA Journal of the American Water Resources Association, Vol.18(1)*, 117-120 (1982).

[11]   Y. Zhang, L. Liu, J. Wang, J. Chen and C. Lu: An index of river health for river plain network regions. In Ecohydrology of surface and groundwater dependent systems: concepts, methods and recent developments. *Proceedings of Symposium JS. 1 at the Joint Convention of the International Association of Hydrological Sciences (IAHS) and the International Association of Hydrogeologists (IAH) held in Hyderabad, India,* 112-121, (2009).

Research Article

Some Results on Fuzzy Compatibility of Metric Spaces

Jayanta Biswas

Barasat Government College, 10 KNC Road, Barasat, West Bengal, India
E-mail - jbiswas37@gmail.com

Abstract

In a metric space (X, d) we have $d(X \times X) \subset \mathbb{R}$ and for a fuzzy set A on X, we have $A(X) \subseteq [0, 1] \subset \mathbb{R}$. Using the usual metric in $\mathbb{R}$ and usual algebraic structures (addition and multiplication) in $\mathbb{R}$, we relate a metric space and a fuzzy set , that will be called "fuzzy compatibility of the metric space with the fuzzy set considered". In this paper, we have introduced some topological properties of metric spaces under the said compatibility.

Motivation: We have fuzzy metric spaces in which fuzziness is internal phenomenon. From this point of view we get motivation to introduce some external phenomenon using fuzziness with metric spaces.

Notations: In a metric space (X, d) we usually denote the functional value of d at $(x, y) \in X^2$ by $d(x, y)$. Instead of using this traditional notation, we denote d by 'o' and for all $(x, y) \in X^2$, we denote $d(x, y)$ by $x \circ y$. Thus we represent
a metric space as $(X, \circ)$, where $\circ : X^2 \to \mathbb{R}$ satisfy
(i) $x \circ y \geq 0, \ \forall x, y \in X$.
(ii) $\forall \ x, y \in X, \ x \circ y = 0$ iff $x = y$.
(iii) $x \circ y = y \circ x, \ \forall x, y \in X$.
(iv) $x \circ z \leq x \circ y + y \circ z, \forall x, y, z \in X$.

Introduction and some Preliminaries: Zadeh introduced fuzzy set in 1965 [4] as a class of objects with a continuum of grades of membership, which is characterized by a membership (characteristic) function which assigns to each object a grade of membership ranging between zero and one, *i.e.*, a fuzzy set *A* on a universe *X* is a function from *X* to the closed interval *[0, 1]*. Heilpern [1] in 1981, introduced the concept of fuzzy contractive mappings and gives a fixed point in linear metric space. Here we are going to establish a new class of metric space which is Fuzzy compatibility of metric space with special contraction. [2] and [3] help us to establish a lot of results.

First we shall recall some basic definition:

(i) The fuzzy union or simply the union $A \cup B$ of the fuzzy sets A and B on a universe X is given by $(A \cup B)(x) = max\{A(x), B(x)\}, \forall\, x \in X$.

(ii) The fuzzy intersection or simply the intersection $A \cap B$ of the fuzzy sets A and B on a universe X is given by $(A \cap B)(x) = min\{A(x), B(x)\}, \forall\, x \in X$.

(iii) The fuzzy complement or simply the complement A^c of a fuzzy set A on a universe X is given by $A^c(x) = 1 - A(x), \forall\, x \in X$.

(iv) The fuzzy difference or simply the difference $A - B$ of the fuzzy sets A and B on a universe X is given by $(A - B)(x) = min\{A(x), 1 - B(x)\}, \forall\, x \in X$.

(v) Let $A_1, A_2, \ldots\ldots, A_n$ be n fuzzy sets on the universes $X_1, X_2, \ldots\ldots, X_n$ respectively. Then the fuzzy Cartesian product of $A_1, A_2, \ldots\ldots, A_n$ is denoted by $A_1 \times A_2 \times \ldots \times A_n$ or by $\times_{i=1}^{n} A_i$ and is defined to be a fuzzy set on the universe $X_1 \times X_2 \times \ldots\ldots \times X_n$, given by
$(\times_{i=1}^{n} A_i)(x_1, x_2, \ldots x_n) = min\{A_1(x_1), A_2(x_2), \ldots, A_n(x_n)\} \,\forall (x_1, x_2, \ldots x_n) \in\ \times_{i=1}^{n} X_i$.

(vi) Let A be a fuzzy set on a universe X and $\alpha \in [0, 1]$. The α-cut of A is given by $A^\alpha = \{x \in X\,|A(x) \geq \alpha\,\}$. And the strong α-cut of A is given by $A^{\alpha+} = \{\,x \in X\,|\,A(x) > \alpha\}$.

(vii) Let $(X, \circ)$ and $(Y, \star)$ be metric spaces. Then a bijection $f : (X, \circ) \rightarrow (Y, \star)$ is said to be an isometry if $x \circ y = f(x) \star f(y), \forall\, x, y \in X$. In this case, $(X, \circ)$ is said to be isometric with the metric space $(Y, \star)$.

(viii) Let $f : X \rightarrow Y$ be a mapping. Then for any fuzzy set A on X, the f-image $f(A)$ of A is a fuzzy set on Y, defined by $f(A)(y) = Sup\{A(x)\,|\,y = f(x)\,\}, \forall\, y \in Y$.

 Results :
1. Properties of metric spaces under fuzzy compatibility:

Definition (1.1)[Fuzzy compatibility of a metric space] Let $(X, \circ)$ be a metric space and A be a fuzzy set on X. The metric space $(X, \circ)$ is said to be compatible with A if there exists $c \in X$ such that $x \circ c = 1 - A(x), \forall\, x \in X$. Such an element $c\ (\in X)$ is called a centre of the metric space $(X, \circ)$ with respect to A.

Example (1.2): Let X be a non-empty set and A be a fuzzy set on X such that $A: X \rightarrow [0, 1]$ is injective and $A(c)=1$ for some $c \in X$. Define $\circ : X^2 \rightarrow \mathbb{R}$ by $x \circ y = |\,A(x) - A(y)|, \forall\, x, y \in X$. Then it can be easily checked that $(X, \circ)$ is a metric space. We see that $c \in X$ and

$\forall\, x \in X, x \circ c = |\, A(x) - A(c)\,| = 1 - A(x)$. Therefore the metric space $(X, \circ)$ is fuzzy compatible with A.

Theorem (1.3): Let the metric space $(X, \circ)$ is compatible with a fuzzy set A on X having a centre c. Then (i) $A(c)=1$. (ii) c is unique as centre. (iii) c is unique such that $A(c) =1$

Proof : (i) We have $x \circ c = 1 - A(x), \forall\, x \in X$. Therefore $0 = c \circ c = 1 - A(c)$ which gives $A(c) = 1$.

(ii) Let c_1 be a centre in X . Then $A(c) = 1 = A(c_1)$. Now $c_1 \circ c = 1 - A(c_1) = 1 - 1 = 0$. Therefore $c_1 = c$ and hence c is unique.

(iii) Let $a \in X$ be arbitrary such that $A(a) = 1$. Now $a \circ c = 1 - A(a) = 1 - 1 = 0$. Therefore $a = c$ and hence c is unique such that $A(c)=1$.

Note (1.4): In Theorem(1.3) we observed that centre of a metric space $(X, \circ)$ which is compatible with a fuzzy set A on X, is unique. Therefore we call this unique centre as

" the centre " in $(X, \circ)$ with respect to A or simply, " the centre " in $(X, \circ)$.

Theorem(1.5): Let the metric space $(X, \circ)$ is compatible with a fuzzy set A on X having the centre c. Then $\forall\, x, y \in X$, $|\, A(x) - A(y)| \le x \circ y \le 2 - A(x) - A(y) \le 2$.

Proof : We have $1 - A(x) = x \circ c \le x \circ y + y \circ c = x \circ y + 1 - A(y)$.

This implies that $x \circ y \ge A(y) - A(x)$.   (1)

Again $1 - A(y) = y \circ c \le y \circ x + x \circ c = x \circ y + 1 - A(x)$.

This implies that $x \circ y \ge A(x) - A(y)$.   (2)

From (1) and (2) we have $|\, A(x) - A(y)| \le x \circ y$, $\forall\, x, y \in X$.   (3)

Now $x \circ y \le x \circ c + c \circ y = 2 - A(x) - A(y) \le 2$.   (4)

From (3) and (4), we have the result.

Note (1.6): From Theorem(1.5) we observed that, if a metric space $(X, \circ)$ be compatible with a fuzzy set A on X, then $|\, A(x) - A(y)| \le x \circ y$, $\forall\, x, y \in X$. Again in Example(1.2) we observed that, for a fuzzy set A on a non-empty set X, $(X, \circ)$ is a metric space which is compatible with A, where $\circ : X^2 \to \mathbb{R}$ is given by $x \circ y = |\, A(x) - A(y)|, \forall\, x, y \in X$. From these facts, we call the metric space of Example(1.2) as the fuzzy compatible metric space with the shortest or minimum metric.

Definition (1.7): A metric space $(X, \circ)$ which is compatible with a fuzzy set A on X and having the centre c, is said to be an invertible metric space with respect to A or simply, an invertible metric space if for every $a \in X$, $\exists\, a' \in X$ such that $a \circ a' = 1\, (= A(c))$. a' is called an inverse of a in X.

Theorem (1.8): Let c be the centre of a metric space $(X, \circ)$ which is compatible with a fuzzy set A on X. Then (i) if c' be an inverse of c then $A(c') = 0$.

(ii) if a' be an inverse of $a\ (\in X)$ in X then $A(a) + A(a') \le 1$.

Proof : (i) We have $c \circ c' = 1$.   (1)

Again $c \circ c' = 1 - A(c')$.   (2)

From (1) and (2) we have $A(c') = 0$.

(ii) We have $1 = a \circ a' \leq a \circ c + c \circ a' = 1 - A(a) + 1 - A(a')$.

This implies that $A(a) + A(a') \leq 1$.

Theorem (1.9): Let $(X, \circ)$ be a metric space which is compatible with a fuzzy set A on X. Then $\forall x \in X, \forall r \, (> 0) \in \mathbb{R}$,

$S(x, r) = \{y \in X \mid x \circ y < r\} \subseteq S_A(x, r) = \{y \in X \mid A(y) \in (A(x) - r, A(x) + r)\}$.

Proof : Let $y \in S(x, r)$ be arbitrary. Then $x \circ y < r$.   (1)

Again $|A(y) - A(x)| \leq x \circ y$.   (2)

From (1) and (2) we have $|A(y) - A(x)| < r$, $i.e., A(y) \in (A(x) - r, A(x) + r)$.

This implies that $y \in S_A(x, r)$. Therefore $S(x, r) \subseteq S_A(x, r)$.

Natural metric space induced by a fuzzy set:

Let A be a fuzzy set on a non-empty set X such that $A : X \to [0, 1]$ is injective and $A(c) = 1$ for some $c \in X$. Then $\forall x \in X$, $\forall r \, (> 0) \in \mathbb{R}$, we have

$S_A(x, r) = \{y \in X \mid A(y) \in (A(x) - r, \ A(x) + r)\}$.

Now for any given $x, y \in X$, the set $\{r \, (> 0) \in \mathbb{R} \mid y \in S_A(x, r)\}$,

$i.e., \{r \, (> 0) \in \mathbb{R} \mid A(y) \in (A(x) - r, A(x) + r)\}$,

$i.e., \{r \, (> 0) \in \mathbb{R} \mid \ |A(x) - A(y)| < r\}$ is bounded below and hence

$Inf \, \{r \, (> 0) \in \mathbb{R} \mid \ |A(x) - A(y)| < \ r\}$ exists.

Now define $\circ : X^2 \to \mathbb{R}$ by $x \circ y = Inf \, \{r \, (> 0) \in \mathbb{R} \mid \ |A(x) - A(y)| < r\}$, $\forall x, y \in X$.

Then clearly $\forall x, y \in X$, $x \circ y \geq 0$. Now let $x, y \in X$ be arbitrary such that $x \circ y = 0$,

$i.e., Inf \, \{r \, (> 0) \in \mathbb{R} \mid \ |A(x) - A(y)| < \ r\} = 0$. This implies that $|A(x) - A(y)| = 0$,

$i.e., A(x) = A(y)$. Therefore x = y (since $A: X \to [0, 1]$ is injective).

Conversely, if $x = y$, then $|A(x) - A(y)| = 0$ and hence

$x \circ y = Inf \, \{r \, (> 0) \in \mathbb{R} \mid \ |A(x) - A(y)| < r\} = 0$.

Now $\forall x, y \in X$ we have $x \circ y = Inf \, \{r \, (> 0) \in \mathbb{R} \mid \ |A(x) - A(y)| < r\}$.

$= Inf \, \{r \, (> 0) \in \mathbb{R} \mid \ |A(y) - A(x)| < r\} = y \circ x$.

Let $x, y, z \in X$ be arbitrary. Then $x \circ z = Inf\{r \, (> 0) \in \mathbb{R} \mid \ |A(x) - A(z)| < \ r\}$.   (1)

$x \circ y = Inf\{r \, (> 0) \in \mathbb{R} \mid \ |A(x) - A(y)| < r\}$.   (2)

$y \circ z = Inf\{r \, (> 0) \in \mathbb{R} \mid \ |A(y) - A(z)| < r\}$.   (3)

Now $|A(x) - A(z)| \leq |A(x) - A(y)| + |A(y) - A(z)|$.   (4)

From (2) it is clear that $|A(x) - A(y)| \leq x \circ y$.   (5)

and from (3) it is clear that $|A(y) - A(z)| \leq y \circ z$.   (6)

Therefore from (4) we have $|A(x) - A(z)| \leq x \circ y + y \circ z$ (by (5) and (6)).   (7)

From (1) and (7) we must have $x \circ z \leq x \circ y + y \circ z$. Therefore $(X, \circ)$ is a metric space.

Now $\forall x \in X$ we have $x \circ c = Inf\{r \, (> 0) \in \mathbb{R} \,|\, |A(x) - A(c)| < r\}.$
$= Inf\{r \, (> 0) \in \mathbb{R} \,|\, 1 - A(x) < r\} = 1 - A(x).$
Therefore the metric space $(X, \circ)$ is compatible with the fuzzy set A on .
This metric space is called the natural metric space induced by the fuzzy set.

Natural fuzzy set induced by a metric space:
Let $(X, \circ)$ be a metric space such that $\exists c \in X$ for which $x \circ c \in [0, 1], \forall x \in X$. Define
$A : X \to [0, 1]$ by $A(x) = 1 - x \circ c , \forall x \in X$. Then clearly A is a fuzzy set on X and the metric
space $(X, \circ)$ is compatible with the fuzzy set A is called the " natural fuzzy set induced by the
metric space $(X, \circ)$".

Example (1.10): Let $(X, \circ)$ be a metric space. Consider the metric space $(X, \star)$ given by
$x \star y = \frac{x \circ y}{1 + x \circ y} , \forall \, x, y \in X.$

Let c be a fixed element of X. Then $x \star c = \frac{x \circ c}{1 + x \circ c} \in [0, 1], \forall x \in \ X.$

Define $A : X \to [0, 1]$ by $A(x) = 1 - x \star c = 1 - \frac{x \circ c}{1 + x \circ c} = \frac{1}{1 + x \circ c}, \forall x \in X.$

Then clearly A is a fuzzy set on X and the metric space $(X, \star)$ is compatible with A having the
centre c.

Example (1.11): Let $(X, \circ)$ be a metric space. Consider the metric space $(X, \star)$ given by
$x \star y = min\{1, x \circ y\}, \forall \, x, y \in X.$ Let c be a fixed element of X.
Then $x \star c = min\{1, x \circ c\} \in [0, 1], \forall \, x \in X.$
Define $A : X \to [0, 1]$ by $A(x) = 1 - x \star c = 1 - min\{1, x \circ c \}, \forall \, x \in X.$
Then clearly A is a fuzzy set on X and the metric space $(X, \star)$ is compatible with A having the
centre c .

A Topology induced by a fuzzy set:
Let A be a fuzzy set on a non-empty set X. $\forall x \in X, \ \forall \, r \, (> 0) \in \mathbb{R},$ define
$S_A(x, r) = \{y \in X \,|\, A(y) \in (A(x) - r, A(x) + r) \},$
$i.e., S_A(x, r) = \{y \in X \,|\, |A(x) - A(y)| < r \}.$
Clearly $x \in S_A(x, r), \forall \, r \, (r > 0) \in \mathbb{R}.$ Now a subset Y of X is said to be an open set in X with
respect to A if for every $y \in Y, \ \exists \, r \, (> 0) \in \mathbb{R}$ such that $S_A(y, r) \subset Y.$

Now we have the following theorems.

Theorem (1.12) : Let A be a fuzzy set on a non-empty set X. Then
(i) Φ , X are open sets in X with respect to A.
(ii) For any $x \in X$ and any $r \, (> 0) \in \mathbb{R} , S_A(x, r)$ is an open set in X with respect to A.
(iii) Arbitrary union of open sets in X with respect to A is an open set in X with respect to A.
(iv) Finite intersection of open sets in X with respect to A is an open set in X with respect to A.

Proof : (i) By default, Φ is an open set in X with respect to A. Again for any $x \in X$ and for any $r \,(> 0) \in \mathbb{R}$, since $S_A(x,r) \subset X$, hence X is an open set in X with respect to A.

(ii) Let $x \in X$ be arbitrary and $r\,(> 0) \in \mathbb{R}$ be arbitrary. Let $y \in S_A(x,r)$ be arbitrary. Then $y \in X$ and $(y) \in (A(x) - r,\ A(x) + r)$.

Let $r_1 = \min\{A(y) - A(x) + r, A(x) + r - A(y)\}\,(> 0)$.

Then clearly $(A(y) - r_1, A(y) + r_1) \subset (A(x) - r, A(x) + r)$.   (1)

We shall show that $S_A(y,r_1) \subset S_A(x,r)$. Let $z \in S_A(y,r_1)$ be arbitrary.

Then $A(z) \in (A(y) - r_1, A(y) + r_1) \subset (A(x) - r, A(x) + r)$ (by (1)). This implies that $z \in S_A(x,r)$. Therefore $S_A(y,r_1) \subset S_A(x,r)$. But $y \in S_A(x,\ r)$ was arbitrary. Therefore $S_A(x,r)$ is an open set in X with respect to A.

(iii) Let $F = \{A_\mu \,|\mu \in I\ \}$ be an arbitrary family of open sets in X with respect to A. We shall show that $\bigcup_{\mu \in I} A_\mu$ is an open set in X with respect to A. Let $x \in \bigcup_{\mu \in I} A_\mu$ be arbitrary. Then $x \in A_{\mu_o}$ for some $\mu_o \in I$. Since A_{μ_o} is an open set in X with respect to A, $\exists r\,(> 0) \in \mathbb{R}$ such that $S_A(x,r) \subset A_{\mu_o} \subset \bigcup_{\mu \in I} A_\mu$. But $x \in \bigcup_{\mu \in I} A_\mu$ was arbitrary. Therefore $\bigcup_{\mu \in I} A_\mu$ is an open set in X with respect to A.

(iv) Let $A_1, A_2, \ldots\ldots, A_n$ be n open set in X with respect to A. We shall show that $\bigcap_{i=1}^{n} A_i$ is an open set in X with respect to A. If $\bigcap_{i=1}^{n} A_i = \Phi$ then proof is complete. Let $\bigcap_{i=1}^{n} A_i \neq \Phi$. Let $x \in \bigcap_{i=1}^{n} A_i$ be arbitrary. Then $x \in A_i$ for $i = 1, 2, \ldots\ldots, n$. For for $i = 1, 2, \ldots\ldots, n$ since A_i is an open set in X with respect to A, $\exists r_1\,(> 0) \in \mathbb{R}$ such that $S_A(\,x,r_i) \subset A_i$.

Then $\bigcap_{i=1}^{n} S_A(x,r_i) \subseteq \bigcap_{i=1}^{n} A_i$.   (1)

Let $r = \min\{r_1, r_2, \ldots\ldots, r_n\}\,(> 0)$. Then clearly $S_A(x,r) \subseteq S_A(x,r_i)$ for $i = 1, 2, \ldots\ldots, n$.

This implies that $S_A(x,r) \subseteq \bigcap_{i=1}^{n} S_A(x,r_i) \subseteq \bigcap_{i=1}^{n} A_i$ (by (1)).

But $x \in \bigcap_{i=1}^{n} A_i$ was arbitrary. Therefore $\bigcap_{i=1}^{n} A_i$ is an open set in X with respect to A.

Let τ_A be the collection of all open sets in X with respect to A. Then from Theorem(1.11), it is clear that τ_A is a topology on X. This topology is called the topology on X induced by A or equivalently, the topology compatible with A on X.

Theorem (1.13): Let $(X, \circ)$ be a metric space which is compatible with a fuzzy set A on X. Let τ_A be the topology on X induced by A. Let τ be the topology on X induced by the metric space $(X, \circ)$. Then $\tau_A \subseteq \tau$.

Proof : Let $B \in \tau_A$ be arbitrary. Let $x \in B$ be arbitrary.

Then $\exists r\,(> 0\,) \in \mathbb{R}$ such that $S_A(x,r) \subseteq B$.   (1)

Now $S(x,r) = \{y \in X\,|x \circ y < r\,\}$ is an open sphere in $(X, \circ)$ centered at x and of radius r.

We shall show that $S(x,r) \subseteq S_A(x,r)$. Let $y \in S(x,r)$ be arbitrary. Then $x \circ y < r$.   (2)

Since the metric space $(X, \circ)$ is compatible with the fuzzy set A on X, by Theorem(1.5) and by (2) we have $|A(x) - A(y)| \leq x \circ y < r$. Therefore $|A(x) - A(y)| < r$.

This implies that $y \in S_A(x,r)$.

Therefore $S(x,r) \subseteq S_A(x,r)$. Therefore $S(x,r) \subseteq S_A(x,r) \subset B$. (by (1))

Therefore $S(x,r) \subset B$. But $x \in B$ was arbitrary. Hence $B \in \tau$. Therefore $\tau_A \subseteq \tau$.

Theorem (1.14): Let A be a fuzzy set on a non-empty set X and $(X, \circ)$ is the natural metric space induced by A. Then the topology τ on X induced by the metric space $(X, \circ)$ and the topology τ_A on X induced by A are equivalent.

Proof: By Theorem(1.6) we have $\tau_A \subseteq \tau$.   (1)

Let $B \in \tau$ be arbitrary. Let $x \in B$ be arbitrary. Then $\exists\, r\,(> 0) \in \mathbb{R}$ such that $S(x,r) \subset B$. (2)

We shall show that $S_A\left(x, \frac{r}{2}\right) \subseteq S(x,r)$, where $S_A(x, \frac{r}{2}) = \{y \in X \mid |A(x) - A(y)| < \frac{r}{2}\}$.(3)

and $S(x,r) = \{y \in X \mid x \circ y < r\} = \{y \in X \mid Inf\{s\,(> 0) \in \mathbb{R} \mid |A(x) - A(y)| < s < r\}$. (4)

Let $y \in S_A(x, \frac{r}{2})$ be arbitrary. Then $|A(x) - A(y)| < \frac{r}{2}$ (by (3)). This shows that

$Inf\{s\,(> 0) \in \mathbb{R} \mid |A(x) - A(y)| < s\} \leq \frac{r}{2} < r$. Therefore $y \in S(x,r)$ (by (4)).

Therefore $S_A\left(x, \frac{r}{2}\right) \subseteq S(x,r)$.   (5)

From (2) and (5) we get $S_A\left(x, \frac{r}{2}\right) \subset B$. But $x \in B$ was arbitrary. Hence $B \in \tau_A$.

Therefore $\tau \subseteq \tau_A$.   (6)

From (1) and (6) we have $\tau = \tau_A$

Corollary (1.14): Every fuzzy set A on a non-empty set X induces a metrisable topology on X and hence the topology is Housdorff.

Theorem(1.15): Let A be a fuzzy set on a nonempty set X and (X, o) is the natural metric space induced by A. Then for any $x \in X$ and for any $r\,(> 0) \in \mathbb{R}$, $S(x, r) = S_A(x, r)$, where $S(x, r) = \{y \in X \mid x \circ y < r\}$ and $S_A(x, r) = \{y \in X \mid |A(x) - A(y)| < r\}$..

Proof: In the proof of Theorem(1.6) we established that $S(x,r) \subseteq S_A(x,r)$.   (1)

Now $\forall r_1 \in (0, \ r)$, we shall prove that $S_A(x, r_1) \subseteq S(x,r)$.

Let $r_1 \in (0, r)$ be arbitrary. Let $y \in S_A(x, r_1)$ be arbitrary. Then $|A(x) - A(y)| < r_1$.

This shows that $Inf\{s\,(> 0) \in \mathbb{R} \mid |A(x) - A(y)| < s\} \leq r_1 < r$, i.e., $x \circ y < r$.

Therefore $y \in S(x,r)$. Therefore $S_A(x, r_1) \subseteq S(x,r)$. Therefore if r_1 be a continuous real

variable which varies in the set $(0, r\,)$, then we have $S_A\left(x, \lim_{r_1 \to r^-}(r_1)\right) \subseteq S(x,r)$,

i.e., $S_A(x,r) \subseteq S(x, \ r)$.   (2)

From (1) and (2) we have $S_A(x,r) = S(x,r)$.

Theorem (1.16): Let A be a fuzzy set on a nonempty set X and $(X, \circ)$ is the natural metric space induced by A. Then for $\alpha \in [0, 1]$, $\forall x, y \in A^{\alpha+}$, $x \circ y \leq 1 - \alpha$, where $A^{\alpha+} = \{x \in X \mid A(x) > \alpha\}$ is the strong α-cut of A.

Proof: We have $\forall x, y \in X, x \circ y = Inf\{r\,(> 0) \in \mathbb{R} \mid |A(x) - A(y)| < r\}$.   (1)

Let $x, y \in A^{\alpha+}$ be arbitrary. Then $A(x) > \alpha$, $A(y) > \alpha$, i.e., $A(x), A(y) \in (\alpha, 1]$.

Hence $|A(x) - A(y)| < 1 - \alpha$.   (2)

From (1) and (2) we have $x \circ y \leq 1 - \alpha$.

Theorem(1.17): Let $(X, \circ)$ be a metric space which is compatible with two fuzzy sets A and B on X having respective centres $c_1, c_2 \in X$. Then
(i) $c_1 = c_2$ iff $A = B$.   (ii) $A(c_2) = B(c_1) \leq 1 - |A(x) - B(x)|, \forall x \in X$.
(iii) $x \circ y \leq 3 - (A(x) + B(y) + E), \forall x, y \in X$, where $E = A(c_2) = B(c_1)$.
(iv) $A(x) + B(x) \leq 1 + E, \forall x \in X$.
Proof: (i) Let $c_1 = c_2$. Now $A(x) = 1 - x \circ c_1 = 1 - x \circ c_2 = B(x), \forall x \in X$. Therefore $A = B$.
Conversely, let $A = B$. Then $A(c_1) = B(c_1)$. This implies that $1 = 1 - c_1 \circ c_2$ which gives $c_1 \circ c_2 = 0$. Therefore $c_1 = c_2$.

(ii) We have $A(c_2) = 1 - c_1 \circ c_2 = B(c_1)$. Therefore $(c_2) = B(c_1)$.   (1)
Now $\forall x \in X, 1 - A(x) = x \circ c_1 \leq x \circ c_2 + c_2 \circ c_1 = 1 - B(x) + c_2 \circ c_1$.
This implies that $c_2 \circ c_1 \geq B(x) - A(x), \forall x \in X$.   (2)
Again $\forall x \in X, 1 - B(x) = x \circ c_2 \leq x \circ c_1 + c_2 \circ c_1 = 1 - A(x) + c_2 \circ c_1$.
This implies that $c_2 \circ c_1 \geq A(x) - B(x), \forall x \in X$.   (3)
From (2) and (3) we have
$c_2 \circ c_1 \geq |A(x) - B(x)|, \forall x \in X, i.e., 1 - A(c_2) \geq |A(x) - B(x)|, \forall x \in X$.
This implies that $A(c_2) \leq 1 - |A(x) - B(x)|, \forall x \in X$.   (4)
From (1) and (4) we have $A(c_2) = B(c_1) \leq 1 - |A(x) - B(x)|, \forall x \in X$.

(iii) $\forall x, y \in X$ we have $x \circ y \leq x \circ c_1 + c_1 \circ y \leq x \circ c_1 + c_1 \circ c_2 + c_2 \circ y$
$= 1 - A(x) + 1 - E + 1 - B(y)$.
This implies that $x \circ y \leq 3 - (A(x) + B(y) + E), \forall x, y \in X$.

(iv) We have $1 - E = c_1 \circ c_2 \leq c_1 \circ x + x \circ c_2 = 2 - (A(x) + B(x)), \forall x \in X$.
This implies that $A(x) + B(x) \leq 1 + E, \forall x \in X$.

Theorem(1.18): If $(X, \circ)$ and $(X, *)$ be metric spaces both of which are compatible with a fuzzy set A on X, then $|x \circ y - x * y| \leq 2(1 - A(x)), \ 2(1 - A(y)), \forall x, y \in X$.
Proof: Let c_1, c_2 be the respective centres in $(X, \circ)$ and $(X, *)$ with respect to A.
Then $A(c_1) = 1 = A(c_2)$ and $A(x) = 1 - x \circ c_1 = 1 - x * c_2, \forall x \in X$.   (1)
From (1) we get $1 = A(c_1) = 1 - c_1 * c_2$.
This implies that $c_1 * c_2 = 0$ so that $c_1 = c_2 = c$ (say).
Therefore $A(x) = 1 - x \circ c = 1 - x * c, \forall x \in X$.
This implies that $x \circ c = x * c = 1 - A(x), \forall x \in X$.   (2)
Now $\forall x, y \in X, \ x \circ y \leq x \circ c + c \circ y = x * c + c * y$ (by (2)).   (3)
Again $\forall x, y \in X, \ x * c = x \circ c$ (By (2)) $\leq x \circ y + y \circ c = x \circ y + y * c$ (by (2)).
This implies that $x \circ y \geq x * c - y * c, \forall x, y \in X$.   (4)
Again $\forall x, y \in X, \ x * y \leq x * c + c * y$.   (5)
And $\forall x, y \in X, \ x * c \leq x * y + y * c$. This implies that $x * y \geq x * c - y * c, \forall x, y \in X$. (6)
From (3) and (4) we have $x * c - y * c \leq x \circ y \leq x * c + c * y, \forall x, y \in X$.   (7)
and from (5) and (6) we get $x * c - y * c \leq x * y \leq x * c + c * y, \forall x, y \in X$.   (8)
From (7) and (8) we get $-2(y * c) \leq x \circ y - x * y \leq 2(y * c), \forall x, y \in X$.
This implies that $|x \circ y - x * y| \leq 2(y * c) = 2(1 - A(y)), \forall x, y \in X$.   (9)

Interchanging x and y in (9), we get $|y \circ x - y \star x| \leq 2(1 - A(x)), \forall x, y \in X$,

i.e., $|x \circ y - x \star y| \leq 2(1 - A(x)), \forall x, y \in X$. $\qquad$ (10)

(9) and (10) give the required result.

Theorem(1.19): Let $(X, \circ)$ be a metric space which is compatible with two distinct fuzzy sets A and B on X having respective centres c_1 and c_2. Then

(i) there may not exist a metric space compatible with $A \cap B$.

(ii) there may not exist a metric space compatible with $A \cup B$.

(iii) there may not exist a metric space compatible with $A - B$, provided $A - B \neq A$.

Proof: (i) Since $A \neq B$, hence $c_1 \neq c_2$. (by theorem(1.17)(i)).

Again $A(c_1) = 1$ and $B(c_2) = 1$.

If possible, let (X, o_1) be a metric space which is compatible with the fuzzy set $A \cap B$ on X having centre c. Then $1 = (A \cap B)(c) = \min\{A(c), B(c)\} \leq A(c), B(c) \leq 1$.

This implies that $A(c) = 1 = B(c)$ and hence $c_1 = c = c_2$ (by Theorem(1.3)).

This contradicts the fact that $c_1 \neq c_2$. Hence the result.

(ii) Since $A \neq B$, hence $c_1 \neq c_2$. (by Theorem(1.17)(i)). Again $A(c_1) = 1$ and $B(c_2) = 1$.

If possible, let (X, o_1) be a metric space which is compatible with the fuzzy set $A \cup B$ on X having centre c. Then $(A \cup B)(c) = 1$. Now $(A \cup B)(c_1) = \max\{A(c_1), B(c_1)\} = A(c_1) = 1$.

Therefore $c_1 = c$ (by Theorem(1.3)).

Again $(A \cup B)(c_2) = \max\{A(c_2), B(c_2)\} = B(c_2) = 1$. Therefore $c_2 = c$ (by Theorem(1.3)).

Therefore $c_1 = c_2$, a contradiction. Hence the result.

(iii) Since $A \neq B$, hence $c_1 \neq c_2$. (by Theorem(1.17)(i)). Again $A(c_1) = 1$ and $B(c_2) = 1$.

If possible, let (X, o_1) be a metric space which is compatible with the fuzzy set $A - B$ on X having centre c. Then $1 = (A - B)(c) = \min\{A(c), 1 - B(c)\}$.

This implies that $A(c) = 1$ and $(c) = 0$. $\qquad$ (1)

Now $A(c) = 1$ implies that $= c_1$ (by Theorem(1.3)). $\qquad$ (2)

Now $1 - x o_1 c = (A - B)(x) = \min\{A(x), 1 - B(x)\}, \forall x \in X$. $\qquad$ (3)

Now $A(c_2) = 1 - c_2 \circ c$ ($\because c = c_1$) $= B(c) = 0$ (by (1)).

Therefore $1 = c_2 \circ c \leq c_2 \circ x + x \circ c = 2 - (A(x) + B(x)), \forall x \in X$.

This implies that $A(x) + B(x) \leq 1$, i.e., $A(x) \leq 1 - B(x), \forall x \in X$. $\qquad$ (4)

From (3) and (4) we get $1 - x o_1 c = (A - B)(x) = \min\{A(x), 1 - B(x)\} = A(x), \forall x \in X$.

Therefore $1 - B = A$, a contradiction. Hence the result.

Theorem (1.20): Let $(X, \circ)$ be a metric space which is compatible with a fuzzy set A on X. For $x \in X$ and $(r > 0) \in \mathbb{R}$, consider the open sphere $S(x, r) = \{y \in X \mid x \circ y < r\}$ in $(X, \circ)$.

Then $r \geq Sup\{|A(x) - A(y)| \mid y \in S(x, r)\}$.

Proof: By Theorem(1.5) we have, for all $y \in S(x, r)$, $|A(x) - A(y)| \leq x \circ y < r$.

Therefore $r \geq Sup\{|A(x) - A(y)| \mid y \in S(x, r)\}$.

Theorem (1.21): Let $(X, \circ)$ be a metric space which is compatible with a fuzzy set A on X. Then A is uniformly continuous on $(X, \circ)$ (considering the usual subspace metric on the closed interval $[0, 1]$).

Proof: Let $\epsilon > 0$ be given arbitrarily. Since $|A(x) - A(y)| \leq x \circ y, \forall x, y \in X$, hence

$|A(x) - A(y)| < \epsilon$ whenever $x \circ y < \delta \,(= \epsilon), \forall x, y \in X.$
This shows that A is uniformly continuous on X.

Theorem (1.22) : Let the metric space $(X, \circ)$ is isometric with the metric space $(Y, \star)$. If $(X, \circ)$ be compatible with a fuzzy set A on X, then $(Y, \star)$ is compatible with the fuzzy set $f(A)$ on Y, where $f: (X, \circ) \to (Y, \star)$ is an isometry.
Proof : We have $x_1 \circ x_2 = f(x_1) \star f(x_2), \forall x_1, x_2 \in X.$ (1)
Let c be the centre in X with respect to A.
Then $A(c) = 1$ and $c \circ x = 1 - A(x), \; \forall \, x \in X.$ (2)
Let $y \in Y$ be arbitrary. Since f is a bijection, there exists a unique $x \in X$ such that $y = f(x)$.
Now $f(A)(y) = Sup\{A(x) | \, y = f(x)\} = A(x) = (A \circ f^{-1})(y).$
Therefore, $f(A)(y) = (A \circ f^{-1})(y), \forall y \in Y.$ (3)
From (3) we get $(A)(f(c)) = (A \circ f^{-1})(f(c)) = A(c) = 1.$
And $f(c) \star f(x) = c \circ x = 1 - A(x) = 1 - (A \circ f^{-1})(f(x)) = 1 - f(A)(f(x)), \forall x \in X.$ (4)
Since f is bijective, from (4) we have $f(c) \star y = 1 - f(A)(y), \forall y \in Y$. Hence $(Y, \star)$ is compatible with $f(A)$.

*** We know that a fuzzy set A on $\mathbb{R}$ is a fuzzy number iff there exists a closed interval $[a, b] \,(\neq \Phi)$ such that
$$A(x) = \begin{cases} 1, & \forall \, x \in [a, b] \\ l(x), & \forall \, x \in (-\infty, a) \\ r(x), & \forall \, x \in (b, \infty) \end{cases}, \; \forall \, x \in \mathbb{R},$$
where $l: (-\infty, a) \to [0, 1]$ is monotonic increasing, continuous from right and $l(x) = 0$ for $x \in (-\infty, w_1)$, for some $w_1 \leq a$ and $r: (b, \infty) \to [0, 1]$ is monotonic decreasing, continuous from left and $r(x) = 0$ for $x \in (w_2, \infty)$, for some $w_2 \geq b$.

Now we have the following theorem.

Theorem (1.23): Let $(\mathbb{R}, \circ)$ be a metric space compatible with a fuzzy set A on $\mathbb{R}$ with centre c.
Then A is a fuzzy number iff $A(x) = \begin{cases} 1, & \text{for } x = c \\ l(x), & \text{for } x < c \\ r(x), & \text{for } x > c \end{cases}, \; \forall \, x \in \mathbb{R},$

where $l: (-\infty, c) \to [0, 1]$ is monotonic increasing, continuous from right and $l(x) = 0$ for $x \in (-\infty, w_1)$, for some $w_1 \leq c$ and $r: (c, \infty) \to [0, 1]$ is monotonic decreasing, continuous from left and $r(x) = 0$ for $x \in (w_2, \infty)$, for some $w_2 \geq c$.
Proof: Let A be a fuzzy number. Since $(\mathbb{R}, \circ)$ is compatible with the fuzzy number A with centre c, hence c is unique in $\mathbb{R}$ such that $A(c) = 1$, and hence $A(x) = \begin{cases} 1, & \forall \, x \in [c, c] \\ l(x), & \forall \, x \in (-\infty, c) \\ r(x), & \forall \, x \in (c, \infty) \end{cases}$,

$\forall \, x \in \mathbb{R}, \; i.e., A(x) = \begin{cases} 1, & \text{for } x = c \\ l(x), & \text{for } x < c \\ r(x), & \text{for } x > c \end{cases}, \; \forall \, x \in \mathbb{R},$

where $l:(-\infty, c) \to [0,1]$ is monotonic increasing, continuous from right and $l(x) = 0$ for $x \in (-\infty, w_1)$, for some $w_1 \le c$ and $r:(c,\infty) \to [0,1]$ is monotonic decreasing, continuous from left and $r(x) = 0$ for $x \in (w_2, \infty)$, for some $w_2 \ge c$.
Converse part is trivial.

Theorem (1.24): Consider the n metric spaces (X_i, o_i) for $i = 1, 2, \ldots\ldots, n$ and consider the product metric space $(X, \circ)$, where $X = \times_{i=1}^{n} X_i$ and $\forall (x_1, x_2, \ldots., x_n), (y_1, y_2, \ldots\ldots, y_n) \in X$,
$(x_1, x_2, \ldots., x_n) \circ (y_1, y_2, \ldots\ldots, y_n) = \sqrt{(x_1 o_1 y_1)^2 + (x_2 o_2 y_2)^2 + \cdots\ldots + (x_n o_n y_n)^2}$.
Let A be a fuzzy set on X such that $(c_1, c_2, \ldots\ldots, c_n)$ is the only element in X for which $A(c_1, c_2, \ldots\ldots, c_n) = 1$.
For each $i \in \{1, 2, \ldots\ldots, n\}$, consider the fuzzy set A_i on X_i given by
$A_i(x) = A(c_1, c_2, \ldots c_{i-1}, x, c_{i+1}, \ldots\ldots, c_n), \forall x \in X_i$.
If $(X, \circ)$ be compatible with A then (X_i, o_i) is compatible with A_i with centre c_i for $i = 1, 2, \ldots\ldots, n$.
Proof: Let $(X, \circ)$ be compatible with A. Since $(c_1, c_2, \ldots\ldots, c_n)$ is the only element in X such that $A(c_1, c_2, \ldots\ldots, c_n) = 1$ hence for every $i \in \{1, 2, \ldots\ldots, n\}$ we can say that c_i is the only element in X_i such that $A_i(c_i) = A(c_1, c_2, \ldots\ldots, c_n) = 1$.
Now for all $(x_1, x_2, \ldots., x_n) \in X, (c_1, c_2, \ldots\ldots, c_n) \circ (x_1, x_2, \ldots., x_n) = 1 - A(x_1, x_2, \ldots., x_n)$.
This implies that $\sqrt{(c_1 o_1 x_1)^2 + (c_2 o_2 x_2)^2 + \cdots\ldots + (c_n o_n x_n)^2} = 1 - A(x_1, x_2, \ldots., x_n)$. (1)
From (1) we have, for each $i \in \{1, 2, \ldots\ldots, n\}, \forall x \in X_i$,
$\sqrt{(c_1 o_1 c_1)^2 + (c_2 o_2 c_2)^2 + \cdots\ldots + (c_{i-1} o_{i-1} c_{i-1})^2 + (c_i o_i x)^2 + (c_{i+1} o_{i+1} c_{i+1})^2 + \cdots\ldots + (c_n o_n c_n)^2}$
$= 1 - A(c_1, c_2, \ldots c_{i-1}, x, c_{i+1}, \ldots\ldots, c_n)$.
This implies that $c_i o_i x = 1 - A_i(x)$ for each $i \in \{1, 2, \ldots\ldots, n\}, \forall x \in X_i$.
This shows that (X_i, o_i) is compatible with A_i and centre c_i for each $i \in \{1, 2, \ldots\ldots, n\}$.

Theorem (1.25): Consider the n metric spaces (X_i, o_i) for $i = 1, 2, \ldots\ldots, n$ and $X = \times_{i=1}^{n} X_i$.
Consider the metric $' \circ '$ on X, given by $\forall (x_1, x_2, \ldots., x_n), (y_1, y_2, \ldots\ldots, y_n) \in X$,
$(x_1, x_2, \ldots., x_n) \circ (y_1, y_2, \ldots\ldots, y_n) = \max\{x_1 o_1 y_1, x_2 o_2 y_2, \ldots\ldots, x_n o_n y_n\}$.
Let A be a fuzzy set on X such that $(c_1, c_2, \ldots\ldots, c_n)$ is the only element in X for which $A(c_1, c_2, \ldots\ldots, c_n) = 1$.
For each $i \in \{1, 2, \ldots\ldots, n\}$, consider the fuzzy set A_i on X_i given by
$A_i(x) = A(c_1, c_2, \ldots c_{i-1}, x, c_{i+1}, \ldots, c_n), \forall x \in X_i$.
If $(X, \circ)$ be compatible with A then (X_i, o_i) is compatible with A_i with centre c_i for $i = 1, 2, \ldots\ldots, n$.
Proof: Let $(X, \circ)$ be compatible with A. Since $(c_1, c_2, \ldots\ldots, c_n)$ is the only element in X such that $A(c_1, c_2, \ldots\ldots, c_n) = 1$ hence for every $i \in \{1, 2, \ldots\ldots, n\}$ we can say that c_i is the only element in X_i such that $A_i(c_i) = A(c_1, c_2, \ldots\ldots, c_n) = 1$.
Now for all $(x_1, x_2, \ldots., x_n) \in X, (c_1, c_2, \ldots\ldots, c_n) \circ (x_1, x_2, \ldots., x_n) = 1 - A(x_1, x_2, \ldots., x_n)$.
This implies that $\max\{c_1 o_1 x_1, c_2 o_2 x_2, \ldots\ldots, c_n o_n x_n\} = 1 - A(x_1, x_2, \ldots., x_n)$. (1)
From (1) we have, for each $i \in \{1, 2, \ldots\ldots, n\}, \forall x \in X_i$,
$\max\{c_1 o_1 c_1, c_2 o_2 c_2, \ldots\ldots, c_{i-1} o_{i-1} c_{i-1}, c_i o_i x, c_{i+1} o_{i+1} c_{i+1}, \ldots\ldots, c_n o_n c_n\}$
$= 1 - A(c_1, c_2, \ldots., c_{i-1}, x, c_{i+1}, \ldots\ldots, c_n)$.
This implies that $c_i o_i x = 1 - A_i(x)$, for each $i \in \{1, 2, \ldots\ldots, n\}, \forall x \in X_i$.
This shows that (X_i, o_i) is compatible with A_i and centre c_i for each $i \in \{1, 2, \ldots\ldots, n\}$.

Theorem(1.26): Let $X_1, X_2, \ldots\ldots, X_n$ be n non-empty sets and $X = \times_{i=1}^{n} X_i$. Let $(X,\circ)$ be a metric space which is compatible with a fuzzy set A on X having centre $(c_1, c_2, \ldots\ldots, c_n)$ $(\in X)$. For each $i \in \{1, 2, \ldots\ldots, n\}$, define $o_i : X_i^2 \to \mathbb{R}$ by
$x_i o_i y_i = (c_1, c_2, \ldots\ldots, c_{i-1}, x_i, c_{i+1}, \ldots\ldots, c_n) \circ (c_1, c_2, \ldots\ldots, c_{i-1}, y_i, c_{i+1}, \ldots\ldots, c_n)$, $\forall x_i, y_i \in X_i$.
And for each $i \in \{1, 2, \ldots\ldots, n\}$, define $A_i : X_i \to [0,1]$ by
$A_i(x_i) = A(c_1, c_2, \ldots\ldots, c_{i-1}, x_i, c_{i+1}, \ldots\ldots, c_n), \forall x_i \in X_i$.
Then for each $i \in \{1, 2, \ldots\ldots, n\}$, (X_i, o_i) is a metric space compatible with A_i having centre c_i.
Proof: Clearly (X_i, o_i) is a metric space for each $i \in \{1, 2, \ldots\ldots, n\}$.
Now for each $i \in \{1, 2, \ldots\ldots, n\}$, $\forall x_i \in X_i$,
$c_i o_i x_i = (c_1, c_2, \ldots\ldots, c_{i-1}, c_i, c_{i+1}, \ldots\ldots, c_n) \circ (c_1, c_2, \ldots\ldots, c_{i-1}, x_i, c_{i+1}, \ldots\ldots, c_n)$
$\qquad = 1 - A(c_1, c_2, \ldots\ldots, c_{i-1}, x_i, c_{i+1}, \ldots\ldots, c_n) = 1 - A_i(x_i)$. Hence the result.

Theorem (1.27): Let $(X,\circ)$ be a metric space compatible with a fuzzy set A on X having the centre c. Let B be a non-empty subset of X and $x \in X$. If x be a limit point of B, then for all $r\,(> 0) \in \mathbb{R}, \exists y\,(\neq x) \in B$ such that $|A(x) - A(y)| < r$.
Proof: Since x is a limit point of B, $\forall r\,(> 0) \in \mathbb{R}, \exists y\,(\neq x) \in B$ such that $y \in S(x, r) \subseteq S_A(x, r) = \{z \in X \mid |A(z) - A(x)| < r\}$. This implies that $|A(y) - A(x)| < r$. This completes the proof.

Theorem (1.28): Let $(X,\circ)$ be a metric space compatible with a fuzzy set A on X having the centre c. Let B be a nonempty subset of X. If c be a limit point of B, then for every $r \in (0, 1]$, $\exists x\,(\neq c) \in B$ such that $x \in A^{(1-r)+}$.
Proof: Since c is a limit point of B, for every $r \in [0, 1], \exists x\,(\neq c) \in B$ such that $x \in S(c, r)$. This implies that $c \circ x = 1 - A(x) < r$, $i.e.,$ $A(x) > 1 - r$. This shows that $x \in A^{(1-r)+}$.

Theorem (1.29): Every metric space $(X,\circ)$ is equivalent to a metric space $(X,\star)$ such that $(X,\star)$ is compatible with a fuzzy set A on X.
Proof: Let $(X,\circ)$ be a metric space. Consider the metric space $(X,\star)$, where $\star : X^2 \to \mathbb{R}$ is given by $x \star y = \frac{x \circ y}{1 + x \circ y}, \forall x, y, \in X$. We know that $(X,\circ)$ and $(X,\star)$ are equivalent metric spaces. Let c be a fixed element in X. Then $c \star x = \frac{c \circ x}{1 + c \circ x}$. Define a fuzzy set A on X by $A(x) = 1 - c \star x, \forall x \in X$. Then clearly $(X,\star)$ is compatible with A having centre c in X. Hence the result.

Another proof: Let $(X,\circ)$ be a metric space. Consider the metric space $(X,\star)$, where $\star : X^2 \to \mathbb{R}$ is given by $x \star y = \min\{1, x \circ y\}, \forall x, y \in X$. We know that $(X,\circ)$ and $(X,\star)$ are equivalent metric spaces. Let c be a fixed element in X. Then $c \star x = \min\{1, c \circ x\} \in [0, 1], \forall x \in X$. Define a fuzzy set A on X by $A(x) = 1 - c \star x, \forall x \in X$. Then clearly $(X,\star)$ is compatible with A having centre c in X. Hence the result.

Theorem (1.30): If $(X,\circ)$ be a metric space such that $x \circ y \in [0, 1], \forall x, y \in X$, then $(X,\circ)$ is compatible with a fuzzy set A on X.
Proof: Let c be a fixed element in X. Then $c \circ x \in [0, 1], \forall x \in X$. Define a fuzzy set A on X by $A(x) = 1 - c \circ x, \forall x \in X$. Then clearly $(X,\circ)$ is compatible with A having centre c in X. Hence the result.

Theorem (1.31): Let $(X,\circ)$ be a metric space and Y is a proper non-empty subset of X such that $Y \circ x + c \circ x = 1, \forall x \in X$, for exactly one $c \in X$, where $Y \circ x = Inf\{x \circ y \mid y \in Y\}$. Then $(X,\circ)$ is compatible with some fuzzy set on X having centre c.

Proof: Clearly $Y \circ x$, $c \circ x \in [0,1], \forall x \in X$. Define a fuzzy set A on X by
$A(x) = Y \circ x = 1 - c \circ x, \forall x \in X$.
Then clearly $(X,\circ)$ is compatible with the fuzzy set A having centre c.

Theorem (1.32): Let $(X,\circ)$ and $(Y,\star)$ be two isometric metric spaces and $(X,\circ)$ is compatible with a fuzzy set A on X having centre c. If $f: (X,\circ) \to (Y,\star)$ and $g: (X,\circ) \to (Y,\star)$ be any two isometries between $(X,\circ)$ and $(Y,\star)$, then (i) $f(c) = g(c) \ iff \ f(A) = g(A)$.
(ii) $f(A)(g(c)) = g(A)(f(c)) \le 1 - |f(A)(y) - g(A)(y)|, \ \forall \ y \in Y$.
(iii) $f(A)(y) + g(A)(y) \le 1 + E, \forall y \in Y$, where $E = f(A)(g(c)) = g(A)(f(c))$.
Proof: Since $(X,\circ)$ is compatible with the fuzzy set A having centre c and $f: (X,\circ) \to (Y,\star)$ and $g: (X,\circ) \to (Y,\star)$ are two isometries, hence by Theorem(1.15), $(Y,\star)$ is compatible with the fuzzy set $f(A)$ having centre $f(c)$ and $(Y,\star)$ is also compatible with the fuzzy set $g(A)$ having centre $g(c)$.
Now the proofs of (i) , (ii) and (iii) follow from Theorem(1.17)(i), Theorem(1.17)(ii) and Theorem(1.17)(iii) respectively.

Theorem (1.33): Let $(X_1, o_1), (X_2, o_2), \ldots \ldots, (X_n, o_n)$ be n metric spaces such that the metric space (X_i, o_i) is compatible with a fuzzy set A_i on X_i having centre c_i , for $i = 1, 2, \ldots \ldots, n$. Then the product metric space $(X,\circ)$ is compatible with the fuzzy set $\times_{i=1}^{n} A_i$ on X having centre $(c_1, c_2, \ldots \ldots, c_n)$, where $X = \times_{i=1}^{n} X_i$ and the product metric $\circ$ is given by
$(x_1, x_2, \ldots \ldots, x_n) \circ (y_1, y_2, \ldots \ldots, y_n) = \max\{x_1 o_1 y_1, x_2 o_2 y_2, \ldots \ldots, x_n o_n y_n\}$,
for all $(x_1, x_2, \ldots \ldots, x_n), (y_1, y_2, \ldots \ldots, y_n) \in X$.
Proof: We have $A_i(c_i) = 1$, for $i = 1, 2, \ldots \ldots, n$.   (1)
and $\forall x \in X_i, c_i o_i x = 1 - A_i(x), \ i = 1, 2, \ldots \ldots \ , n$.   (2)
Now the fuzzy set $\times_{i=1}^{n} A_i$ on X is given by
$(\times_{i=1}^{n} A_i)(x_1, x_2, \ldots, x_n) = \min\{A_1(x_1), A_2(x_2), \ldots, A_n(x_n)\}, \forall(x_1, x_2, \ldots, x_n) \in X$. (3)
Then $(c_1, c_2, \ldots \ldots, c_n) \in X$ and
$(\times_{i=1}^{n} A_i)(c_1, c_2, \ldots, c_n) = \min\{A_1(c_1), A_2(c_2), \ldots \ldots, A_n(c_n)\} = 1$ (by (1)).
And $\forall(x_1, x_2, \ldots \ldots, x_n) \in X$ we have
$(c_1, c_2, \ldots \ldots, c_n) \circ (x_1, x_2, \ldots \ldots, x_n) = \max\{c_1 o_1 x_1, c_2 o_2 x_2, \ldots \ldots, c_n o_n x_n\}$
$\qquad\qquad\qquad = \max\{1 - A_1(x_1), 1 - A_2(x_2), \ldots \ldots, 1 - A_n(x_n)\}$ (by (2))
$\quad = 1 - \min\{A_1(x_1), A_2(x_2), \ldots \ldots, A_n(x_n)\} = 1 - (\times_{i=1}^{n} A_i)(x_1, x_2, \ldots \ldots, x_n)$ (by (3)).
Therefore $(X,\circ)$ is compatible with the fuzzy set $\times_{i=1}^{n} A_i$ on X having centre $(c_1, c_2, \ldots \ldots, c_n)$.

Theorem (1.34): Let $(X_1, o_1), (X_2, o_2), \ldots \ldots, (X_n, o_n)$ be n metric spaces such that the product metric space $(X,\circ)$ is compatible with a fuzzy set A on X having centre $(c_1, c_2, \ldots \ldots, c_n)$, where $X = \times_{i=1}^{n} X_i$ and the product metric $\circ$ is given by $(x_1, x_2, \ldots \ldots, x_n) \circ (y_1, y_2, \ldots \ldots, y_n) = \max\{x_1 o_1 y_1, x_2 o_2 y_2, \ldots \ldots, x_n o_n y_n\}$, for all $(x_1, x_2, \ldots \ldots, x_n), (y_1, y_2, \ldots \ldots, y_n) \in X$.
Then there exists fuzzy sets $A_1, A_2, \ldots \ldots, A_n$ on $X_1, X_2, \ldots \ldots, X_n$ respectively such that (X_i, o_i) is compatible with A_i having centre c_i, for $i = 1, 2, \ldots \ldots, n$ and $A = \times_{i=1}^{n} A_i$.
Proof: We have $A(c_1, c_2, \ldots \ldots, c_n) = 1$.   (1)
and $(c_1, c_2, \ldots \ldots, c_n) \circ (x_1, x_2, \ldots \ldots, x_n) = \max\{c_1 o_1 x_1, c_2 o_2 x_2, \ldots \ldots, c_n o_n x_n\}$

$= 1 - A(x_1, x_2, \ldots \ldots, x_n), \forall\, (x_1, x_2, \ldots \ldots, x_n) \in X.$ \hfill (2)

From (2) it is clear that $c_i o_i x_i \in [0,1]$, for $i = 1, 2, \ldots \ldots, n$.

For $= 1, 2, \ldots \ldots, n$, define $A_i : X_i \to [0,1]$ by $A_i(x_i) = 1 - c_i o_i x_i$, $\forall x_i \in X_i$.

Then clearly $A_i(c_i) = 1$ and $c_i o_i x_i = 1 - A_i(x_i)$, for $i = 1, 2, \ldots \ldots, n$.

Therefore, for $i = 1, 2, \ldots \ldots, n$, (X_i, o_i) is compatible with A_i on X_i having centre c_i.

Now $\times_{i=1}^{n} A_i : X \to [0,1]$ is given by $\forall\, (x_1, x_2, \ldots \ldots, x_n) \in X$,

$(\times_{i=1}^{n} A_i)(x_1, x_2, \ldots \ldots, x_n) = \min\{A_1(x_1), A_2(x_2), \ldots \ldots, A_n(x_n)\}.$ \hfill (3)

Again from (2) we have $\forall\, (x_1, x_2, \ldots \ldots, x_n) \in X$,

$A(x_1, x_2, \ldots \ldots, x_n) = 1 - (c_1, c_2, \ldots \ldots, c_n) \circ (x_1, x_2, \ldots \ldots, x_n)$

$= 1 - \max\{c_1 o_1 x_1, c_2 o_2 x_2, \ldots \ldots, c_n o_n x_n\} = \min\{1 - c_1 o_1 x_1, 1 - c_2 o_2 x_2, \ldots \ldots, 1 - c_n o_n x_n\}$

$= \min\{A_1(x_1), A_2(x_2), \ldots \ldots, A_n(x_n)\} = (\times_{i=1}^{n} A_i)(x_1, x_2, \ldots \ldots, x_n).$

Therefore $A = \times_{i=1}^{n} A_i$.

Theorem (1.35): Let $(Y, \star)$ be a metric space compatible with a fuzzy set A on Y having centre c in Y. Then any extension $(X, \circ)$ of $(Y, \star)$ is compatible with a fuzzy set B on X having the same centre c and B is an extension of A from Y to X, provided $c \circ x \in [0, 1], \forall x \in X - Y$.

Proof: Let $(X, \circ)$ is any extension of $(Y, \star)$ such that $c \circ x \in [0, 1], \forall x \in X - Y$.

Clearly $\forall x \in Y,\ c \star x = c \circ x = 1 - A(x).$ \hfill (1)

Define $B : X \to [0, 1]$ by $\forall x \in X, B(x) = \begin{cases} A(x), & \forall x \in Y \\ 1 - c \circ x, & \forall x \in X - Y \end{cases}$ \hfill (2)

Then $B(c) = A(c) = 1$ and $\forall x \in X,\ c \circ x = \begin{cases} 1 - A(x), & \forall x \in Y \\ 1 - B(x), & \forall x \in X - Y \end{cases} = 1 - B(x)$ (by (2)).

Therefore $(X, \circ)$ is compatible with a fuzzy set B on X having the same centre c and B is an extension of A from Y to X.

Theorem (1.36): Let $(X, \circ)$ be a metric space and (Y, o_1), (Z, o_2) be two metric subspaces of $(X, \circ)$, compatible with fuzzy sets A on Y and B on Z respectively having common centre $c \in Y \cap Z$ such that $A = B$ on $Y \cap Z$. Then the metric subspace $(Y \cup Z, o_3)$ of $(X, \circ)$ is compatible with a fuzzy set on $Y \cup Z$.

Proof: Define $D : Y \cup Z \to [0, 1]$ by $\forall x \in Y \cup Z, D(x) = \begin{cases} A(x), & \forall x \in Y \\ B(x), & \forall x \in Z - Y \end{cases}$ \hfill (1)

Then $D(c) = A(c) = 1$. Now from (1), it is clear that $\forall x \in Y \cup Z,\ D(x) = 1 - c \circ x$, i.e., $c o_3 x = 1 - D(x), \forall x \in Y \cup Z$. Hence the result.

Theorem (1.37): Let $(X, \circ)$ be a metric space compatible with a fuzzy set A on X. Then there exists a quotient space $(Y, \star)$ of $(X, \circ)$, compatible with an injective fuzzy set on Y.

Proof: Let c be the centre in X with respect to A.

Then $A(c) = 1$ and $c \circ x = 1 - A(x), \forall x \in X.$ \hfill (1)

Define a binary relation ρ on X by $\rho = \{(x, y) \in X^2 \mid A(x) = A(y)\}$

Clearly ρ is an equivalence relation on X and hence we have the quotient set $X_\rho = $ the set of all ρ-equivalence classes.

Define $\star : X_\rho \times X_\rho \to \mathbb{R}$ by $[x] \star [y] = |A(x) - A(y)|,\ \forall [x], [y] \in X_\rho$.

We shall show that $\star$ is well-defined.

Let $[x], [x_1], [y], [y_1] \in X_\rho$ be arbitrary such that $[x] = [x_1]$, $[y] = [y_1]$. Then $A(x) = A(x_1)$ and $A(y) = A(y_1)$ so that $[x] \star [y] = |A(x) - A(y)| = |A(x_1) - A(y_1)| = [x_1] \star [y_1]$. Therefore $\star$ is well-defined. Clearly $\star$ is a metric on X_ρ.

Define $B: X_\rho \to [0, 1]$ by $B([x]) = A(x)$, $\forall\, [x] \in X_\rho$.

Then $\forall [x], [y] \in X_\rho, [x] = [y]$ iff $A(x) = A(y)$ iff $B([x]) = B([y])$.

Therefore B is well-defined and injective.

We see that $[c] \in X_\rho$ and $B([c]) = A(c) = 1$ (by (1)) and

$[c] \star [x] = |A(c) - A(x)| = |1 - A(x)| = 1 - A(x) = 1 - B([x]), \forall [x] \in X_\rho$.

Therefore the quotient space $(X_\rho, \star)$ of $(X, \circ)$, is compatible with the injective fuzzy set B with centre $[c]$ in X_ρ.

2. Subspace Topology

Let $(X, \circ)$ be a metric space compatible with a fuzzy set A on X having the centre c and Y be a non-empty subset of X. Consider the subspace $(Y, \star)$ of the metric space $(X, \circ)$. Then clearly $(Y, \star)$ is compatible with the fuzzy set $A_{/Y} : Y \to [0, 1]$, provided $c \in Y$, where $A_{/Y}$ is the restriction of A to Y.

Theorem (2.1): Let $(X, \circ)$ be a metric space compatible with a fuzzy set A on X having the centre c. Let Y be a non-empty subset of X. If for some $y \in Y, \exists r \in (0, 1]$ such that $y \in A^{(1-r)+}$, then the subspace $(Y, \star)$ of the metric space $(X, \circ)$ is compatible with the fuzzy set $A_{/Y}$, provided $S(y, r) \subset Y$.

Proof: To establish the result, it is sufficient to prove that $c \in Y$. Since $y \in A^{(1-r)+}$, hence $A(y) > 1 - r$. This implies that $1 - A(y) < r, i.e., c \circ y < r$. This implies that $c \in S(y, r) \subset Y$. Therefore $c \in Y$.

Theorem (2.2): Let $(X, \circ)$ be a metric space compatible with a fuzzy set A on X having the centre c. Let B be a non-empty subset of X. Then c is an interior point of B iff $A^{(1-r)+} \subset B$, for some $r \in (0, 1]$.

Proof: Let c be an interior point of B. Then $\exists r_1 (> 0) \in \mathbb{R}$ such that $S(c, r_1) \subset B$. If $r_1 \le 1$, then take $r = r_1$. If $r_1 > 1$, take any $r \in (0, 1]$ and in this case $r < r_1$.

Therefore, in any case $S(c, r) \subset B$.   (1)

Let $x \in A^{(1-r)+}$ be arbitrary. Then $A(x) > 1 - r$. This implies that $1 - A(x) < r$, i.e. $c \circ x < r$. This implies that $x \in S(c, r) \subset B$ (by (1)). Therefore $x \in B$.

Therefore $A^{(1-r)+} \subset B$.

Conversely let $A^{(1-r)+} \subset B$ for some $r \in (0, 1]$. To prove c is an interior point of B, it is sufficient to show that $S(c, r) \subset B$. Let $x \in S(c, r)$ be arbitrary. Then $c \circ x = 1 - A(x) < r$. This implies that $A(x) > 1 - r$ so that $x \in A^{(1-r)+} \subset B$. Therefore $x \in B$. Hence $S(c, r) \subset B$. Hence the result.

Theorem (2.3): Let $(X, \circ)$ be a metric space compatible with a fuzzy set A on X having the centre c. If a sequence $\{x_n\}$ in X is convergent in X then the sequence $\{A(x_n)\}$ is convergent in the metric subspace $[0, 1]$ of the usual metric space of real numbers.

Proof: Let $\epsilon > 0$ be given arbitrarily. Let $\{x_n\}$ converge to l in X. Since A is uniformly continuous on $X, \exists \delta > 0$ such that $|A(x) - A(l)| < \epsilon$, $\forall x \in X$ with $x \circ l < \delta$.   (1)

Then $\exists m \in \mathbb{N}$ such that $x_n \circ l < \delta, \ \forall n \geq m$. $\qquad$ (2)
Now (1) and (2) imply that $|A(x_n) - A(l)| < \epsilon, \ \forall n \geq m$.
Therefore the sequence $\{A(x_n)\}$ converges to $A(l)$ in $[0,1]$.

Corollary (2.4): Let $(X, \circ)$ be a metric space compatible with a fuzzy set A on X having the centre c. If a sequence $\{x_n\}$ in X converges to c then the sequence $\{c \circ x_n\}$ is a null sequence in the metric subspace $[0,1]$ of the usual metric space of real numbers.

Theorem (2.5): Let $(X, \circ)$ be a metric space compatible with a fuzzy set A on X. If a sequence $\{x_n\}$ in X is a Cauchy sequence in X then the sequence $\{A(x_n)\}$ is convergent in the metric subspace $[0,1]$ of the usual metric space of real numbers.
Proof: Let $\epsilon > 0$ be given arbitrarily. Let $\{x_n\}$ be a Cauchy sequence in X.
Then $\exists m \in \mathbb{N}$ such that $x_{n+p} \circ x_n < \epsilon, \ \forall n \geq m, \forall p \geq 1$. $\qquad$ (1)
Now $|A(x_{n+p}) - A(x_n)| \leq x_{n+p} \circ x_n < \epsilon, \ \forall n \geq m, \forall p \geq 1$ (by Theorem(1.5) and (1)).
This shows that $\{A(x_n)\}$ is Cauchy in $[0,1]$. But $[0,1]$ is a complete metric subspace of the usual metric space of real numbers. Therefore the sequence $\{A(x_n)\}$ is convergent in $[0,1]$.

Theorem (2.6): [Extension Theorem] Let $(X, \circ)$ be a metric space and Y be a dense set in X. Let the metric subspace $(Y, \star)$ of $(X, \circ)$ is compatible with a fuzzy set A on Y. Then A can be extended uniquely to a fuzzy set B on X such that $(X, \circ)$ is compatible with B.
Proof : If $Y = X$ then the proof is obvious.
Let $Y \neq X$. Define $B : X \to [0, 1]$ as follows:
For $x \in Y$ we declare $B(x) = A(x)$. If $x \in X - Y$ then x is a limit point of Y (since closure of Y is X) and hence there is a sequence $\{x_n\}$ in Y converging to x. Since every convergent sequence is Cauchy, $\{x_n\}$ is a Cauchy sequence in Y and $A : Y \to [0, 1]$ being uniformly continuous on Y (by Theorem(1.21)), the sequence $\{A(x_n)\}$ is a Cauchy sequence in $[0, 1]$ (with respect to the usual metric). $[0, 1]$ being complete metric subspace of the usual metric space $\mathbb{R}$ of real numbers (since $[0, 1]$ is a closed set in the complete metric space $\mathbb{R}$), the sequence $\{A(x_n)\}$ converges to a unique point y (say) in $[0, 1]$. We set $B(x) = y$.
To show that B is well-defined, we show that $B(x)$ depends only on x and is independent of the choice of the sequence $\{x_n\}$ in Y converging to x. Let $\{y_n\}$ be another sequence in Y converging to x. Now $x_n \star y_n = x_n \circ y_n \leq x_n \circ x + y_n \circ x \to 0$ as $n \to \infty$. Therefore, $\lim_{n \to \infty}(x_n \star y_n) = 0$.
Let $\epsilon > 0$ be arbitrary. Then by uniform continuity of A, $\exists \delta > 0$ such that $x_1, x_2 \in Y$, $x_1 \star x_2 < \delta$ implies that $|A(x_1) - A(x_2)| < \epsilon$.
Since $\lim_{n \to \infty}(x_n \star y_n) = 0$, $\exists m \in \mathbb{N}$, such that $\forall n \geq m, x_n \star y_n < \delta$ which gives $|A(x_n) - A(y_n)| < \epsilon$. Thus $|A(x_n) - A(y_n)| \to 0$, as $n \to \infty$. $\qquad$ (1)
Since $A(x_n) \to y$ as $n \to \infty$, from (1) we have $A(y_n) \to y$ as $n \to \infty$.
Hence corresponding to each $x \in X - Y$, the value of $y \ (= B(x))$ assigned to B in $[0, 1]$ is uniquely determined, *i.e.*, $B : X \to [0, \ 1]$ is well-defined. Clearly B is an extension of A to X as a fuzzy set on X.
We now show that B is uniformly continuous on X. Let $\epsilon > 0$ be preassigned arbitrarily. By uniform continuity of A on Y, $\exists \delta > 0$ such that $a_1, a_2 \in Y, a_1 \star a_2 < \delta$ implies that $|A(a_1) - A(a_2)| < \frac{\epsilon}{2}$. $\qquad$ (2)
Let $x_1, x_2 \in X$ be arbitrary such that, $x_1 \star x_2 < \frac{\delta}{2}$. It is enough to show that

$|B(x_1) - B(x_2)| < \epsilon$. Since $x_1, x_2 \in X = \bar{Y}$ (= the closure of Y), there are sequences $\{y_n\}$ and $\{z_n\}$ in Y converging to x_1, x_2 respectively. Then $m \in \mathbb{N}$ such that $y_n \star x_1 < \frac{\delta}{4}$ and $z_n \star x_2 < \frac{\delta}{4}$, $\forall n \geq m$. Now $y_n \star z_n = y_n \circ z_n \leq y_n \circ x_1 + x_1 \circ x_2 + z_n \circ x_2 < \frac{\delta}{4} + \frac{\delta}{2} + \frac{\delta}{4} = \delta, \forall n \geq m$

and hence $|A(y_n) - A(z_n)| < \frac{\epsilon}{2}$, $\forall n \geq m$ (by (2)).

Then $\lim_{n \to \infty} |A(y_n) - A(z_n)| = |B(x_1) - B(x_2)| \leq \frac{\epsilon}{2} < \epsilon$

This shows that B is uniformly continuous on X.

Hence B is unique, since we know that if $f, g : (M, \circ_1) \to (S \ \circ_2)$ be continuous functions from the metric space $(M, \circ_1)$ to the metric space $(S \ \circ_2)$, and if Z is a dense subset of M such that $f(x) = g(x), \forall x \in Z$, then $f = g$.

Now we shall show that $(X, \circ)$ is compatible with B. If $Y = X$ then there is nothing to prove. Let $Y \neq X$. Since $(Y, \star)$ is compatible with the fuzzy set A on Y hence $\exists c \in Y$ (c being the centre in Y with respect to A) such that $A(c) = 1$ and $c \star y = 1 - A(y), \forall y \in Y$.

Now $c \in X$ (since $Y \subset X$) and $B(c) = A(c) = 1$.

Let $x \in X$ be arbitrary. If $x \in Y$ then $c \circ x = c \star x = 1 - A(x) = 1 - B(x)$
$$(\text{since } B(x) = A(x), \forall x \in Y).$$

Let $x \in X - Y$. Then there exists a sequence $\{x_n\}$ in Y converging to x (since $\bar{Y} = X$).

Now $\forall n \in \mathbb{N}, c \circ x_n = c \star x_n = 1 - A(x_n)$.   (3)

Since $\{x_n\}$ is convergent, hence $\{x_n\}$ is Cauchy in $(Y, \star)$ and hence $\{A(x_n)\}$ is Cauchy in $[0, 1]$ (since A is uniformly continuous on $(Y, \star)$).

Since $[0, 1]$ is a complete metric subspace of the usual metric space $\mathbb{R}$ of real numbers, hence $\{A(x_n)\}$ converges to some point $y \in [0, 1]$ and $B(x) = y$.

Taking the limit as $n \to \infty$ on both sides of (3) we get $c \circ x = 1 - y = 1 - B(x)$.

Hence $(X, \circ)$ is compatible with B. This completes the proof.

Corollary (2.7): Let Y be a non-empty set in a metric space $(X, \circ)$ such that the metric subspace $(Y, \star)$ of $(X, \circ)$ is compatible with a fuzzy set A on Y. Then A can be extended to B as a fuzzy set on the metric subspace $(\bar{Y}, \circ_1)$ of $(X, \circ)$ such that $(\bar{Y}, \circ_1)$ is compatible with B, where $\bar{Y}$ is the closure of Y in $(X, \circ)$.

Theorem (2.8) [Completion Theorem]: Let $(X, \circ)$ be a metric space compatible with a fuzzy set A on X and $(Y, \star)$ be a completion of $(X, \circ)$. Then $(Y, \star)$ is compatible with a fuzzy set on Y.

Proof: Since $(Y, \star)$ is a completion of $(X, \circ)$, hence $(X, \circ)$ is isometric with a dense subspace $(Z, \circ_1)$ of $(Y, \star)$.

Since $(X, \circ)$ is isometric with $(Z, \circ_1)$ and $(X, \circ)$ is compatible with the fuzzy set A on X, hence , by Theorem(1.22), $(Z, \circ_1)$ is compatible with the fuzzy set $f(A)$ on Z, where $f : (X, \circ) \to (Z, \circ_1)$ is an isometry.

Since $(Z, \circ_1)$ is a dense subspace of $(Y, \star)$ and $(Z, \circ_1)$ is compatible with the fuzzy set $f(A)$ on Z, hence by Theorem(2.6), $f(A)$ can be extended to a fuzzy set B on Y such that $(Y, \star)$ is compatible with B. This completes the proof.

Theorem (2.9): Let $(X, \circ)$ be a compact metric space compatible with a fuzzy set A on X. Then $A(X)$ is compact in the metric subspace $[0,1]$ of the usual metric space $\mathbb{R}$ of real numbers.

Proof: We know that $A : X \to [0, 1]$ is uniformly continuous on X. Since $(X, \circ)$ is compact and

continuous image of a compact set is compact, hence the result.

Theorem (2.10): Let $(X,\circ)$ be a connected metric space having at least two elements such that it is compatible with a fuzzy set A on X. Then A cannot be a Crisp set.
Proof: Let c be the centre in X with respect to A. Since $A: X \to [0,1]$ is uniformly continuous on X and $(X,\circ)$ is connected, then if A be a Crisp set then A is a constant function. Therefore
$$A(x) = A(c) = 1, \forall x \in X. \tag{1}$$
Since $(X,\circ)$ is compatible with A having the centre c, hence c is the only element in X such that $A(c) = 1$. Therefore from (1) we have $X = \{c\}$ which is not the case. Hence the result.

Theorem (2.11): Let $(X,\circ)$ be a metric space compatible with a fuzzy set A on X having centre c .
(i) If B be a connected set in X then $A(B)$ is connected in the metric subspace $[0,1]$ of the usual metric space $\mathbb{R}$ of real numbers.
(ii) If B be a connected set in X having at least two elements and $c \in B$ then $A(B)$ is an interval in the metric subspace $[0,1]$ of the usual metric space $\mathbb{R}$ of real numbers.
Proof: (i) We know that $A: X \to [0,1]$ is uniformly continuous and hence continuous. Also we know that if $f: (Y,\circ_1) \to (Z,\circ_2)$ be a continuous function from the metric space $(Y,\circ_1)$ to the metric space $(Z,\circ_2)$ and if W be a connected set in Y, then $f(Y)$ is a connected set in Z. Hence $A(B)$ is connected in the metric subspace $[0,1]$ of the usual metric space $\mathbb{R}$ of real numbers.

(ii) By (i), $A(B)$ is connected in the metric subspace $[0,1]$ of the usual metric space $\mathbb{R}$ of real numbers. Given that $c \in B$. Since B has at least two elements, let $x(\neq c) \in B$. Since c is unique element in X such that $A(c) = 1$, hence $A(x) \neq 1$. This shows that $A(B)$ has at least two elements and hence $A(B)$ is an interval in $[0,1]$, since we know that, a subset V of the real line $\mathbb{R}$, with at least two points, is connected if and only if V is an interval.

Theorem (2.12): Let $(X,\circ)$ be a metric space compatible with a fuzzy set A on X having centre c . If $(X,\circ)$ is connected, then $A(X) = [a, 1]$, where $a = Inf\{A(x)|x \in X\}$ is assumed by A.
Proof : We know that , every continuous real valued function from a connected metric space $(X,\circ)$ takes on all values between any two , it assumes. Since $a = Inf\{A(x)|x \in X\}$ is assumed by A and $A(c) = 1 = Sup\{A(x)|x \in X\}$, hence $A(X) = [a, 1]$, since $A: (X,\circ) \to [0, 1]$ is continuous.

Conclusion: In this article, we have established many topological properties in a metric space $(X,\circ)$ under its fuzzy compatibility with a fuzzy set A in X. Also we have studied some propries of A in the setting of this fuzzy compatibility.

Declaration of competing interest: We declare that we have no known competing financial interests or personal relationships that could have appeared to influence the work reported in this paper.

References

[1] S. Heilpern: Fuzzy mappings and fixed point theorem, *J. Math. Anal. Appl.* **83**, 566-569 (1981).
[2] G. J. Klir and B. Yuan: Fuzzy sets and fuzzy logic-theory and applications, *Prentice Hall P T R*, (1995).
[3] M. N. Mukherjee: Elements of Metric spaces, *Academic publishers*, (2005).
[4] L. A. Zadeh: Fuzzy Sets, *Information and Control*, **8**, 338-353 (1965).

Applications of perturbative and non-perturbative methods to 1D anharmonic vibration

Uttam Sinha Mahapatra

Associate Professor,Department of Physics, Barasat Government College, Barasat, Kolkata-700124, Email: mahapatrauttamsinha@gmail.com

Abstract : Quantum mechanical solution for one dimensional oscillator problem with different kind of anharmonicities have been studied with the help of basis set expansion procedure via some perturbative and non perturbative techniques. Rayleigh-Schrödinger (RS) variant perturbation theory (PT) up to third order in energy(second order in wave function) have been applied. Both Möller-Plesset(MP) and Epstein-Nessbet (EN) partitionings of the Hamiltonian have been employed. It is observed that EN partitioning based RSPT has better convergence behaviour than it's MP conterpart, in general. The performance of perturbative methods are compared with configuration interaction (CI) based energies. In addition, we have also applied those methodologies to find out the anharmonicity constant of of the potential energy curve of some diatomic molecules. It is found that CI results predicts anharmonicity constants well in comparision with experiments, whereas for PT methods one should go beyond third order in energy to have sensible predictions.

I   Introduction:

A large number of systems under certain approximations can be governed by harmonic oscillator equation when studies involved is the neighbourhood of a stable equillibrium position.The vibration of atom in molecules,atoms(ions) in solid about their equillibrium, can be well approximated(with small oscillations) by simple harmonic motion(SHM) equation. The underlying potential energy function of SHM is quadratic in nature where $v(x) = \frac{1}{2}kx^2$

with x as displacement from equilibrium position, and the angular frequency is $\omega = \sqrt{(k/m}$, m being the reduced mass of the oscillator. In real oscillations,however, oscillation amplitude is not small always due to strong perturbing influence of its neighbour (and possibly due to temperature effect) but if such an influence can be approximated by a function $v(x) = \beta x^3 + \gamma x^4 + \cdots$, and the total potential energy function $v(x) = \frac{1}{2}kx^2 + \beta x^3 + \gamma x^4 + \cdots$ (which is a positive definite function) and the oscillator in such potential is called anharmonic quantum mechanical oscillator(AHO). Exact quantum solution of the AHO problem does not exist. There exists many numerically oriented quantum mechanical methods([1]for an exaustive review) which are used to extract a set of lowest eigenvalues and eigenfunctions in an approximate ways. In order to solve the AHO problem we explore a few simple quantum-mechanical methods such as (1) Configuration expansion, or Configuration Interaction (CI) (2) Rayleigh-Schrodinger based perturbation methods(PT) in the following.

We organize the work as follows. First we outline the theoretical essentials pertaining to CI and PT methods. Secondly, we describe the computational implementation. Finally, we present some numerical results to highlight the usefulness of the(also drawbacks) methods followed by the concluding remarks.

II   Theory:

In order to discuss the methodologies used to describe the AHO problem, we indicate the unperturbed problem associated with, i.e. of simple harmonic oscillator. The eigen-value equation of un-perturbated harmonic oscillator is given by,

$$H_0|\phi_\mu\rangle = \epsilon_\mu|\phi_\mu\rangle; \quad \forall \mu = 0, 1 \cdots \infty \tag{1}$$

where $H_0 = -\frac{\hbar^2}{2m}\frac{d^2}{dx^2} + \frac{1}{2}kx^2$, defining $\omega = \sqrt{\frac{k}{m}}$, $\alpha = \sqrt{(\frac{m\omega}{\hbar})}$ and normalized wavefuctions ϕ_μ's are given by $\phi_\mu = \sqrt{(\frac{\alpha}{\sqrt{\pi}\,n!2^n})}\exp^{\frac{(-\alpha^2 x^2)}{2}} H_n(\alpha\ x)$ with corresponding eigenvalues $\epsilon_\mu = (\mu + \frac{1}{2})\hbar\omega$

The AHO problem is governed by the following equation

$$\mathcal{H}|\psi_n\rangle = \mathcal{E}_n|\psi_n\rangle \ \ \forall n = 0, 1 \cdots \infty \tag{2}$$

where $\mathcal{H} = H_0 + v(x)$ [$v(x)$, a polynomial of finite order in x].

As we have already indicated that exact quantum mechanical solution of eq.2 does not exist, so we will try for an approximate solution to this equation, where we focus at some approximate eigenstates of $\mathcal{H}$ which are energetically lowest lying, and to do that we expand ψ_n in terms of known complete set of functions $\{\phi_\mu\}$. In practice, however, we keep finite number of ϕ_μ from the infinity of $\{\phi_\mu\}$, i.e. we work in a function space which is subcomplete. In principle, one goes on increasing the dimension of this subcomplete space till a predefined numerical accuracy is acheived.

(1) CI method:

We concentrate, say, on n=0, and thus substituting $\psi_0 = \sum_{\mu=0}^{d-1} c_\mu \phi_\mu$ in eq.2 we land up in an equation which is defined in a finite subspace of the infinite hilbert space of the original eigenvalue equation(i.e. eq, 2). For notational convenience we use H instead of $\mathcal{H}$.

$$H \sum_{\mu=0}^{d-1} c_\mu |\phi_\mu\rangle = E_0 \sum_{\mu=0}^{d-1} c_\mu |\phi_\mu\rangle \tag{3}$$

premultiplying this equation by $\langle\phi_\nu|$ and $\forall \nu = 0, 1 \cdots$ d-1 we get d equations

$$H_{00}c_0 + H_{01}c_1 + \cdots + H_{0,d-1}c_{d-1} = E_0 c_0$$

$$H_{10}c_0 + H_{11}c_1 + \cdots + H_{1,d-1}c_{d-1} = E_0 c_1$$

$$\cdots\cdots$$

$$\cdots\cdots$$

$$H_{d-1,0}c_0 + H_{d-1,1}c_1 + \cdots + H_{d-1,d-1}c_{d-1} = E_0 c_{d-1}$$

Defining the Hamiltonian matrix

$$\mathbf{H} = \begin{pmatrix} H_{00} & H_{01} & \ldots & H_{0,d-1} \\ H_{10} & H_{11} & \ldots & H_{1,d-1} \\ \vdots & \vdots & \ddots & \vdots \\ H_{d-1,0} & H_{d-1,1} & \ldots & H_{d-1,d-1} \end{pmatrix}$$

where $\mathrm{H}_{ij} = \int dx\ \phi_i\ H(x)\ \phi_j = \epsilon_i\ \delta_{ij} + \int dx\ \phi_i\ v(x)\ \phi_j$

and the coefficient matrix is

$$
\mathbf{C} = \begin{pmatrix} c_0 \\ c_1 \\ \vdots \\ c_{d-1} \end{pmatrix}
$$

Defining thus H and C the above set of linear algebraic equations are cast as a matrix eigenvalue equation,

$$
\mathbf{H} \, \mathbf{C} = E_0 \, \mathbf{C} \tag{4}
$$

on diagonaliging eq.4, we get d eigenvalues (we symbolize these by a set $\{E_n\}$) and d eigenvectors (CI eigenvalues and eigenvectors). If we had used a complete orthonormal basis $\{\phi_\mu\}\forall \mu = 0, 1, \cdots \infty$, we would have obtained an equation identical to eq.2 except, of course, $\mathbf{H}$ would have been an infinite matrix. The eigenvalue of the matrix H in such a situation are exactly equal to the eigenvalues of the oerator $\mathcal{H}$(we do not know how to diagonalize an infinite matrix). Although, the eigenvalues of the matrix equation are apprxomitate solutions of orginal AHO problem, they have a very interesting property, an upper bound property with respect to the exact eigensolutions of eq.2 in the following sense:

$$
E_0 > \mathcal{E}_0 \, , E_1 > \mathcal{E}_1 \, , E_2 > \mathcal{E}_2 \, , E_3 > \mathcal{E}_3,
$$

$$
\vdots
$$

$$
and \;\; in \;\; the \;\; limit \;\; of \;\; d \;\; \longrightarrow \infty
$$

$$
E_0 \sim \mathcal{E}_0 \, , E_1 \sim \mathcal{E}_1 \, , E_2 \sim \mathcal{E}_2 \, , E_3 \sim \mathcal{E}_3
$$

The set of functions $\{\phi_\mu\}\forall \mu = 0, 1, \cdots d-1$, called unperturbed functions which act as basis functions for the expansion of approximate solution of ψ_0, in this way a CI method is also called a basis set expansion method. Within a specified basis space CI method delivers the best numerical results and these results are taken as reference to all other methods which also uses same basis space. We will discuss now a few PT methods which are also based on basis set expansion method.

(2) PT methods:

In a perturbation method the finite number of eigensolutions (i.e. ϕ_μ and λ_μ's) of H_0 are taken as building blocks. We define an operator Ω with it's representation in terms of these zeroth order quantities alongwith the perturbation operator(perturbing potential) $v(x)$ ($= \mathcal{H}$ -H_0), such that acting on ϕ_0 it produces exact state Ψ_0.

$$|\psi_0\rangle = \Omega|\phi_0\rangle \tag{5}$$

This equation also dictates that the operator Ω should reduce to unit operator if the perturbation $v(x)$ is switched off and then Ψ_0 reduces to ϕ_0. As each of the unperturbed functions in the set $\{\phi_\mu\}$ is normalised so ψ_0 is not. When $v(x)$ is switched on– the ground state wave function ψ_0 grows, additionally, beyond the function space defined by ϕ_0 and expanded into the entire function space defined by $\{\phi_\mu\}$. We assume that the weight of the unperturbed function ϕ_0 remains unmodified, in that we advocate using unnormalized total function when perturbation is on.

$$|\psi_0\rangle = |\phi_0\rangle + c_1|\phi_1\rangle + \cdots \tag{6}$$

Premultiplying above equation by $\langle\phi_0|$ (also using eq.5)we get so called intermediate normalization condition.

$$\langle\phi_0|\Omega|\phi_0\rangle = 1 \tag{7}$$

which suggests us to write $\Omega = 1 + \chi$ and $\psi_0 = \phi_0 + \sum_n^{\neq 0} c_n \phi_n$.

We stress here again that if ϕ_0 is a normalized function Ψ_0 is not, so that we have relation like these $\langle\phi_0|\phi_0\rangle = 1, \langle\psi_0|\psi_0\rangle \neq 1, \langle\phi_0|\psi_0\rangle = 1$

Now substituting eq. 5 in eq.**??** we get

$$\mathcal{H}\Omega|\phi_0\rangle = E\Omega|\phi_0\rangle \tag{8}$$

As discussed earlier we use a finite set of unperturbed eigen-functions of H_0 among infinite of them to define our "working" function space which form a subcomplete space with completeness and orthogonality property in the sense: $\langle\phi_\mu|\phi_\nu\rangle = \delta_{\mu\nu}$

and $\sum_{\mu=0}^{d-1} |\phi_\mu\rangle\langle\phi_\mu| = I(identity)$ which may also be written as, $|\phi_0\rangle\langle\phi_0| + \sum_{\mu=1}^{d-1} |\phi_\mu\rangle\langle\phi_\mu| = I$. We will use these two important identities in our development of perturbation theory.

Projecting eq.8 by $\langle\phi_0|$ we have,

$$\langle\phi_0|\mathcal{H}\Omega|\phi_0\rangle = E\langle\phi_0|\Omega|\phi_0\rangle = E \tag{9}$$

State energy is determined, provided the operator Ω is known to us.

Using expressions in eqs. 9 and 8 we have,

$$\mathcal{H}\Omega|\phi_0\rangle = \langle\phi_0|\mathcal{H}\Omega|\phi_0\rangle\Omega|\phi_0\rangle \tag{10}$$

To furnish a workable strategy to find Ω we partition $\mathcal{H}$ into $\mathcal{H} = \mathcal{H}_0 + V$, where $\mathcal{H}_0$ is readily managable to solve exactly, the rest portion of the hamiltonian is the perturbation which is defined by $V = \mathcal{H} - \mathcal{H}_0$, we emphasize here that $\mathcal{H}_0$, in general, different from the hamiltonian H_0 of SHO problem. Depending upon the choice there may be different partitionings of the given hamiltonian. It is also worthwhile to comment that the convergence of the perturbation series (either in energy or in wavefunction) crucially depends on partitioning type. For the time being we only assume that eigen-solutions of $\mathcal{H}_0$ is possible.

Using the partitioning of our hamiltonian $\mathcal{H}$ and carrying out some mathematical manipulations we arrive at the working set of equations of the operator Ω, which is non-perturbative in nature.

$$(\mathcal{H}_0 + V)\Omega|\phi_0\rangle = \langle\phi_0|(\mathcal{H}_0 + V)\Omega|\phi_0\rangle\Omega|\phi_0\rangle$$

$$\mathcal{H}_0\Omega|\phi_0\rangle + V\Omega|\phi_0\rangle = \langle\phi_0|\mathcal{H}_0\Omega|\phi_0\rangle\Omega|\phi_0\rangle + \langle\phi_0|V\Omega|\phi_0\rangle\Omega|\phi_0\rangle$$

$$\mathcal{H}_0\Omega|\phi_0\rangle + V\Omega|\phi_0\rangle = \lambda_0\langle\phi_0|\Omega|\phi_0\rangle\Omega|\phi_0\rangle + \langle\phi_0|V\Omega|\phi_0\rangle\Omega|\phi_0\rangle$$

$$(\lambda_0 - \mathcal{H}_0)\Omega|\phi_0\rangle = V\Omega|\phi_0\rangle - \langle\phi_0|V\Omega|\phi_0\rangle\Omega|\phi_0\rangle$$

Where the symbol $\lambda_0 = \langle\phi_0|\mathcal{H}_0|\phi_0\rangle$ has been employed. Expanding $\Omega = 1+\Omega^{(1)}+\Omega^{(2)}+\cdots$

substituting this in the last expressions we arrive at our final working equation which will determine orderwise expansion of wavefunction and energy. So we have

$$(\lambda_0 - \mathcal{H}_0)(1 + \Omega^{(1)} + \Omega^{(2)} + \cdots)|\phi_0\rangle = V(1 + \Omega^{(1)} + \Omega^{(2)} + \cdots)|\phi_0\rangle$$
$$- \langle\phi_0|V(1 + \Omega^{(1)} + \Omega^{(2)})|\phi_0\rangle(1 + \Omega^{(1)} + \Omega^{(2)} + \cdots)|\phi_0\rangle$$

Taking perturbation V as a quatity of order one, from previous expression we have

equating terms of zeroth order $(\lambda_0 - \mathcal{H}_0)|\phi_0\rangle = 0$ as zeroth order expansion

or,

$$\mathcal{H}_0|\phi_0\rangle = \lambda_0|\phi_0\rangle \tag{11}$$

This is eigen-value equation of unperturbed Hamiltonian.

Similarly equating all terms of order one we also get,

$$(\lambda_0 - \mathcal{H}_0)\Omega^{(1)}|\phi_0\rangle = V|\phi_0\rangle \tag{12}$$

Projecting by $\langle\phi_\nu|$ we get, $\langle\phi_\nu|(\lambda_0 - \mathcal{H}_0)\Omega^{(1)}|\phi_0\rangle = \langle\phi_\nu|V|\phi_0\rangle$

or, $(\lambda_0 - \lambda_\nu)\langle\phi_\nu|\Omega^{(1)}|\phi_0\rangle = \langle\phi_\nu|V|\phi_0\rangle$

or,

$$\omega_{\nu 0}^{(1)} = \frac{\langle\phi_\nu|V|\phi_0\rangle}{(\lambda_0 - \lambda_\nu)} \tag{13}$$

This is 1st order correction to the wavefunction.

In the similar manner we collect all terms of order two which reads as using the resolution of identity and using orthonormality of unperturbed functions and intermediate normalization condition:

$(\lambda_0 - \mathcal{H}_0)\Omega^{(2)}|\phi_0\rangle = V\Omega^{(1)}|\phi_0\rangle - \langle\phi_0|V|\phi_0\rangle\Omega^{(1)}|\phi_0\rangle$

Again projecting by $\langle\phi_\nu|$ we get,

$(\lambda_0 - \lambda_\nu)\langle\phi_\nu|\Omega^{(2)}|\phi_0\rangle = \langle\phi_\nu|V\Omega^{(1)}|\phi_0\rangle - \langle\phi_\nu|\Omega^{(1)}|\phi_0\rangle\langle\phi_0|V|\phi_0\rangle$

$$\omega_{\nu 0}^{(2)} = \sum_\beta{}' \frac{\langle\phi_\nu|V|\phi_\beta\rangle\langle\phi_\beta|V|\phi_0\rangle}{(\lambda_0 - \lambda_\nu)(\lambda_0 - \lambda_\beta)} - \frac{\langle\phi_0|V|\phi_0\rangle\langle\phi_\nu|V|\phi_0\rangle}{(\lambda_0 - \lambda_\nu)^2} \tag{14}$$

where prime denotes that the sum excludes $\beta=0$, and the last equation furnish all the second order components of Ω.

Now we turn our attention to the energy expression in eq.9. Once we calculate different components of Ω i.e. $\omega_{\nu 0}^{(1)}$ $\forall$ $\nu = 1, 2, \cdots (d-1)$ and $\omega_{\nu 0}^{(2)}$ $\forall$ $\nu = 1, 2, \cdots (d-1)$ we can obtain the energy correction

$E^{(2)}$, $E^{(3)}$ etc. using eq.9. $E = \langle \phi_0 | H\Omega | \phi_0 \rangle$

Using wave operator contribution up to second order we get energy corrected up to third order as $E[3] = \langle \phi_0 | (\mathcal{H}_0 + V)(1 + \Omega^{(1)} + \Omega^{(2)} | \phi_0 \rangle$

$= \langle \phi_0 | \mathcal{H}_0 (1 + \Omega^{(1)} + \Omega^{(2)}) | \phi_0 \rangle$

$+ \langle \phi_0 | V (1 + \Omega^{(1)} + \Omega^{(2)}) | \phi_0 \rangle$

$= \lambda_0 \langle \phi_0 | \Omega | \phi_0 \rangle + \langle \phi_0 | V(1 + \Omega^{(1)} + \Omega^{(2)}) | \phi_0 \rangle$

$= \lambda_0 + \langle \phi_0 | V | \phi_0 \rangle + \langle \phi_0 | V\Omega^{(1)} | \phi_0 \rangle + \langle \phi_0 | V\Omega^{(2)} | \phi_0 \rangle$

Here $\lambda_0 = \langle \phi_0 | \mathcal{H}_0 | \phi_0 \rangle$. $E^{(1)} = \langle \phi_0 | V | \phi_0 \rangle$ is the first order correction and $E^{(2)} = \langle \phi_0 | V\Omega^{(1)} | \phi_0 \rangle$ is the 2nd order correction to the energy eigen-value.

$E^{(3)} = \langle \phi_0 | V\Omega^{(2)} | \phi_0 \rangle = \sum_{\nu \neq 0} \langle \phi_0 | V | \phi_\nu \rangle \langle \phi_\nu | \Omega^{(2)} | \phi_0 \rangle$ is the third order correction to the energy eigen-value.

III COMPUTATIONAL DETAILS:

Using the zeroth order functions (we designate these also as basis functions) ϕ_μ from eq.1 we define the matrix elements of operator $V(x)$. The matrix representation of total hamiltonian operator $\mathcal{H}$ is then kept on the main memory which is used in subsequent computations. In general, the perturbation $V(x)$ may have any structure (it may be a high order polynomial or Morse type) we have calculated $H_{\mu\nu} = \int \phi_\mu V(x) \phi_\nu dx$ using numerical integration. Up to 11 harmonic oscillator functions are used. AS H is a hermitian matrix only lower traingular matrix elements are stored. To find out the numerical integrations we limit ourselves in the domoain -20 a.u.$\leq$ x $\leq$ 20 a.u. with 500 grid points.

In CI calculations use has been made of symmetrical diagonalization method of Householder. All the matrix elements $\omega_{\beta 0}^{(1)}, \omega_{\beta 0}^{(2)}$ were computed first and were kept in fast memory which were used in subsequent energy caculations. We have already indicated that defining zeroth order hamiltonian is very important, which has direct bearing to the convergence properties of the perturbation series. In the following we discuss two popular partitioning schemes which are employed in the perturbation calculations.

- SPECIFICATION OF $\mathcal{H}_0$:-

In Möller-Plesset method specification of $\mathcal{H}_0$ is as following:

$H_0 = \sum_i \epsilon_i a_i^\dagger a_i$

where $\lambda_i = \langle \phi_i | H_0 | \phi_i \rangle = \epsilon_i$

where a_i and $a_i^\dagger$ are usual particle annihilation creation operators in occupation number representation. But in Epstein-Nesbett method $H_0 = \sum_i h_i a_i^\dagger a_i$

where $h_i = \langle \phi_i | H | \phi_i \rangle$ i.e. all the diagonal terms of total hamiltonian $\mathcal{H}$ are included. So in MP partition the diagonal matrix elements of V(x) are included in the perturbation. The zeroth order hamiltonians in two cases are connected by $h_i = \lambda_i + \langle \phi_i | V(x) | \phi_i \rangle$ This is worthwhile to comment that as diagonals of H are included in H_0, in EN scheme first order energy shift $E^{(1)} = 0$.

IV   Results and discussions:-

In this section we discuss the results obtained when we solve an AHO problem by the numerical codes we have developed with CI and PT theories. To begin with and to test the code first we take the perturbing term $V(x) = \beta x^2$. The results obtained with the code with CI and MP based second order and third order results are plotted [see Figure 1] along with their EN counterparts. We have difined energy deviation $\Delta(E) = E(method) - E(exact)$ for each method and plotted these deviations for the sake of better representation.

The exact eigenenergies of the AHO hamiltonian with potential energy term$= \frac{1}{2}(k+2\beta)x^2$ would be $(n+1/2)\omega_0$, where $\omega_0 = \sqrt{\frac{(k+2\beta)}{m}}$. We note from Fig. 1   that for β values up to 1.0, essentially, there is no deviation of CI results in comparison to exact ground state energy values. However PT methods shows increasing deviation with increased β, however,
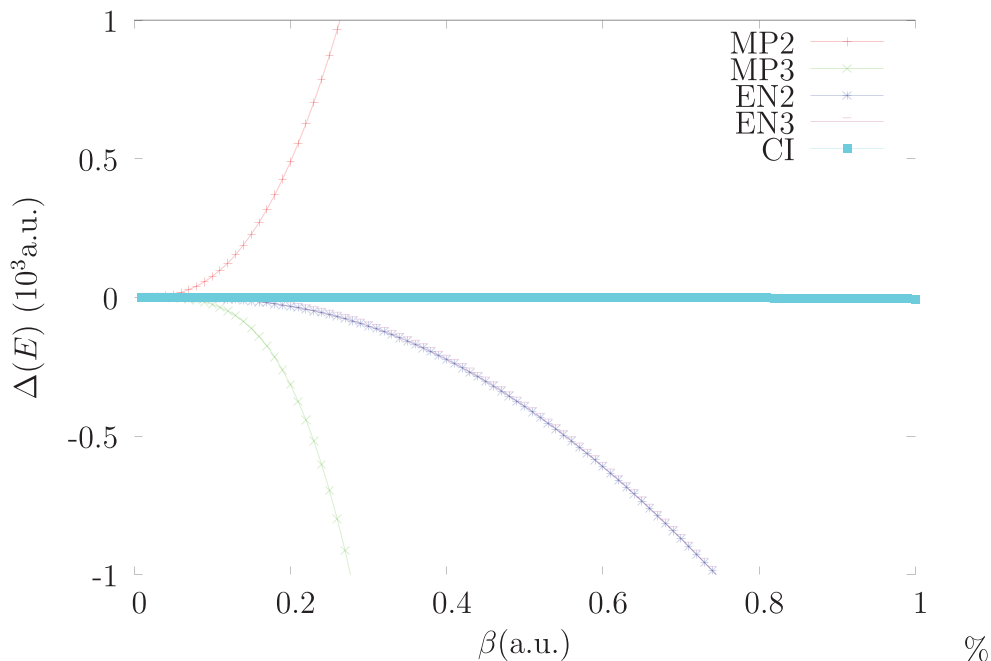
Figure 1: Performance of different method with respect to Exact result

EN results are closer to exact energy values compared to their MP counterparts.

In Fig.2 we have plotted energy values computed via MP2,MP3,EN2,EN3 alongwith CI along vertical axis and β along horizontal axis. For β up to 0.4 a.u all the methods perform fairly well, but with increasing β values performance of MP variants go down compared to their EN counterparts- the latter lies very close to CI values. Though EN3 goes in the opposite side to the CI compared to EN2 the former lies closer.

(2)Molecular applications:

For a reallistic application of the above-mentioned methods we now turn to the molecular vibrational problem with electronic Σ states of some diatomic molecules such as H_2, Be_2,F_2 molecules. As the molecules have only one vibrational degree of freedom it may be a test case to the CI and PT methods.

To begin with we first

compute the H_2 molecular dissociation curve by quantum mechanical(QM) full configuration interaction (FCI) method by GAMESS programme package [3] with a correlation consistent basis of triple-zeta variety. This basis although is not the best one it is enough to describe the behaviour of electrons in the ground state of H_2 molecule. The computed potential energy (PE) curve (V(R)$\sim$ R) is shown in Fig.3. (shown by QM data. We have
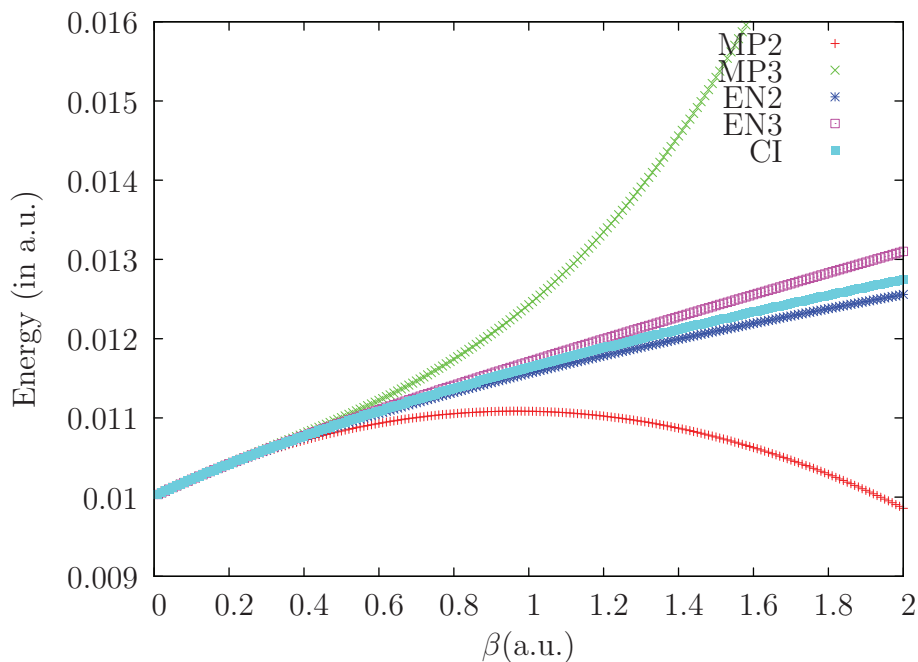
Figure 2: Plot of Energy with different Perturbation methods alonwith CI as function of β
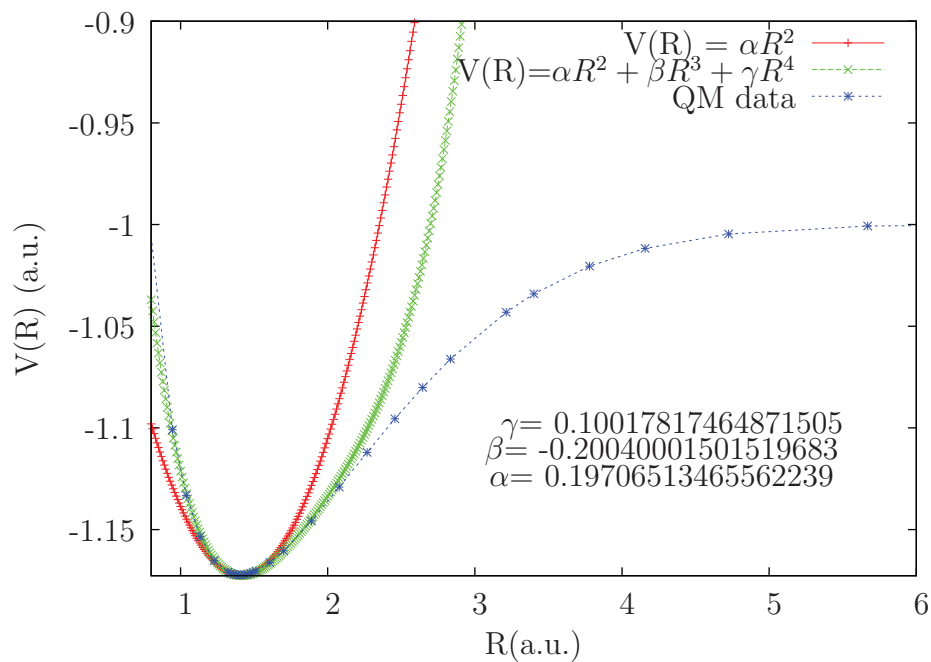
Figure 3: Taylor series expansion of V(R) in harmonic and anharmonic approx.

Table I: Spectroscopic constants of different molecules in
their ground electronic sate

Molecule	r_e (a.u.)	D_e (cm^{-1})	w_0 (cm^{-1})	$w_0\delta$ (cm^{-1})
H2	1.404(1.404)	33231.8(36780.8)	4385.0(4395.0)	123.5(126.0)
Be_2	4.73(4.64)	637.59(929.7)	243.19(222.6)	23.19
F_2	2.73(2.68)	12244.2(13389.5)	837.091(917)	15.55(11.2)

used the least square fitting procedure by finite order polynomials to have different fitted curves which approximately reproduces the given QM data. This polynomial function V(R) appear in the AHO problem. The harmonic approximation to this (red one) given by V(R) = 0.197065 x^2 as indicated in this Figure 3. The PE function of the vibrating H_2 molecule within harmonic approximation was used througout all the earlier applications of the project work. To get a more reallistic PE function we have taken some anharmonic terms of the true PE function. This case is indicated by V(R) = 0.197065 x^2 -0.20040 x^3 + 0.10017 x^4 (the green curve). This curve is almost coincident with the actual Potentian Energy Curve(PEC) to the left region of equilibrium (the minimum of PEC) and up to 2.6 a.u to the right side of the minima of the PEC. So we hope the second approximation to the PEC will represent the low lying vibrational energy levels of H_2. We have shown some spectroscopic datas of interest of the molecules in Table I : such as equilibrium bond length r_e,w_0, D_e for completeness. The anharmonicity parameter $w_0\delta$can be found approximately by the equation[4]

$$\omega' = \omega_0(n + 1/2) - \omega_0\delta(n + 1/2)^2 \tag{15}$$

ω_0 and ω' are the vibrational frequencies within harmonic and anharmonic approximations. The parameter $\omega_0\delta$ is called anhamonicity parameter. In Table I: we have presented corresponding experimental results within paraenthesis, whenever available. We see that our computed anhamonicity parameter (with CI method) for H_2 compares well with experiment. The anharmonicity parameter computed with EN PT methods deviates more than 50 cm^{-1} with respectet to experimental values, whereas MP methods predicts wrong sign.

This observation is reallistic in the sense the EN methods has better converegence properties and better representation of the situation as it takes diagonal matrix elements of the perturbing PE into zeroth order hamiltonian. In the example of Be_2 molecule, a very weakly bound one(dissociation energy is about 1/50 to that of H_2 molecular dissociation energy) , the potential energy function is taken from [5]. The expression for potential energy function v(x)= 1.5641536325 -85.6497682557/x 1986.92186292421/x^2 -25126.00202709961/x^3 + 183500.14891968661/x^4 -716552.61701591201/x^5 + 742394.41596868971/x^6 + 4932817.907090691/x^7 -14847343.558330741/x^8 -29948723.652553861/x^9+ 227010834.923468591/x^{10} -439134574.931347671/x^{11} + 300474684.366797271/x^{12}. Numerical optimization of this function (by solving $\frac{dv}{dx}$=0) gives r_e=4.73 a.u. and computing double derivative $(\frac{d^2v}{dx^2})_{r=r_e}$ gives the stiffness constant k. v(x) and V(x) are related by V(x)=v(x)-0.5kx^2. We see, given the difficulty of the very weak binding molecule, the results are in the correct direction which also confirms that the current model can predict first hand information regarding the correct eigenvalue structure of the molecular vibrational hamiltonian. The remaining deviation of anharmonicity constant lies in the accurate computation of the potential energy functions, discussions of which are out of the scope in the current study. In the same way, we have used the PEC of F_2 molecule and we see that the computed anaharmonicity constant is very close to the experiment, given the potential function which is moderate one[6].

V   Conclusion and Summarizing remarks:

We have employed some quantum mechanical methods to solve the AHO problem. All the methods, namely non perturbative CI and perturbative MP and EN partitionings based Rayleigh-Schrödinger PT methods are among them. All these methods are applied to ground vibrational state, although, they can be applied to excited vibrational states, in principle. In the pilot application with small β all methods perform well and can be used to extract reallistic inference for few lowest vibrational states. Finally, the methods are applied to find some spectroscopic parameters of vibrational problem of real molecules which valididate the usefulness of the methods described and applied here to some extant.

References

[1] J. C. Light, T. Carrington: Discrete-variable representations and their utilization, Adv. Chem. Phys. **114**, 263-310 (2000)

[2] T. H. Schucan, H. A. Weidenmüller: Perturbation theory for the effective interaction in nuclei, Ann. Phys. **72**, 483-509 (1972)

[3] GAMESS: The General Atomic and Molecular Electronic Structure System (GAMESS) is a general ab initio quantum chemistry package (a non-commercial quantum chemistry package). See www.msg.ameslab.gov/gamess.

[4] P. M. Morse: Diatomic Molecules According to the wave Mechanics.II. Vibrational levels, Phys. Rev**34**, 57-64 (1929)

[5] U. S. Mahapatra and S. Chattopadhyay: Single reference coupled cluster calculations for weakly bound alkaline-earth metal dimers in the ground state: a useful perturbative scheme for an iterative triples correction, Mol. Phys. **110**, 75-83 (2012)

[6] U. S. Mahapatra, B. Datta, and D. Mukherjee: A size-consistent state specific multi-reference coupled cluster theory: formal developments and molecular applications, J. Chem. Phys. **110**, 6171-6188 (1999).

Research Article

Density functional theory and its application for the structure and electronic properties of rutile MO$_2$ (M=Cr, V)

Animesh Ghosh, Muniya Mondal and Sarajit Biswas[*]

[1]Department of Physics, Barasat Government College, 10 K. N. C. Road, Kolkata-700124

*Email for Correspondence: sarajit.biswas@bgc.ac.in

Abstract In this work, the density functional theory is discussed and it is applied for the investigation of the structural and electronic properties of rutile transition metal dioxides MO$_2$ (M=Cr, V). Different Cr-O/V-O, Cr-Cr/V-V bond lengths and <Cr-O-Cr/<V-O-V, <O-Cr-O/<O-V-O bond angles are calculated and are compared with the experimental results. The magnitudes of different bond lengths and bond angles are consistent with experimental values. In the high-temperature tetragonal structure (space group I4$_2$/mnm), CrO$_2$ is found to be a half-metallic ferromagnet with a conductive/insulating spin majority/minority channel. On the other hand, VO$_2$ is found to be a nonmagnetic metal with both spin channels being conductive. It is revealed in this study that the partial filling of the Cr-t$_{2g}$ (d$_{xy}$, d$_{yz}$ and d$_{xz}$) orbitals for the spin majority channel is responsible for the half-metallic behaviour of CrO$_2$. For the V-counterpart, VO$_2$ the partial filling of V-t$_{2g}$ orbitals for both spin majority and spin minority channels is responsible for the metallic behaviour of VO$_2$. The p-d hybridization is responsible for the ferromagnetism in CrO$_2$, whereas opposite spin orientations in the two spin channels is responsible for the non-magnetic behaviour of VO$_2$.

1. Introduction

The transition metal oxides (TMOs) have unprecedented diversity in physical properties. The electrical and magnetic properties of TMOs have technological importance. At ambient conditions, these compounds belong to the rutile structure of a tetragonal unit cell with space group symmetryI4$_2$/mnm. Six O-atoms surrounding a V atom form an octahedron. Although the TMOs (TiO$_2$, VO$_2$, CrO$_2$, SnO$_2$, RuO$_2$, IrO$_2$ etc.) have an identical geometrical structure, they show a variety of electrical, magnetic, optical and mechanical properties. For example, the Ti-counterpart TiO$_2$ is an insulator with a band gap of 3.0 eV [1, 2]. At ambient conditions, rutile CrO$_2$ is a ferromagnetic half-metal [3, 4], The Ru counterpart, RuO$_2$ exhibits metallic conductivity at room temperature. This compound is considered as a promising material for electrical contact material, electrode conductors in the integrated circuits and optical thin film in ceramic resistors [5-8]. The tin oxide (SnO$_2$) is an n-type semiconductor with a wide band gap of~3.6 eV at 300K [9], which is suitable for transparent electrodes, far-infrared detectors, gas sensors and optoelectronic devices [10, 11]. The Ir-counterpart IrO$_2$ is a metal in the ambient pressure, which is used as electrodes in the application of high-density memory devices [12].

Rutile CrO_2, commonly known as chromium dioxide, is a remarkable material that has attracted significant attention due to its unique structural and electronic properties [3-5, 15-22]. Understanding the crystal structure and electronic characteristics of rutile CrO_2 is crucial for exploring its potential applications in various fields, including spintronic, magnetic storage devices, and emerging technologies. This introduction provides an overview of the importance of studying rutile CrO_2, the motivation behind investigating its structure and electronic properties, and the objectives of this study.

At present, the study of spintronic-based devices has become attractive due to their massive applications in the field of programmable logic elements, magneto-logic-random access memory (MRAM), non-volatile information devices and other reconfigurable circuits[13, 14]. Rutile CrO_2 has gained prominence in recent years due to its potential applications in advanced electronic devices. Its distinctive properties, such as its half-metallic behaviour and magnetic properties make it an attractive candidate for spintronic, where the spin of electrons is exploited for information storage and processing. By harnessing the unique characteristics of rutile CrO_2, it may be possible to develop more efficient and versatile electronic devices. Therefore, a comprehensive understanding of its crystal structure and electronic properties is essential. Spintronics or spin electronics refers to the utilization of electron quantum property called the spin in addition to the charge and mass of an electron. The capabilities of spintronic devices critically depend on the spin polarization of the underlying material. In this area, half-metallic ferromagnets (HMFs) are of particular interest, especially CrO_2 is considered a strong candidate for spintronic devices. Full spin polarization can be realized in CrO_2 because it is conductive in one spin channel and insulating in the other spin channel. It is also interesting to look for half-metals based on semiconductors. Many reports have been revealed to realize full spin polarization with a ferromagnetic Curie temperature Tc = 394 K in the half-metal CrO_2 [15-20]. Consequently, CrO_2 is widely used in the research works of half-metallic ferromagnetic electrodes to ensure highly spin-polarized current sources [21, 22]. The crystal structure of rutile CrO_2 plays a pivotal role in determining its properties and behaviour.

The V-counterpart, VO_2 has also received irreducible attention due to the rich variety in their structural, electronic and magnetic properties, along with their use in several applications [23-33]. It is currently considered one of the promising materials for oxide electronics. In the rutile phase, VO_2 is a nonmagnetic metal. VO_2 has been the most studied of all the vanadium oxides [23, 24] because it exhibits a structural phase transition (SPT) from the high temperature (HT) rutile phase to the low temperature (LT) monoclinic phase, along with a metal-insulator transition (MIT) at nearly room temperature (TMI = 341 K). It is appropriate for electrical, optical, thermal sensing and memory-based electronic devices due to the features resulting from MIT in VO_2 [25]. Even with a slight drop in temperature from TMI, an abrupt increase in electrical resistivity exceeding

several orders of magnitude is seen. The high electrical resistance of VO_2 makes it suitable for use in device manufacturing procedures. This compound is a nonmagnetic metal in the HT rutile phase. It adopts monoclinic M1 (space group $P2_1$/c) and M2 (space group C_2/m) insulating structures in the LT phase [26, 27]. For, The MIT in LT-VO_2 has several origins. It is believed that either a Mott-Hubbard transition [26] or a Peierls transition is responsible for the MITs in VO_2 [27].

The electronic properties of the two MO_2 (M=Cr, V), such as its band structure, the density of states (DOS), and magnetic behaviour are crucial for understanding its conductivity, magnetism and potential applications in the diverse field of materials science and technology. Exploring these properties will provide valuable knowledge for the design and development of novel electronic devices and materials. Thus the study of rutile MO_2 is of great importance due to their unique structural and electronic properties. Investigating their crystal structure and electronic characteristics will enable a deeper understanding of their behaviour and pave the way for the development of novel electronic devices. The objectives of this study involve utilizing theoretical techniques such as DFT to elucidate the structure and electronic properties of rutile CrO_2 and VO_2, contributing to the advancement of materials science and technology. The primary objective of this study is to investigate the crystal structure and electronic properties of rutile CrO_2 and VO_2 using density functional theory.

2. Methods of Calculations

Self-consistent spin-polarized electronic structure calculations of CrO_2 and VO_2 were carried out using density functional theory (DFT) [34, 35] as implemented in the tight-binding linearized - muffin-tin-orbitals (TB-LMTO) [36, 37] method. The local density approximations (LDA) [36, 38] were employed for exchange correlation functional. Both CrO_2 and VO_2 consist of a three-dimensional framework of distorted CrO_6 and VO_6 octahedra respectively, in which the distortion is due to a slight compression of the octahedral environment along the c-axis and the shift of Cr and V atoms from the centre. Both CrO_2 and VO_2 have an octahedral structure with the space group I4/m (space group number). The lattice parameters used for pure CrO_2 are a = b = 4.422Å and c = 2.917 Å with α=β=γ=90°. The primitive unit cell of CrO_2 contains two equivalent Cr and four equivalent O atoms with Cr atoms located at (0.0, 0.0, 0.0) and O atoms located at (0.302, 0.302, 0) [3]. On the other hand, the lattice parameters used for the structure of $VO_2$are a=b=4.5546 Å, c=2.8514 Å with α=β=γ=90°. The primitive unit cell of VO_2 also contains two equivalent V and four equivalent O atoms with V atoms located at (0.0, 0.0, 0.0) and O atoms located at (0.3001, 0.3001, 0.0) [39].

Before discussing the result it is mandatory to discuss some important points of density functional theory (DFT). Following are some important points about DFT which are very important for calculating DOS and electronic band structures.

2.1. Density Functional Theory (DFT)

Density-functional theory [34, 35] is one of the most popular and successful quantum mechanical approaches to matter. It is nowadays routinely applied for calculating, e.g., the binding energy of molecules in chemistry and the band structure of solids in physics. First applications relevant for fields traditionally considered more distant from quantum mechanics, such as biology and mineralogy are beginning to appear. Superconductivity, atoms in the focus of strong laser pulses, relativistic effects in heavy elements and atomic nuclei, classical liquids, and magnetic properties of alloys have all been studied with DFT. DFT owes this versatility to the generality of its fundamental concepts and the flexibility one has in implementing them. Despite this flexibility and generality, DFT is based on quite a rigid conceptual framework. This section introduces some aspects of this framework in general terms. In DFT, the many-body problem is addressed by mapping the interacting many-electron system onto an equivalent non-interacting system, where the electrons move independently in an effective potential. The key idea is to describe the electronic structure in terms of the electron density rather than individual electron wavefunctions. This reduces the complexity of the problem from dealing with the wave function of each electron to working with the electron density, which is a three-dimensional function of position.

To study the chemical and physical properties of a many-particle system (atoms, molecules, or solids), the electronic structure and total energy must be precisely determined. The electronic structure of basic systems can be satisfactorily explained by the solution of the Schrödinger equation (SE) since all system information is inherited in its wave function (ψ). For small numbers of atoms and molecules, numerically exact solutions can be achieved. Now, one needs to solve the SE related to the relevant system to find ψ. While the SE is relatively straightforward to solve for small systems, solving it for large systems becomes quite difficult.

For a large interacting system, one needs to consider a many-particle wave function. The many-body SE for the nuclei and electrons of a system has the following form,

$$\hat{H}\psi(\mathbf{r}, \mathbf{R}, t) = E\psi(\mathbf{r}, \mathbf{R}, t) \dots\dots\dots\dots\dots\dots\dots\dots\dots\dots\dots\dots\dots\dots\dots\dots (1)$$

This wave equation appears to be very simple but it is very difficult to solve it because the Hamiltonian $\hat{H}$ contains many terms as given below:

$$\hat{H} =$$

$$-\sum_N \frac{\hbar^2}{2M} \nabla_N^2 - \sum_i \frac{\hbar^2}{2m_e} \nabla_i^2 + \frac{1}{4\pi \epsilon_0} \frac{1}{2} \sum_{N \neq M} \frac{Z_N Z_M e^2}{|\mathbf{R}_N - \mathbf{R}_M|} +$$

$$\frac{1}{4\pi\epsilon_0} \frac{1}{2} \sum_{i \neq j} \frac{e^2}{|\mathbf{r}_i - \mathbf{r}_j|} - \frac{1}{4\pi\epsilon_0} \sum_{i,N} \frac{Z_N e^2}{|\mathbf{r}_i - \mathbf{R}_N|} \dots\dots\dots\dots\dots\dots\dots(2)$$

where M and Z_N, Z_M are the mass and charge of the nucleus, m_e and e are the mass and charge of an electron. The nuclear coordinates are given by R_N, R_M and the electronic coordinates are given by r_i, r_j.

However, approximation at several levels is needed to solve this SE. The first simplification of the SE's simplification is the Born-Oppenheimer approximation. The Born-Oppenheimer assumption states that nuclei are substantially heavier than electrons [40, 41]. The nuclei move far more slowly than the electrons as a result. The electrons are essentially in a condition of immediate equilibrium, whereas the nuclei remain stationary in their set positions. SE then takes the form

$$\left(-\sum_i \frac{\hbar^2}{2m_e}\nabla_i^2 + V_{ee} + V_{ext}\right)\psi_i(\mathbf{r_1}, \mathbf{r_2} \dots \mathbf{r_i} \dots \mathbf{r_N}) = E\psi_i(\mathbf{r_1}, \mathbf{r_2} \dots \mathbf{r_i} \dots \mathbf{r_N}) \dots\dots\dots\dots\dots\dots\dots(3)$$

where $V_{ee} = \frac{1}{4\pi\epsilon_0}\frac{1}{2}\sum_{i\neq j}\frac{e^2}{|\mathbf{r_i}-\mathbf{r_j}|}$ is electron-electron interaction and $V_{ext} = \frac{1}{4\pi\epsilon_0}\sum_{i,N}\frac{Z_N e^2}{|\mathbf{r_i}-\mathbf{R_N}|}$ is the electron-nucleus interaction.

It is still very difficult to solve Eqn. (3) due to the many-electron nature one needs further approximations to solve it. The next approximation towards solving SE was the Hartree approximation [42, 43]. According to Hartree approximation (HA), the total wave function of the system can simply be represented by the product of the wave function of each single particle (electron) wave function in the following way:

$$\psi = \psi_1(\mathbf{r}).\psi_2(\mathbf{r}).\psi_3(\mathbf{r}) \dots \psi_N(\mathbf{r}) \dots\dots\dots\dots\dots\dots\dots\dots\dots\dots\dots\dots\dots(4)$$

An electron moves under the influence of the average field (called the Hartree potential, V_H) of the other electrons which is given by

$$V_H(\mathbf{r}) = e^2 \sum_{j\neq i}^{N} \int \frac{|\psi_j(\mathbf{r_j})|^2}{|\mathbf{r_i}-\mathbf{r_j}|} d\mathbf{r_j} \dots\dots\dots\dots\dots\dots\dots\dots\dots\dots\dots\dots\dots\dots\dots\dots(5)$$

SE equation then takes the form

$$\left[\frac{-\hbar^2}{2m_e}\nabla_i^2 + V_H(\mathbf{r}) + V_{ext}(\mathbf{r})\right]\psi_i(\mathbf{r_i}) = E_i\psi_i(\mathbf{r_i}) \dots\dots\dots\dots\dots\dots\dots\dots\dots(6)$$

$$\Rightarrow \left[\frac{-\hbar^2}{2m_e}\nabla_i^2 + e^2 \sum_{j\neq i}^{N} \int \frac{|\psi_j(\mathbf{r_j})|^2}{|\mathbf{r_i}-\mathbf{r_j}|} d\mathbf{r_j} + V_{ext}(\mathbf{r})\right]\psi_i(\mathbf{r_i}) = E_i\psi_i(\mathbf{r_i}) \dots\dots\dots\dots\dots(7)$$

In the HA, two basic principles of quantum physics namely the antisymmetry principle and Pauli's exclusion principle were not considered. Also correlation and exchange interaction among the N-electrons were not accounted for in the HA. However, Fock corrected the HA with a few approximations which is known as the Hartree-Fock approximation (HFA) [44, 45]. According to HFA, the N-electron wave function can be replaced by the linear combination of the non-interacting single-electron wave function as below:

$$\Psi(1,\dots,N) = \frac{1}{\sqrt{N!}}\begin{vmatrix} \psi_1(1) & \psi_1(2) & \cdots & \psi_1(N) \\ \psi_2(1) & \psi_2(2) & \cdots & \psi_2(N) \\ \vdots & \vdots & \ddots & \vdots \\ \psi_N(1) & \psi_N(2) & \cdots & \psi_N(N) \end{vmatrix}$$

$$\dots\dots\dots\dots\dots\dots\dots\dots\dots\dots\dots\dots(8)$$

Then SE takes the form

$$\left[\frac{-\hbar^2}{2m_e}\nabla_i^2 + V_H(\mathbf{r}) + V_{ext}(\mathbf{r}) + V_x(\mathbf{r})\right]\psi_i(\mathbf{r_i}) = E_i\psi_i(\mathbf{r_i}) \dots\dots\dots\dots\dots\dots\dots(9)$$

where V_x= exchange potential comes from the antisymmetric nature of wave function and is given by,

$$V_x(\mathbf{r}) = -e^2 \sum_{j=i}^{N} \int \frac{\psi_j^*(\mathbf{r_j})\psi_i(\mathbf{r_j})\psi_j(\mathbf{r_i})}{|\mathbf{r_i}-\mathbf{r_j}|\psi_i(\mathbf{r_i})} d\mathbf{r_j} \dotfill (10)$$

And from Eqn. (9), we have

$$\left[\frac{-\hbar^2}{2m_e}\nabla_i^2 + V_{ext}(\mathbf{r}) + e^2 \sum_{j\neq i}^{N} \int \frac{|\psi_j(\mathbf{r_j})|^2}{|\mathbf{r_i}-\mathbf{r_j}|} d\mathbf{r_j} - e^2 \sum_{j=i}^{N} \int \frac{\psi_j^*(\mathbf{r_j})\psi_i(\mathbf{r_j})\psi_j(\mathbf{r_i})}{||\mathbf{r_i}-\mathbf{r_j}||\psi_i(\mathbf{r_i})} d\mathbf{r_j} \right] \psi_i(\mathbf{r_i})$$

$$= E_i\psi_i(\mathbf{r_i}) \dotfill (11)$$

Following the above approximations, massive computer resources are needed even for tiny systems to capture the detailed wave function, which is a function of 3N variables. DFT can be used to handle the SE for a many-body system satisfactorily. The approach first forth by Kohn, Hohenberg and Sham in the 1960s uses an effective one-body system to explain a real system [34, 35]. This is achieved by substituting the electronic density, which fluctuates only in three spatial coordinates, for the complex many-body wave function, which is the SE equation's solution. This density functional is the only one that can determine the energy of the system. Two theorems namely Hohenberg-Kohn (HK) 1st and 2nd theorem are the heart of the DFT.

The first HK theorem is stated as,

The ground-state energy is a unique functional of the electron density n(r).

This suggests that the ground state properties of a many-electron system can be uniquely represented by an electron density that depends on only three factors. This theorem gives a one-to-one mapping between the ground state charge density and ground state wave function and is mathematically represented as

$$E = E[n(\mathbf{r})] \dotfill (12)$$

The second HK theorem is stated as

The electron density that minimizes the energy of the overall functional is the true ground electron density.

$$i.e., E[n(\mathbf{r})] \geq E_0[n_0(\mathbf{r})] \dotfill (13)$$

The next effort for solving SE was the Kohn-Sham (KS) approximation [35]. The KS approach was the method that is most frequently adopted instead of minimizing the system's energy. All potential terms are expressed by a single effective potential, V_{eff} (r) by the Kohn-Sham approximation. Then SE equation takes the following form:

$$\left(-\frac{\hbar^2}{2m_e}\nabla_i^2 + V_{eff}(\mathbf{r}) \right) \psi_i(\mathbf{r}) = E_i\psi_i(\mathbf{r}) \dotfill (14)$$

This equation is known as the Kohn-Sham equation.

where $\qquad V_{eff}(\mathbf{r}) = V_{KS}(\mathbf{r}) \qquad$ ($V_{KS}(\mathbf{r})$ is called the Kohn-Sham potential)

$$= V_{ext}(\mathbf{r}) + V_H(\mathbf{r}) + V_{xc}(\mathbf{r}) \dots\dots\dots\dots\dots\dots\dots\dots\dots\dots\dots\dots\dots\dots(15)$$

The Hartree and exchange-correlation potential are calculated from the knowledge of electron density n(r) and are given by,

$$V_H(\mathbf{r}) = \frac{e^2}{4\pi\epsilon_0} \int \frac{n(\mathbf{r_j})}{|\mathbf{r}-\mathbf{r_j}|} d\mathbf{r_j} \dots\dots\dots\dots\dots\dots\dots\dots\dots\dots\dots\dots\dots\dots(16)$$

and $\qquad V_{xc}(\mathbf{r}) = \int \frac{\delta E_{XC}[n(r)]}{\delta n(r)} d\mathbf{r_j} \dots\dots\dots\dots\dots\dots\dots\dots\dots\dots\dots\dots\dots(17)$

$$\text{Then } V_{eff}(\mathbf{r}) = V_{ext}(\mathbf{r}) + \frac{e^2}{4\pi\epsilon_0} \int \frac{n(\mathbf{r_j})}{|\mathbf{r}-\mathbf{r_j}|} d\mathbf{r_j} + \int \frac{\delta E_{XC}[n(r)]}{\delta n(r)} d\mathbf{r_j} \dots\dots\dots\dots\dots(18)$$

The KS equation can also be written as,

$$\left(-\frac{\hbar^2}{2m_e} \nabla_i^2 + V_{KS}(\mathbf{r}) \right) \psi_i(\mathbf{r}) = E_i \psi_i(\mathbf{r}) \dots\dots\dots\dots\dots\dots\dots\dots\dots (19)$$

with $\qquad\qquad n(\mathbf{r}) = \sum_{i=1}^{N} |\psi_i(\mathbf{r})|^2 \dots\dots\dots\dots\dots\dots\dots\dots\dots\dots\dots\dots\dots (20)$

The interactive system can be effectively turned into a non-interacting system in this fashion and SE is then can be easily solved by computer implementation of the KS equation.

The algorithm used to solve SE using DFT is given below.

1. Guess the initial electron density n($\mathbf{r}$).

2. Construct the effective potential: $V_{eff}(\mathbf{r}) = V_{ext}(\mathbf{r}) + V_H[n(\mathbf{r})] + V_{xc}[n(\mathbf{r})]$.

3. Solve Kohn-Sham equation: $\left[-\frac{\hbar^2}{2m_e} \nabla^2 + V_{eff}(\mathbf{r}) \right] \psi_i(\mathbf{r}) = E_i \psi_i(\mathbf{r})$

4. Re-calculate the new electron density $n'(\mathbf{r}) = \sum |\psi_i(\mathbf{r})|^2$ and compare it with n($\mathbf{r}$).

(i) If$n'(\mathbf{r}) = n(\mathbf{r})$, then self-consistency is reached and the total ground state energy, magnetic moment, forces, band structure, densities of states, band gap etc. can then be calculated.

ii). If $n'(\mathbf{r}) \neq n(\mathbf{r})$, new n($\mathbf{r}$) is given and the above steps are repeated.

The flow chart of the DFT computer programming is shown below
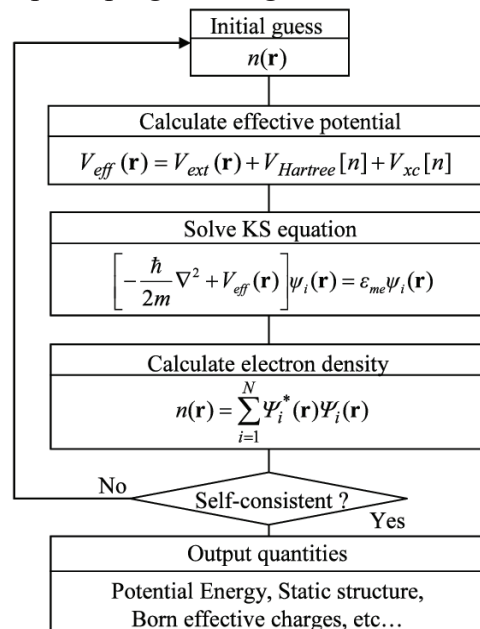
The most challenging aspect is determining the E_{xc} functional, as the exchange-correlation component of the total energy functional is still unknown. As a result, KS-DFT presents challenges in handling the exchange and correlation relationship. The correlation energy is yet not determined rigorously. The two most effective techniques for handling exchange and correlation energy are the Local-Density Approximation (LDA) [36, 38] and the Generalized Gradient Approximation (GGA) [46, 47]. There are several simulation packages available for DFT computations. Among them, the tight-binding linearized-muffin-tin-orbital (TB-LMTO) software packages [44-46] were utilized in our DFT calculations for the structure and electronic properties of CrO_2 and VO_2.

3. Results and discussions
3.1. Crystal structure of CrO_2 and VO_2

The crystal structure of Cr/VO_2 is shown in Fig. 1. Each Cr/V-atom has six oxygen coordination, forming a Cr/VO_6 octahedron. Out of these six O-atoms, four lie in the basal plane and the remaining two lie in the apical plane of the Cr/VO_6 octahedra. Every Cr/V site is located at the centre of the Cr/VO_6 octahedron. It is emerged from the LDA calculations that four neighbouring CrO_6 and VO_6 octahedra form a Cr-Cr and V-V square well (SW) respectively and found in the ab plane. In each Cr-Cr or V-V SW, Cr or V atoms in the opposite diagonal positions (z = 1 or z = 0) lie in the same mirror plane, i.e., every mirror symmetry preserves by the Cr/V-atoms at the opposite diagonal positions, as shown in Fig. 1(b). The calculated Cr-O, Cr-Cr bond distances and <Cr-O-Cr, <O-Cr-O bond angles are reported in Table 1. All the Cr-Cr double chains have uniform (2.9132 Å) bond distances. Additionally, the uniform Cr-Cr distances in the Cr-Cr square well column is responsible for the non-formation of Cr-Cr tetramers. All the <Cr-O-Cr bond angles are uniform (= 130.33°). The Cr-atoms within the Cr-Cr SWs are connected via O-atoms. The calculated different bond lengths and bond angles of CrO_2 are consistent with other reports [3].
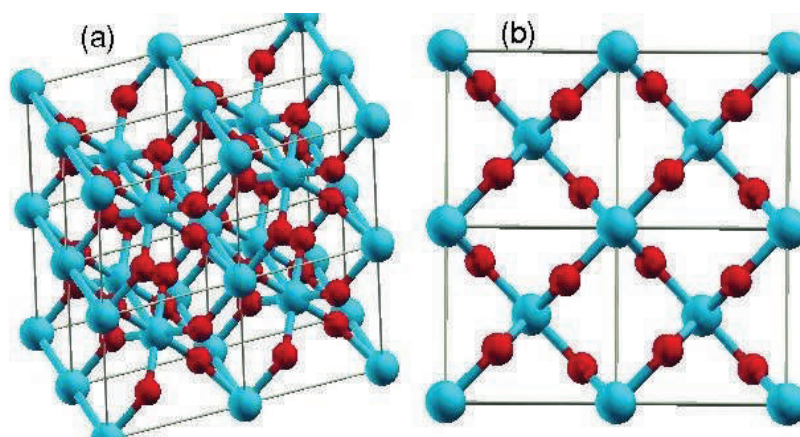
Fig. 1: The crystal structure of Cr/VO_6. The Cyan spheres represent Cr/V atoms and the red spheres represent O atoms.

Table 1: Calculated Cr-O, Cr-Cr bond distances and <Cr-O-Cr, <O-Cr-O bond angles of CrO_2 in the rutile structure.

	Apical	Basal
Cr-O bond distances (Å)	1.9132×2	1.8886×4
Cr-Cr distances (Å)	2.9132	2.9132
<O-Cr-O angles (°)	180	90×2
<Cr-O-Cr angles (°)	130.33×2	130.33×2

For the V counterpart, VO_2, the V-O distances measured as 1.9203Å and 1.9349Å for the apical and basal oxygen respectively (see Table 2). These distances are in good agreement with other report [39]. All V-atoms of the upper plane (z = 1) are connected to V-atoms of the lower plane (z = 0) via O atoms with uniform <V–O–V angle = 95.828°, which is also consistent with the values of 95.8° as measured by Korotin et al. The uniform V–V distance running in the c-direction is 2.8514 Å. Note that the reported value of V–V distances was 2.851 Å. The uniform V–O distance running in the c-direction is 1.9211 Å. All the V–V distances (in the ab plane) in the SWs have a uniform magnitude of 3.5220 Å. All the<O–V–O angles in the basal plane are uniform having a value of 90° (×4), which is also reflected in other reports. In the apical plane, it has the magnitude of 180°. The V atoms in the SW are connected via the O atom With <O–V–O bond angle = 132.086°. The V-atoms of the upper plane are connected to that at the lower plane via O-atoms with a uniform <V–O–V angle of 95.941°. The uniform V–V distances in the c-direction are 2.8528 Å.

Table 2: Calculated V-O, V-V bond distances and <V-O-V, <O-V-O bond angles of VO_2 in the rutile structure.

	Apical	Basal
V-O bond distances (Å)	1.9349×2	1.9203×4
V-V distances (Å)	3.5220	3.5220
<O-V-O angles (°)	180	95.828(×2)
<V-O-V angles (°)	132.086× 2	132.016

3.2. Electronic structure of CrO_2

We concentrate on the band structure of CrO_2. The total band structure of CrO_2 for the spin majority and spin minority spin channels are shown in Fig. 2(a) and 2(b) respectively. The system is metallic in the majority spin channel and insulting the minority spin channel. For the spin majority channel, the bands mainly found below -2.0 eV are the O-2p bands and the bands. The six

bands mainly found between -2.0 eV to 1.0 eV are the Cr-t_{2g} bands, whereas the four bands mainly found between 1.0 eV to 5.0 eV are the Cr-e_g bands [see Fig. 2(a)]. It is unambiguous that the Cr-t_{2g} orbitals are partially occupied by the available two Cr-3d electrons, whereas the Cr-e_g orbitals (d_{x^2}- and $d_{3z^2 - r^2}$) remain unoccupied. Therefore, the sharing of the available two electrons by the three Cr-t_{2g} orbitals (d_{xy}, d_{yz} and d_{xz}) is responsible for the metallic behaviour of CrO_2 for the spin majority channel. For the spin minority channel [Fig. 2(b)], both the Cr-t_{2g} (found mainly between 0.3 eV to 2.5 eV) and Cr-e_g (found mainly between 2.5 eV to 5.5 eV) orbitals are found unoccupied. Therefore, the system is insulating in the spin minority channel. Thus, considering both spin channels, CrO_2 is half-metallic.
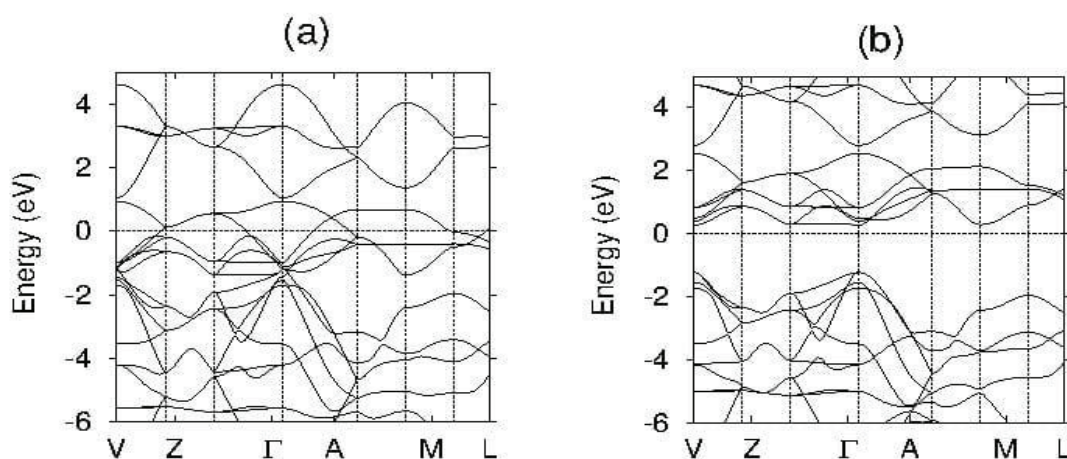
Fig. 2: Total band structure of CrO_2 for the spin majority channel (a) and spin minority channel (b). E_F represents the Fermi energy.

Our next motivation was to investigate the DOS of CrO_2. Figure 3 displays the total density of states (TDOS) and projected density of states (PDOS) of Cr-3d and O-2p orbitals. The system is found metallic in the spin majority channel, whereas it is insulating in the spin minority channel with a semiconducting spin gap of $E_g \sim 1.85$ eV. Considering both spin channels, the system is thereby half-metallic. It is obvious from this figure that the DOS in the close vicinity of the Fermi level (E_F) is dominated by the Cr-3d character. The octahedral crystal field splits the Cr-3d manifold into triply degenerate t_{2g} and doubly degenerate e_g bands. It is obvious from Fig. 3 that the t_{2g} and e_g PDOS are well separated from each other in both spin channels, which indicates 100% spin polarization. The Cr-t_{2g} and e_g PDOS are observed in between -1.3 eV to 1.07 eV and 1.34 eV to 4.50 eV respectively for the spin majority spin channel. In the spin minority channel, the corresponding PDOS are found between 0.35 eV to 2.6 eV and 3.1 eV to 6.1 eV respectively. For the spin majority channel, the available two Cr-3d electrons are distributed among the three t_{2g} states in such a manner that the occupied states are shifted below E_F and partially occupied states are found near E_F. The two e_g states are found unoccupied and are pushed above E_F. The scenario is different in the spin minority channel for which the entire Cr-3d bands are found above E_F. The O-

2p orbitals are mainly found between –7.24 eV to –1.6 eV and –7.07 eV to –1.54 for the spin majority and spin minority channels respectively. The O-2p orbitals are hybridized with Cr-3d orbitals, resulting in ferromagnetism in CrO_2.
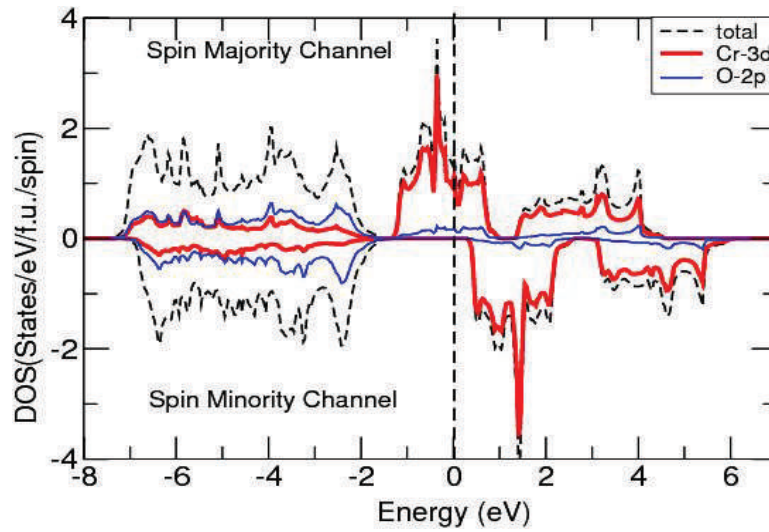

Fig. 3: Calculated TDOS, Cr-3d and O-2p PDOS in the LDA calculations. The spin majority channel is metallic, whereas the spin minority channel is insulating with a semiconducting gap of Eg ~ 1.85 eV. E_F represents the Fermi energy.

3.3. Electronic structure of VO$_2$

The formal valence V in VO_2 is 4+, i.e. the number of V-3d electrons is one ($3d^1$). The octagonal crystal field also splits V-3d orbitals into triply degenerate V-t_{2g} and doubly degenerate V-e_g orbitals. The V-t_{2g} states further split into V-d_{xy}, d_{yz} and d_{xz} orbitals, while the V-e_g states split into $d_{x^2-y^2}$ and $d_{3z^2-r^2}$ orbitals. Fig. 4 demonstrates the total band structure of VO_2 for the spin majority channel (a) and the spin minority channel (b). It is noticeable that the band structures are identical in both spin channels.
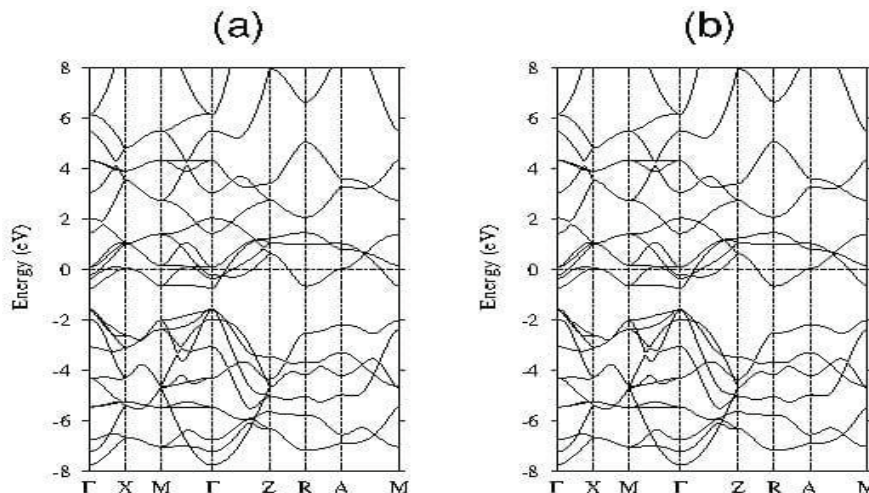
Fig. 4: Total band structure of VO_2 for spin majority channel (a) and spin minority channel (b). E_F represents the Fermi energy.

The twelve bands found below -1.5 eV are coming out from the O-2p orbitals. The six bands found mainly between. -1.0 eV to 2.0 eV are coming out from V-t_{2g} orbitals. The four bands found above 2.0 eV arise from the V-e_g orbitals. It is noteworthy that the V-t_{2g} orbitals are partially occupied in both spin channels, resulting in the metallic behaviour of VO_2.

The TDOS (black), PDOS of V-3d (red) and O-2p (green) orbitals are shown in Fig. 5. Here the TDOS near E_F is also dominated by the V-3d orbitals. It is interestingly found that TDOS and PDOS profiles are identical for both spin channels. In contrast to CrO_2 (for which an energy gap is found between the Cr-t_{2g} and e_g orbitals, as shown in Fig. 3), no energy gap is observed between the valance and conduction bands. In both spin channels, the V-t_{2g} orbitals are observed in the energy range of -0.85 to 1.62 eV, whereas the V-e_g orbitals are found in the energy range of 1.62 to 5.0 eV. It is evident that the V-t_{2g} orbitals are also partially occupied by the single electron for both spin channels and this sharing of the single electron by the three V-t_{2g} orbitals (d_{xy}, d_{yz} and d_{xz}) is responsible for the metallic behaviour of VO_2 in both spin channels. Therefore, considering both spin channels, VO_2 is metallic. No p-d hybridization is observed in the DOS calculations which is also consistent with the bands structure calculations [see Figs. (4(a) and 4(b)], implying opposite orientations of spins in the spin majority and spin minority channels. Hence, the present system is nonmagnetic.
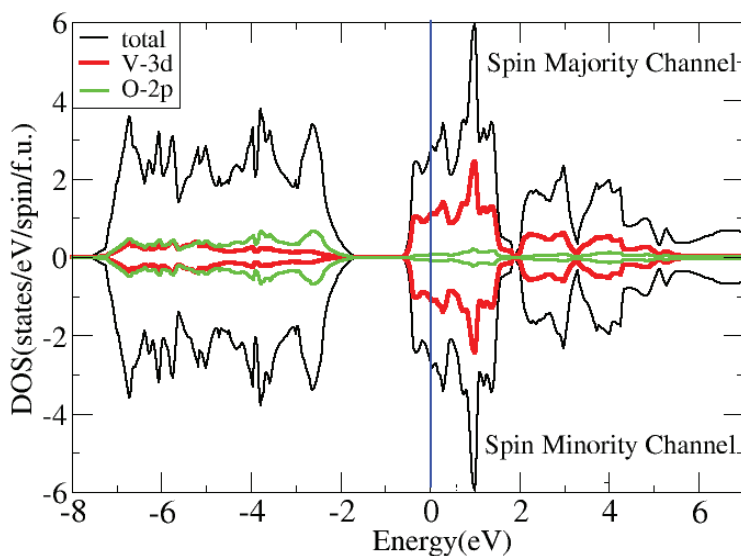
Fig. 5: The TDOS (black), V-3d (red) and O-2p (green) PDOS of VO_2. E_F represents the Fermi energy.

4. Conclusions

The structure and electronic properties of CrO_2 and VO_2 are studied. The material CrO_2 is observed to be a half-metallic ferromagnet with conductive/non-conductive spin majority/minority channel. On the other hand, VO_2 is observed to be a non-magnetic metal with both spin channels being

conductive. The sharing of the available two Cr-3d electrons by the three Cr-t_{2g} (d_{xy}, d_{yz} and d_{xz}) orbitals is responsible for the metallic behaviour of this material for the spin majority channel. On the other hand, the sharing of the available one V-3d electrons by the three V-t_{2g} orbitals is responsible for the metallic behaviour of this material for both spin majority channels. The p-d hybridization is responsible for the ferromagnetism of CrO_2, whereas opposite spin orientations in the two spin channels are responsible for the non-magnetic behaviour of VO_2.

References

[1] H. Tang, F. Levy, H. Berger and P. E. Schmid: Urbach tail of anatase TiO_2. *Phys. Rev. B* **52** (11), 7771-7774 (1995).

[2.] V. Duzhko, V. Y. Timoshenko, F. Koch and T. Dittrich: Photovoltage in nano crystalline porous TiO_2. *Phys. Rev. B* **64**(7), 075204 (2001).

[3] M. A. Korotin, V. I. Anisimov, D. I. Khomskii and G. A. Sawatzky: CrO_2: a self-doped double exchange ferromagnet. *Phys. Rev. Lett* **80** (19), 4305–4308 (1998).

[4.] H. T. Jeng and G. Y. Guo: First-principles investigations of the orbital magnetic moments in CrO_2. *J. Appl. Phys.* **92** (2), 951-957 (2002).

[5] B. R. Maddox, C. S. Yoo, D. Kasinathan, W. E. Pickett and R. T. Scalettar: High-pressure structure of half-metallic CrO_2. *Phys. Rev. B* **73**, 144111 (2006).

[6.] D. J. Pedder: Silver-ruthenium dioxide contacts. *Electrocompon. Sci. Technol.* **2**(4), 259–261 (1976) .

[7.] A. K. Goel, G. Skorinko and F. H. Pollak: Optical properties of single-crystal rutile RuO_2 and IrO_2 in the range 0.5 to 9.5 eV. *Phys Rev B* **24**(12), 7342–7350 V.

[8.] N. C. Halder: Electron tunnelling and hopping possibilities in RuO_2 thick films. *Electrocompon. Sci. Technol.* **11**(1), 21–34 (1983).S

[9] S. W. Lee, Y. W. Kim and H. Chen: Electrical properties of Ti-doped SnO_2 thin films prepared by the metal-organic chemicalvapor deposition method. *Appl. Phys. Lett.* **78**(3), 350–352 (2001).

[10.] K. L. Chopra, S. Major and D. K. Pandya: Transparent conductors-a status review. *Thin Solid Films* **102**(1), 1–46 (1983).

[11] J. Galy and G. Miehe: Ab initio structures of and VO_2 high-pressure phases. *Solid State Sci.* **1**(6), 433–448 (1999).

[12] B. W. Yu, W. R. Zhu, W. Jian and G. Hong: Spin-dependent transport in Fe-doped carbon nanotubes. *Phys. Rev. B*, **75**, 235415 (2007)

[13] K. L. Yao, Y. Min, Z. L. Liu, H. G. Cheng, S. C. Zhu and G. Y. Gao: First-principles study of transport of V-doped boron nitride nanotube. *Phys. Lett. A* **372**(34), 5609–13 (2008).

[14] G. M. Muller, J. Walowski, M. Djordjevic, G. X. Miao, A. Gupta, A. V. Ramos et al.: Spin polarization in half-metals probed by femtosecond spin excitation. *Nat. Mat.* **8**, 56–61 (2009).

[15] M. S. Anwar, F. Czeschka, M. Hasselberth, M. Porcu and J. Aarts: Long-range supercurrents through half-metallic ferromagnetic CrO_2. *Phys. Rev.* **82**, 100501(R) (2010).

[16] M. S. Anwar and J. Aarts: Anomalous transport in half-metallic ferromagnetic CrO_2. *Phys. Rev. B* **88**, 085123 (2013).

[17] H. Fujiwara, M. Sunagawa, K. Terashima, T. Kittaka et al.: Intrinsic spin polarized electronic structure of CrO_2 epitaxial film revealed by bulk sensitive spin-resolved photoemission spectroscopy. *Appl. Phys. Lett.* **106**, 202404 (2015).

[18] H. Takeda, Y. Shimizu, Y. Kobayashi, M. Itoh et al.: Local electronic state in the half-metallic ferromagnet CrO_2 investigated by site-selective ^{53}Cr NMR measurements. *Phys. Rev. B* **93**, 235129 (2016).

[19] A. Singh, C. Jansen, K. Lahabi and J. Aarts: High-quality CrO_2 nanowires for dissipationless spintronics. *Phys. Rev. X* **6**, 041012 (2016).

[20] A. M. Bratkovsky: Tunneling of electrons in conventional and half-metallic systems: towards very large magnetoresistance. *Phys. Rev. B* **56**, 2344 (1997).

[21] S. Sughara and M. A. Tanaka: Spin metal–oxide–semiconductor field-effect transistor using half-metallic–ferromagnet contacts for the source and drain. *Appl. Phys. Lett*. **84**(13), 2307 (2004).

[22] B. Zhang, J. Sun, J. Leng, C. Zhang and J. Wang: Tunable two dimensional ferromagnetic topological half-metal CrO_2 by electronic correction and spin direction, *Appl. Phys. Lett.* **117**, 222407 (2020).

[23] S. S. N. Bharadwaja, C. Venkatasubramanian, N. Fieldhouse, S. Ashok, M. W. Horn and T. N. Jackson: Low temperature charge carrier hopping transport mechanism in vanadium oxide thin films grown using pulsed dc sputtering. *Appl. Phys. Lett.* **94,** 222110 (2009).

[24] T. Driscoll, S. Palit, M. M. Qazilbash, M. Brehm, F. Keilmann, B. G. Chae, S. J. Yun, H. T. Kim, et al.: Dynamic tuning of an infrared hybrid-metamaterial resonance using vanadium dioxide. *Appl. Phys. Lett.* **93**, 024101 (2008).

[25] Z. Yang, C. Ko and S. Ramanathan: Oxide Electronics Utilizing Ultrafast Metal-Insulator Transitions. *Annu. Rev. Mater. Res*. **41**, 337 (2011).

[26] R. M. Wentzcovitch, W. W. Schulz and P. B. Allen: VO_2: Peierls or Mott-Hubbard? A view from band theory. *Phys. Rev. Lett*. **72**, 3389 (1994).

[27] T. M. Rice, H. Launois and J. P. Pouget: Comment on "VO_2: Peierls or Mott-Hubbard? A View from Band Theory" *Phys. Rev. Lett.* **73**, 3042 (1994).

[28] Z. Tao, T. R. T. Han, S. D. Mahanti, P. M. Duxbury, F. Yuan, C. Y. Ruan, K. Wang and J. Wu: Decoupling of structural and electronic phase transitions in VO_2. *Phys. Rev. Lett*. **109**(16), 166406 (2012).

[29] J. Laverock, S. Kittiwatanakul, A. A. Zakharov, Y. R. Nilu, B. Chen, S. A. Wolf, J. W. Lu and K. E. Smith: Direct observation of decoupled structural and electronic transitions and an ambient pressure monoclinic like metallic phase of VO_2. *Phys. Rev. Lett.* **113**(21), 216402 (2014).

[30] J. H. Park, J. M. Coy, T. S. Kasirga, C. Huang, Z. Fei Z, S. Hunter and D. H. Cobden: Measurement of a solid-state triple point at the metal-insulator transition in VO_2. *Nat.* **500**, 431–434 (2013)

[31] B. T. O'Callahan, A. C. Jones, J. H. Park, D. H. Cobden, J. M. Atkin and M. B. Raschke: Inhomogeneity of the ultrafast insulator-to-metal transition dynamics of VO_2. *Nat. Commun.* **6**(1), 6849 (2015).

[32] B. Yan, X. Li, Z. Bai, L. Lin, G. Chen, X. Song, D. Xiong, D. Li and X. Sun: Superior sodium storage of novel VO_2 nano-microspheres encapsulated into crumpled reduced graphene oxide. *J. Mater. Chem. A* **5**(10),4850-4860 (2017).

[33] Y. Chen, S. Zhang, F. Ke, C. Ko, S. Lee, K. Liu, B. Chen, J. W. Ager, R. Jeanloz, V. Eyert and J. Wu: Pressure-temperature phase diagram of vanadium dioxide. *Nano. Lett.* **17**(4), 2512 (2017).

[34] P. Hohenberg and W. Kohn: Inhomogeneous electron gas. *Phys. Rev. B* **136**, B864 (1964).

[35] W. Kohn and L. J. Sham: Self-consistent equations including exchange and correlation effects. *Phys. Rev*. **140**, A1133 (1965).

[36] O. K. Andersen and O. Jepsen: Explicit, first-principles tight binding theory. *Phys. Rev. Lett*. **53***, 2571 (1984).

[37] O. K. Andersen: Linear methods in band theory. *Phys. Rev. B***12**, 3060 (1975).

[38] J. P. Perdew and Y. Wang: Accurate and simple analytic representation of the electron gas correlation energy. *Phys. Rev. B***45**, 13244 (1992).

[39] V. Eyert: The metal-insulator transitions of VO_2: A band theoretical approach *Ann. Phys*. **11**, 9 (2002).

[40] M. Born and J. R. Oppenheimer: Zur Quantentheorie der Molekel. *Ann. Phys.* **389** (20), 457 (1927).

[41] N. J. Hoboken: Born-Oppenheimer Approach: Diabatization and Topological Matrix, Wiley & Sons, USA, 2006, pp. 26-57.

[42] J. A. Gaunt: A Theory of Hartree's Atomic Fields. *Proc. Camb. Philos. Soc.* **24** (2), 328 (1928).

[43] D. R. Hartree and W. Hartree: Self-consistent field, with exchange, for beryllium. *Proc. Royal Soc. Lond. A.* **150** (869), 9 (1935).

[44] V. A. Fock: Näherungsmethode zur Lösung des quantenmechanischen Mehrkörperproblems. *Z. Phys.* **61** (1), 126 (1930).

[45] V. A. Fock: Selfconsistent field "mit Austausch für Natrium. *Z. Phys.* **62** (11), 795 (1930).

[46] J. P. Perdew and Y. Wang: Accurate and simple density functional for the electronic exchange energy: Generalized gradient approximation. *Phys. Rev. B* **33**, 8800 (1986).

[47] K. Burke, J. P. Perdew and Y. Wang: Generalized gradient approximation for the exchange-correlation hole of a many-electron system. *Phys. Rev. B* **54**, 16533 (1996).

[48] O. Jepsen and O. K. Andersen, The STUTTGART TB-LMTO program, version 47 (2000). https://www2.fkf.mpg.de/andersen/ LMTODOC/LMTODOC.html.

Research Article

Studies on the Nutrient Uptake by Two Thelastomatid Nematodes (Nematoda: Oxyuroidea) of the Cockroach, *Periplaneta americana*

Jayati Ghosh*, Tasnin Sultana, Jayati Chakraborty

Post Graduate Department of Zoology, Barasat Govt. College, West Bengal, India.
*Associate Professor, Post Graduate Department of Zoology, Barasat Govt. College
Corresponding author email: jayatizoology@gmail.com

Abstract: Thelastomatid nematodes are obligate parasites in the hind gut of cockroaches. In the present work, investigation on the quantitative uptake of some simple carbohydrates (Glucose, fructose, lactose) and proteins was performed from Thelastomatid Nematodes, *Hammerschmidtiella diesingi* and *Thelastoma aligarhica* isolated from *P. americana*. Our results revealed that in *H. diesingi* lactose uptake is highest (156.25 ± 19.44 µg/ml) followed by Fructose (142.5 ± 24.74 µg/ml) and Glucose (58.3 ± 11.73 µg/ml). Whereas, in *T. aligarhica* maximum utilization of glucose (197.5± 10.61 µg/ml) was found followed by fructose (147.9 ± 5.04 µg/ml) and lactose (107.5 ± 7.07 µg/ml). Glucose uptake in T. *aligarhica* is about 3.38 times higher compared to *H. diesingi.* Our observation is size difference and habitat preference may be linked with such differing carbohydrate utilization. *H. diesingi* has a preference for anterior hind gut of *P. americana*. Therefore, high lactase activity in these region probably played a role in high lactose uptake in *H. diesingi*. The study also showed that utilization of exogenous protein is very less compared to sugar uptake in these parasites.

Keywords: Cockroach . Pinworm . Nutrients . Uptake . Hindgut

Introduction:

Oxyurid nematodes are omnipresent and plentiful in *Periplaneta americana,* often occurring in 80% of laboratory populations [1]. These worms belong to the family Thelastomatidae (order Oxyurida) sub-family Thelastomatide and are very common in hind part of intestinal tract of cockroaches [2, 3]. These entomophilic nematodes are endoparasites and only lay their eggs outside of host body for dispersal. After host ingestion, juveniles hatch out and undergo several molts to become adult worm. It is a large family, currently represented by about 31 genera. Cockroach hind gut complex bacterial microfauna are the main food source of these nematodes [4]. Thelastomatids worms mainly remains as mixed population of different pinworms [5] or in association with different protozoan fauna like ciliates, flagellates and amoebas. In India, three species of Thelastomatidae in the gut of *Periplaneta americana* viz *Hammerschmidtiella diesingi*, *Thelastoma aligarhica* and *Periplaneticola mirzaiawas* described

by Basir in 1940 [6]. *Hammerschmidtiella diesingi* was found to be most prevalent and available in *P. americana*. Very little information is available on the interaction of these nematodes with each other and with the host species. The nature of pathological effect these worms may have upon the host is not well investigated. Generally, these worms are not lethal to their host but may have some effect on health and reproductive potential.

All parasites require a supply of energy for biosynthesis of macromolecules, growth, mechanical activity, reproduction etc. A major part of energy source utilized by the parasite is in the form of carbohydrates.

Despite the possession of mouth and functional gut in the helminth, uptake of glucose or soluble carbohydrate occurs in these parasites across their outer body surface [7, 8]. In cockroach gut the food contents are mostly semi liquid in nature. The pharynx of oxyuroid show considerable variation in structure and acts as a powerful pumping organ. Similar to carbohydrate, protein also forms the main nutritional requirement of adult worm as they produce large number of eggs in the alimentary tract [9]. Little is known about the metabolism and carbohydrate and protein uptake in oxyurid nematodes. Investigations into the nutrient uptake pattern of two different Thelastomatid nematodes under *in vitro* conditions have been performed to understand the preference and variation of sugar and protein uptake pattern. This study might also have significant impact on pest control program.

Material and Methods

Dissection of Cockroach and collection of pinworm

The cockroaches (*Periplaneta americana)* were collected and immobilized by warm water and then dissected out. The digestive systems were removed. The hindgut was taken out and kept in watch glass containing saline solution (0.67% NaCl in distilled water). Adult female pinworms *Hammerschimidtiella diesingi* (Hammerschmidt, 1838) and *Thelastoma aligarhica* (Basir, 1940) were collected from hind gut.

Incubation of worms in different sugar solution and measurement of sugar uptake by 3, 5-dinitrosalicylic acid (DNS) assay described by Miller[10]

Standard glucose, fructose and Lactose soln. were prepared. Immediately after isolation worms were kept in 0.06% of monosaccharides glucose, fructose and disaccharide lactose solution and incubated at 37 °C for 6 hours. After incubation is completed, the amount of reducing sugar present in the nutrient media were calculated spectrophotometrically by DNS

method. Control absorbance was obtained by replacing nutrient media with water. Reducing sugar uptake per worm was calculated using the following formula:-

$$\text{Sugar uptake per worm (µg/ml)} = \frac{\text{Standard sugar content at 540 nm O.D. - Sample sugar content after Incubation at 540 nm}}{\text{Number of worms incubated}}$$

Incubation of worms in protein solution and measurement of protein uptake

Bovine serum albumin (BSA) powder was dissolved in distilled water and diluted to a concentration of 1 µg/ml and a protein standard curve was prepared using Lowry's method (Lowry *et al.* 1951). Worms were incubated for 6 hrs and absorbance measured at 650 nm. Protein uptake per worm was calculated using the following formula:-

$$\text{Protein uptake per worm} = \frac{\text{Standard protein content at 650 nm O.D. - Sample protein content after incubation at 650 nm}}{\text{Number of worms incubated}}$$

Statistical Analysis

All tests were carried out in triplicate and the results obtained in the study were statistically analyzed and the data were expressed in mean ± S.D. Data analyzed using paired Student's t-test ($p < 0.05$).

Results

The uptake data of different simple carbohydrates by oxyurid nematode *Hammerschmidtiella diesingi* and *Thelastoma aligarhica* are tabulated quantitatively in Table 1 and same are represented graphically in Figure 1, 2 and 3. After the 6 hours of incubation, both the worms utilized these three simple carbohydrates namely glucose, fructose and lactose but the results showed that these uptake is preferential. In *H. diesingi* lactose uptake is highest (156.25 ± 19.44 µg/ml) followed by Fructose (142.5 ± 24.74 µg/ml) and Glucose (58.3 ± 11.73 µg/ml) (Figure 1). Whereas, in *T. aligarhica* maximum utilization of glucose (197.5± 10.61 µg/ml) followed by fructose (147.9 ± 5.04 µg/ml) and lactose (107.5 ± 7.07 µg/ml) were found (Figure 2).
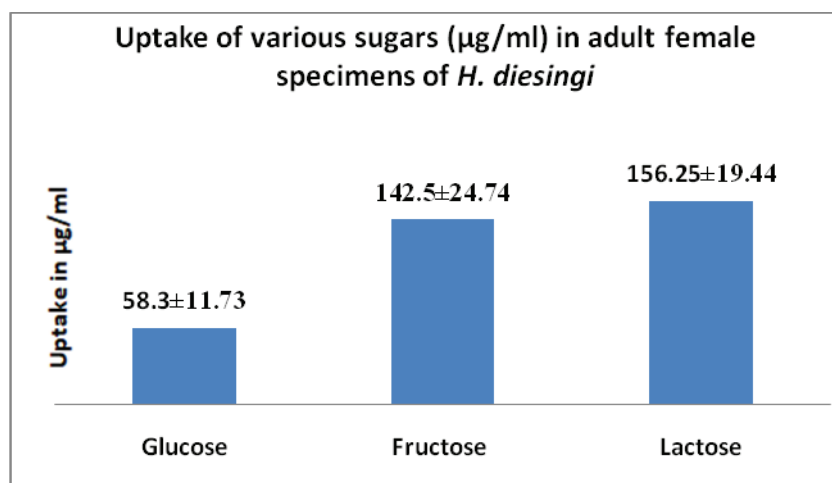
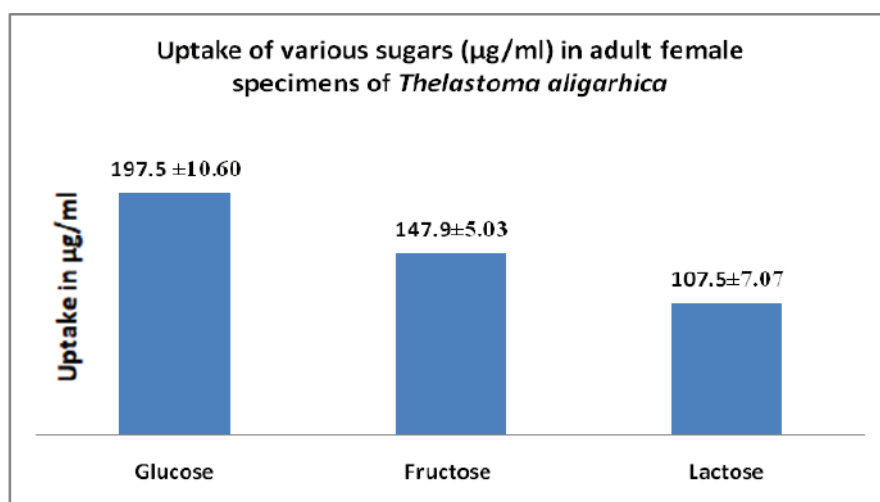**Figure1.** Uptake of various sugars (µg/ml) in adult female specimens of *H. diesingi*

Figure2. Uptake of various sugars (µg/ml) in adult female specimens of *Thelastoma aligarhica*

In *H. diesingi*, the lactose uptake is more than two times higher than glucose uptake. Glucose utilization varied between two worms markedly (Table 1) (Figure 3). Fructose uptake is almost similar in the two groups. Lactose is less preferred as exogenous nutrient in *T. aligarhica* whereas mostly preferred by *H. diesingi*.

Table 1. Uptake of various sugars (µg/ml) in adult female specimens of *H. diesingi* Chitwood, 1932 and *T. aligarhica* (Basir, 1940) after 6 hrs incubation. Data were expressed in mean ± S.D

Carbohydrate as Nutrient	*Hammerschmidtiella diesingi*	*Thelastoma aligarhica*
Glucose	58.3 ± 11.73^{a1}	197.5± 10.61^{b1}
Fructose	142.5 ± 24.74^{a2}	147.9 ± 5.04^{a2}
Lactose	156.25 ± 19.44^{a3}	107.5 ± 7.07^{c2}

Mean ± SD with the same letter in a row are not significantly different at $p < 0.05$ between two worms. Mean ± SD with the same number in a column are not significantly different at $p < 0.05$
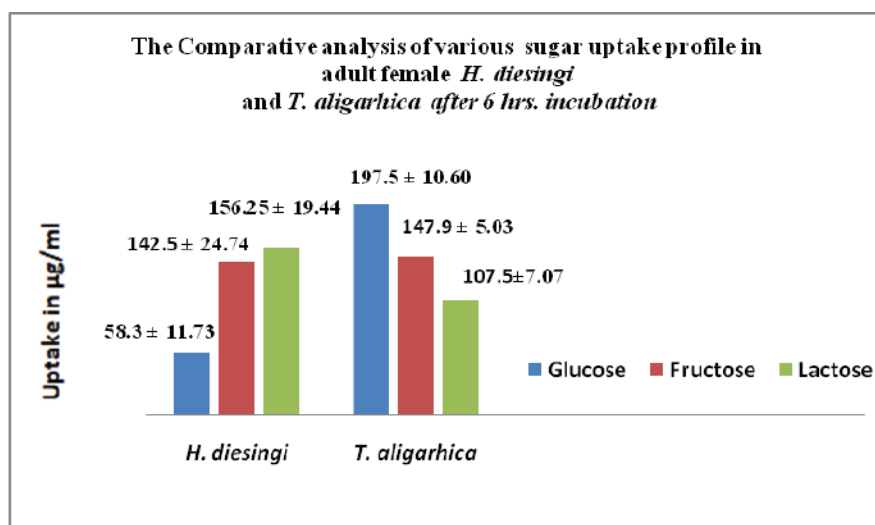
Figure 3. The Comparative analysis of various sugar uptake in adult female *H. diesingi* and *T. aligarhica* after 6 hours of incubation

It is also evident that uptake of glucose is about 3.38 times higher in T. *aligarhica* compared to *H. diesingi.* The results of protein uptake study indicate very clearly that utilization of exogenous protein is very less compared to carbohydrates in the medium. These worms choose carbohydrate as their main energy source rather than protein. Uptake of BSA was found to be highest in *H. diesingi* than T. *aligarhica* (Table 2) (Figure 4).
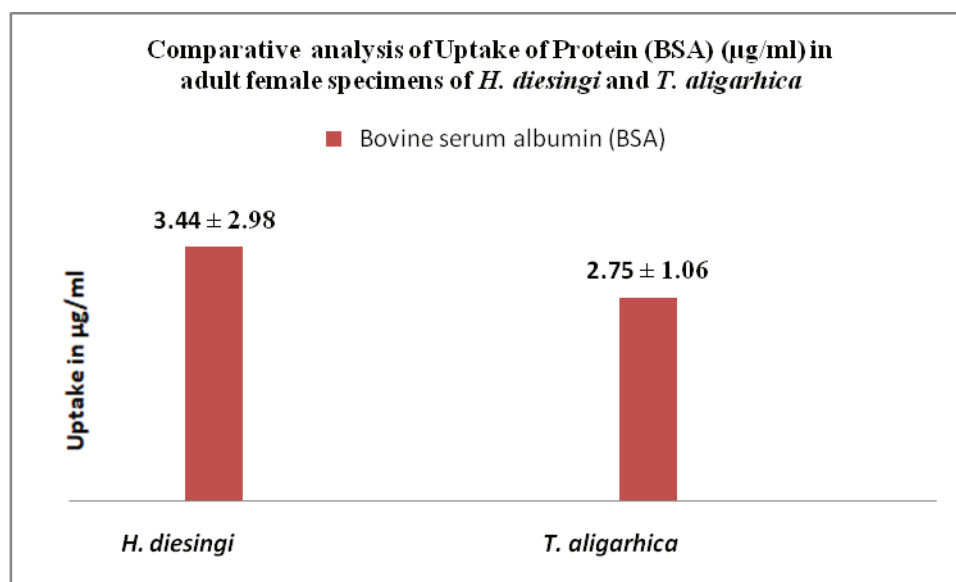
Figure 4 Comparative analysis of Uptake of Protein (BSA) (µg/ml) in adult female specimens of *H. diesingi* and *T. aligarhica*

Table 2 Uptake of Protein (BSA) (µg/ml) in adult female specimens of *H. diesingi* Chitwood, 1932 and *Thelastoma aligarhica* (Basir, 1940) after 6 hrs incubation. Data were expressed in mean ± S.D

Protein as Nutrient	*Hammerschmidtiella diesingi*	*Thelastoma aligarhica*
Bovine serum albumin (BSA)	3.44 ± 2.98^a	2.75 ± 1.06^b

Mean ± SD with the different letter in a row are significantly different at $p < 0.05$ between two worms.

Discussion

Carbohydrates are chief energy source in all parasites. Helminths when live in the intestine of hosts, they utilize food from the gastrointestinal tract. The metabolism of these parasites depends on the feeding habits and the rich nourishment available in the gut of the host. These worms use this nourishment for their normal development and growth.

It is generally believed that nematodes uptake glucose against a concentration gradient and use the endogenous carbohydrate as an energy source when it cannot be obtained

from outside. Such observations are based on *in vitro* studies of a number of helminths [12]. Cavier and Savel, 1951 reported that nematode can make use of other sugar also [13]. It is generally accepted that intestinal worms has two routes of nutrient uptake. Major portion of nutrients are taken by oral aperture and rest across the cuticle. These nematodes are different from ascaroids on the basis of esophageal morphology (oxyuroids having a posterior bulbar enlargement) and shape of the adult females (oxyuroids having a pointed tail) [14]. Presence of muscular pharynx in oxyuroids suggests that main route of entry of nutrients occurs through mouth.

These adult nematodes are essentially anaerobic. In this environment, the nematodes depend primarily on carbohydrate metabolism because non-carbohydrate nutrients like protein and lipids do not contribute in the intestinal oxidation-reduction reactions as in anaerobic processes [15]. This is indicated in pinworms of the present study also. Thelastomatids utilized very small amount of proteins compared to carbohydrates.

T. aligarhica is a larger species than *H. diesingi*. Average length of *T. aligarhica* is 3300μm and width is 300 μm [6]. Average length of *H. diesingi* is 2666.7 μm and width 240.5 μm [16]. These size differences are probably one of the reasons of higher uptake of glucose and other simple carbohydrates. It has been reported that there is a lack of trophic segregation among various pinworm species but species differs in consumption rate. In a three species co infection, *L. appendiculatum* ate more than *Thelastoma bulhoesi*, which ate more than *H. diesingi* [17]. Therefore large size and high consumption rate may be the reason for higher uptake of nutrients in *Thelastoma* compared to *Hammerschmidtiella*.

Adamson and Noble (1992) found that in single species infection both *Thelastoma* sp. and *H. diesingi* prefer to stay at extreme anterior end of hind gut but in co infection *Thelastoma* sp. was more spread out in the gut than *H. diesingi* and it tended to be more

posteriorly located occurring in the second fifth fraction of the hindgut [18]. Hominick & Davey (1973) reported that *H. diesingi* is a mucosal wall specialist in hind gut of *P. americana*. It relies mainly on fine granular material of bacterial origin and positions its mouth close to the intima [19]. The region of the anterior hindgut or colon is preferred by *H. diesingi* may be a least active area and so the amount of energy required to maintain its position is also may be less. Whereas *T. aligarhica* extended more posteriorly needs more energy to adjust and positioning in the fluctuating conditions of colon. Therefore, size difference as well as relative position of worms in the hind guts may be the reason of higher uptake of carbohydrates in *T. aligarhica*.

Here, the lactose preference over glucose in *H. diesingi* may be a consequence of high lactase activity close to intestinal epithelium at the junction of mid and hind gut. Gilmour (1961) quotes various workers who obtained lactase in their experimental insects [20]. Glycosidase activities in the cockroach *Byrsotria fumigata* on several disaccharides has been reported by Fisk and Rao, 1964. They observed high β-galactosidase activity on lactose in the fore and mid gut and low activity in the hind gut [21]. According to their observation, oligosaccharide availability was limited in the hindgut. Our observation corroborated well with this work and we conclude that *H. diesingi* utilized lactose mostly because of high lactase activity in midgut or anterior hind gut which is their preferred location. As *T. aligarhica* localized in the posterior hindgut where lactase activity is low they preferentially choose glucose as the main energy substrate.

Proteins play a very significant role in the construction of egg shell, nutrition and the formation of larval bodies. In intestinal nematode parasites the amino acids requirements are met from the content of their hosts as suggested by the Shishova, *et al.*, 1970, Von Brand, 1973[22,12]. It is a known fact that not only amino acids but dipeptides and whole protein molecules can be ingested by helminthes [9]. In our study, two Thelastomatids worms utilized protein from the medium but in much lesser quantity.

Conclusion

The present investigation indicated that two species of the oxyurid worms have different carbohydrate preference in the gut of *P. americana*. Lactose is preferred by *H. diesingi* whereas; in *T. aligarhica* maximum utilization of glucose was observed.

Acknowledgements

References:

[1] V. H.Tsai, K.M. Cahill: Parasites of the German cockroach (*Blattella germanica* L.) in New York City. *Journal of Parasitology,* **56**, 375-377 (1970).

[2] M. M. Shah: Some studies on insect parasitic nematodes (Oxyurida, Thelastomatoidea, Thelastomatidae) from Manipur, North-East India. *ActaParasitologica,* **52**, 346–362 (2007).

[3] A. R. Jex, M. A. Schneider, H.A. Rose, T.H. Cribb: The Thelastomatoidea (Nematoda: Oxyurida) of two sympatric Panesthiinae (Blattodea) from southeastern Queensland, Australia: taxonomy, species richness and host specificity. *Nematology*, **7**, 543–575 (2005).

[4] M. Adamson: Evolutionary patterns in life histories of Oxyurida. *International Journal for Parasitology*, **24**, 1167–1177 (1994).

[5] S. Ozawa, C.S.Vicente, K. Sato, T. Yoshiga, N. Kanzaki and K. Hasegawa: First report of the nematode. *Leidynema appendiculata* from *Periplaneta fuliginosa*. *Acta Parasitol* , **59**, 219–228 (2014).

[6] M.A. Basir: Nematodes parasitic in Indian cockroaches. Proc Indian Acad Sci Sect (B) 12, 8–16 (1940).

[7] A. A. Siddiqi, W. A. Nizami: Gas content of swim-bladder of *Wallago attu* and oxygen consumption in *Isoparorchis hypselobagri* Trematoda. Z. Parasitenkd **47**, 263-268 (1975).

[8] D. P. Thompson, T. G. Geary: The structure and function of helminth surfaces in Biochemistry and Molecular Biology of parasites (j.j.marr, ed.), 1st ed. Academic press, New York (1995).

[9] J. D. Smyth: Animal Parasitology. Cambridge University Press (LPE), U.K. (1996).

[10] G. L. Miller: Use of dinitrosalicylic acid reagent for determination of reducing sugar. Analytical Chemistry **31(3)**, 426–428 (1959).

[11] O. H. Lowry, N. J. Rosebrough, A. L. Farr, R. J. Randall: Protein Measurement with the Folin Phenol Reagent. *J Biol Chem*, **193**,265-275 (1951).

[12] T. Von brand: Biochemistry of Parasites. Academic Press, New York and London (1973).

[13] R. Cavier, J. Savel: Chemical composition of *Ascaris lumbricoides* from swine. Bull. Soc. Chem. Biol., 33: 447 – 454 (1951).

[14] W. Yorke, P. A. Maplestone : The Nematode parasites of vertebrates. P. Blakiston's Son & Co Philadelphia (1926).

[15] T. C. Cheng: General parasitology (Academic Press) (1971).

[16] M. V. Blanco, P. Lax, J. C. R. Dueñas, C. N. Gardenal and M. E. Doucet: Morphological and molecular characterization of the entomoparasitic nematode *Hammerschmidtiella diesingi* (Nematoda, Oxyurida, Thelastomatidae). *Acta Parasitologica*, **57**, 302–310 (2012).

[17] S. Connor, M. Adamson: Niche overlap among three species of pinworm parasitic in the hindgut of the American cockroach, Periplaneta americana. *Journal of Parasitology*, **84**, 245–247 (1998).

[18] M. L. Adamson, H. Noble: Structure of the pinworm (Oxyurida: Nematoda) guild in the hindgut of the American cockroach, *Periplaneta americana*. *Parasitology,* **104**, 497–507 (1992).

[19] W. M. Hominick, K. G. Davey: The influence of host stage and sex upon the composition of the population of 2 species of thelastomatids parasitic in the hind gut of *Periplaneta americana*. *Canadian Journal of Zoology*, **50**, 945–952 (1972).

[20] D. Gilmour: The Biochemistry of Insects. Academic Press, New York (1961).

[21] F. W. Fisk, B.R. Rao: Digestive carbohydrases of the Cuban burrowing cockroach. Ann. Entomol. Soc. Am 5740-5744 (1964).

[22] O. A. Shishova-Kasatochkina, N. A. Lev: Protein uptake in *A. suum*. Riga. IzdatePstvo Zinatne 103-104. Gelan, Moscow, USSR (1970).

Contents

AUREOLE

Guidelines to Authors for Humanities, Social Sciences and Science Subjects

Guidelines to Authors for Science Subjects AUREOLE –An Academic Journal (ISSN 0976 –9625) is a well intended endeavour of the Barasat Government College to facilitate publication of papers/articles in the do main of Humanities, Science and Social Science.

- Full-length papers should be limited to 10 printed pages.
- The **title zone** of the manuscript should be the upper-half portion of the first page and should include the title, names and addresses of the authors, abstract and keywords.
- The **abstract** should clearly state the rationale, objectives, methods, views and important conclusions of the study. It should not exceed 180 words (10 pt in MSWord).
- The abstract should be followed by not more than five **keywords** indicating the contents of the paper and useful for abstracting purposes (10 pt in MSWord).
- The **main text** of the paper should start from 3 lines below the Keywords in the first page. The paper should be organized in different sub-sections. Sub-section headings are to be typed in bold running text and flushed with the left-margin. The following scheme of organization of the paper in different sub-section may be considered to be adhered to: Introduction, Specific Problem to study and Methodology, New Insights or Views, Results, Discussion, Acknowledgements, References. Wherever appropriate, results and discussion can be combined and Acknowledgements be omitted (12 pt in MSWord).
- **Introduction** should be brief and limited to the statement of the problem and aim of the study.
- **Specific Problem to Study** should be clearly spelled out and **Methodology** applied to study the same should be clearly stated. For well-known methods, citation of reference will suffice.
- **New Insights and Views** which are relevant and are specifically applied to resolve the problem under study are to be clearly mentioned.
- **Results and Discussion** should be clear to readers in different disciplines . Regarding the units of any measurement, authors are to stick to SI system.
- **Tables** should be included within the text at relevant place with a heading stating its contents clearly and concisely. Numericaldata and calculations should be thoroughly checked.
- **Figures** should be included within the main text of the paper at relevant places and should be of proportional size (with the text)as well as legible. Legends to the illustrations should be typed below the figure and information in the legend should not be repeated in the text and similarly, the same data should not be represented in both graph and table form. All figures, whether photographs, maps, graphs or line drawings should be numbered consecutively.
- **Line drawings** of high quality and in the desired size would have to be included in the running text of the main body of the paper.Any inscription should be clearly legible.
- **Photographs if any**, should be of high contrast, black and white or colour and of suitable size and should be embedded within the maintext.
- **Acknowledgements** should mention only guidance or assistance received in real terms, and financial grant provided by anagency. Acknowledgements for inspiration, typing etc., need not be mentioned.
- **References** in text, to be cited by author, would have to be in numerals within square brackets as [1] etc. Multip le citations should be in multiple numbers within the square brackets as [2-7, 10, 15] where the first part indicates that references numbered 2 to 7 are all cited.